

Utah State University

DigitalCommons@USU

All Graduate Theses and Dissertations

Graduate Studies

5-2014

Laboratory Modeling of Erosion Potential in Dam Foundations Due to Foundation Voids

Tyler K. Coy
Utah State University

Follow this and additional works at: <https://digitalcommons.usu.edu/etd>



Part of the [Civil and Environmental Engineering Commons](#)

Recommended Citation

Coy, Tyler K., "Laboratory Modeling of Erosion Potential in Dam Foundations Due to Foundation Voids" (2014). *All Graduate Theses and Dissertations*. 3899.

<https://digitalcommons.usu.edu/etd/3899>

This Thesis is brought to you for free and open access by the Graduate Studies at DigitalCommons@USU. It has been accepted for inclusion in All Graduate Theses and Dissertations by an authorized administrator of DigitalCommons@USU. For more information, please contact digitalcommons@usu.edu.



LABORATORY MODELING OF EROSION POTENTIAL IN DAM FOUNDATIONS
DUE TO FOUNDATION VOIDS

By

Tyler K. Coy

A thesis submitted in partial fulfillment
of the requirements for the degree

of

MASTER OF SCIENCE

in

Civil and Environmental Engineering

Approved:

Dr. John D. Rice
Major Professor

Dr. James A. Bay
Committee Member

Dr. Gilberto E. Urroz
Committee Member

Dr. Mark R. McLellan
Vice President for Research and
Dean of the School of Graduate Studies

UTAH STATE UNIVERSITY
Logan, Utah

2014

Copyright © Tyler K. Coy 2014

All Rights Reserved

ABSTRACT

Laboratory Modeling of Erosion Potential in Dam Foundations

Due to Foundation Voids

by

Tyler K. Coy, Master of Science

Utah State University, 2014

Major Professor: Dr. John D. Rice
Department: Civil and Environmental Engineering

Many earthen dams and levees throughout the United States and the world have been built on top of karst formations or jointed bedrock, leading to problems with internal erosion. The large hydraulic pressures and gradients that dam construction imposes on the dam or levee itself and especially the soil adjacent to these open and/or soil-filled voids can have a very negative effect on the integrity of the dam or levee. These voids can be a conduit for soil erosion to occur and, over time, lead to the partial or complete failure of the structure. The voids that are already filled with soil can oftentimes be cleared out due to the high pressures and gradient imposed by the reservoirs that are considerably higher than the soil has ever before seen. The clearing of these voids allows for an exit point for more soil to follow.

The purpose of this study is to better understand the effects and interaction that different size voids can have on a variety of soils when hydraulic loading is imposed.

Hydraulic loading may consist of a constant differential hydraulic head imposed across the sample and/or cyclic hydraulic loading such as the rising and lowering of the water table. Tests were performed with a vertical flow down through the soil exiting out of the void and also flow entering in at the void charging the soil and then exiting out of the same void. The downward flow represents the seepage due to the high heads that the dam or levee imposes on the soil and the charging and then rapid drawdown of the soil is representative of piezometric surface change in elevation due to reservoir fluctuation or large rainfall events. The information gathered in these tests will be used to help in risk assessment studies of existing dams and levees and in future construction.

(185 pages)

PUBLIC ABSTRACT

Laboratory Modeling of Erosion Potential in Dam Foundations

Due to Foundation Voids

Tyler K. Coy

Earthen dams and levees create high gradients and increased hydraulic pressures in the underlying soil, which can lead to erosion and other challenges. Karst formations and other defects such as cracks in the foundation and/or abutments can lead to failure mechanisms such as internal erosion. Generally these voids or cracks are filled with soil, but due to the increased pressures and gradients that dams and levees create, the original soil is pushed out, thus creating a void that acts as a conduit for more soil to follow. Different soils will erode at different rates and some even create a natural filter, preventing further erosion from occurring, but due to these increased gradients and the cyclic changes that can occur throughout the seasons these filters can be broken down, allowing for erosion to continue and potentially lead to complete failure of the structure unless certain reparatory measures are taken. In the lab we have simulated different conditions that exist in the field and the results of testing a variety of soils can be found in this paper.

ACKNOWLEDGMENTS

I along with Utah State University would like to thank the United States Army Corps of Engineers for financial, technical, and administrative assistance in funding and managing this project and for making the information discovered in this study possible.

I would also like to thank my major professor, Dr. John Rice, for his continued guidance and support throughout the duration of this project. Without his insight and expertise none of this would have been possible. I would also like to thank my committee members, Dr. James Bay and Dr. Gilberto Urroz, for their support and guidance throughout the duration of my project.

I would also like to give special thanks to all of my family and friends for your support throughout this project. I especially want to thank my dear wife for making all of this possible. For her continued love, encouragement, and support during this entire process.

Tyler Coy

CONTENTS

Page	
ABSTRACT.....	iii
PUBLIC ABSTRACT	v
ACKNOWLEDGMENTS.....	vi
LIST OF TABLES.....	ix
LIST OF FIGURES.....	x
CHAPTER	
1: INTRODUCTION.....	1
2: REVIEW OF RELATED LITERATURE	4
2.1 Introduction.....	4
2.2 Sinkholes.....	4
2.3 Internal Erosion	8
2.4 Karst Problems.....	9
2.5 Open Void Test Cell (previous laboratory work)	12
2.6 Case History	13
3: FOUNDATION VOID EROSION TEST CELL.....	20
3.1 Testing Apparatus.....	20
3.2 Data Collection	23
3.3 Procedure Setup.....	24
4: ANALYSIS OF RESULTS.....	28
4.1 Teton Dam Shell of Embankment Soil.....	29
4.2 East Branch Dam Core of Embankment Soil	39
4.3 Sand with Clay Soil.....	59
4.4 Teton Dam Core of Embankment Soil Test #1	68
4.5 Teton Dam Core of Embankment Soil Test #2	78
4.6 Teton Dam Core of Embankment Soil Test #3	82
5: SUMMARY AND CONCLUSIONS	86

REFERENCES..... 90

APPENDIX 92

LIST OF TABLES

Table	Page
1 Six subcategories of sinkholes with cross section and information (Waltham et al. 2005)	7
2 Continuing erosion criteria into an open defect (Fell et al. 2008).....	9
3 Soil properties	26
4 Summary of tests.....	29
5 Hydraulic loading cycles for East Branch Dam test	42
6 Calculated stresses at top of void in Figure 35.....	58
7 Hydraulic loading cycles for Sand-Kaolinite test	60
8 Hydraulic loading cycles for Teton Dam Core test #1	69
9 Hydraulic loading cycles for Teton Dam Core test #2	79

LIST OF FIGURES

Figure	Page
1	Deposits of gypsum and anhydrite (Johnson 2008) 10
2	Gypsum-karst located at abandoned Upper Mangum Dam filled with soil (Johnson 2008)..... 11
3	Gypsum-karst located at abandoned Upper Mangum Dam (Johnson 2008)..... 11
4	Photo of apparatus (Lei et al. 2002) 12
5	Sketch of apparatus (Lei et al. 2002) 13
6	Typical cross section of embankment dam (Greene et al. 2010) 14
7	Left rim sinkholes at Center Hill Dam (Brimm 2010) 18
8	Location of the two main construction projects on Center Hill Dam (Brimm 2010) 19
9	Schematic drawing of foundation void erosion test cell 21
10	Photo of foundation void test cell 22
11	Sensor number and location..... 24
12	Teton Shell before saturation 30
13	Teton Shell after saturation 31
14	Teton Shell immediately following the start of flow 32
15	Teton Shell immediately following the start of flow 33
16	Teton Shell at end of test..... 34
17	Teton Shell at end of test..... 35
18	Eroded soil in lower reservoir 35
19	Natural soil filter around open void..... 36

20	Flow vs. Time of Teton Shell test	37
21	Pressure vs. Time of Teton Shell test.....	38
22	East Branch Core before initial saturation.....	40
23	East Branch Core before initial saturation.....	41
24	Horizontal Erosion.....	43
25	Initial upward erosion	44
26	Increased void size and stoping rate	44
27	Opening of void and drastic increase in stoping rate.....	45
28	Drastic stoping and failure	46
29	Pressure vs. Time of sensor #2	47
30	Pressure vs. Time of sensor #3	47
31	Low permeable zone.....	51
32	Calculated gradients between piezometers 1, 2, and 3 and the void during discharge of cycle 19.....	52
33	Calculated gradients between piezometers 1, 2, and 3 and the void during discharge of cycle 25.....	52
34	Total head that each sensor reached during charging of the East Branch soil	54
35	E. B. Cycle 10 Slide 6.0 analysis showing discharge total head drops around the void.....	55
36	E. B. Cycle 20 Slide 6.0 analysis showing discharge total head drops around the void.....	56
37	Changes in stress in the soils around the void a) during discharge, and b) during charging.	59
38	Test after 8 days.....	62
39	Test after 9 days.....	62

40 Test after 10 days..... 63

41 Test after 11 days..... 63

42 Complete failure of sample..... 64

43 Total head that each sensor reached during charging of the Sand-Kaolinite soil 65

44 Sand-Kaolinite Cycle 4 Slide 6.0 analysis showing discharge total head drops
around the void..... 66

45 Sand-Kaolinite Cycle 6 Slide 6.0 analysis showing discharge total head drops
around the void..... 67

46 Air pocket during cycle 6 of Sand-Kaolinite test..... 68

47 Day 2 Cycle 2 of Teton Core Test #1 70

48 Day 12 Cycle 13 of Teton Core Test #1 71

49 Day 14 Cycle 17 of Teton Core Test #1 (Time – 9:10 a.m.)..... 71

50 Day 14 Cycle 17 of Teton Core Test #1 (Time – 1:22 p.m.)..... 72

51 Day 14 Cycle 18 of Teton Core Test #1 (Time – 7:20 p.m.)..... 72

52 Total head that each sensor reached during charging of the Teton Core test #1
soil 73

53 Teton Dam Core test #1 Cycle 8 Slide 6.0 analysis showing discharge gradients
around the void..... 74

54 Teton Dam Core test #1 Cycle 8..... 74

55 Teton Dam Core test #1 Cycle 14 Slide 6.0 analysis showing discharge gradients
around the void..... 75

56 Teton Dam Core test #1 Cycle 14..... 75

57 Teton Dam Core test #1 Cycle 17 Slide 6.0 analysis showing discharge
gradients around the void..... 76

58 Teton Dam Core test #1 Cycle 17..... 76

59	Hydraulic fracturing of soil matrix	78
60	Teton Core test #2 end of cycle 1	80
61	Teton Core test #2 after charge and just before drainage of cycle 2.....	80
62	Teton Core test #2 one hour after start of drainage of cycle 2	81
63	Teton Core test #2 at failure 2.5 hours after start of drainage of cycle 2	81
64	Teton Core test #3 before start of test.....	83
65	Teton Core test #3 35 days after start of test (visible channels marked in red) ..	84
66	Teton Core test #3 43 days after start of test (visible channels marked in red) ..	84
66	Teton Core test #3 43 days after start of test (visible channels marked in red) ..	84
A- 1	Test 3 on East Branch Core during Cycle 1 charge	93
A- 2	Test 3 on East Branch Core during Cycle 2 charge	93
A- 3	Test 3 on East Branch Core during Cycle 3 charge	94
A- 4	Test 3 on East Branch Core during Cycle 4 charge	94
A- 5	Test 3 on East Branch Core during Cycle 5 charge	95
A- 6	Test 3 on East Branch Core during Cycle 6 charge	96
A- 7	Test 3 on East Branch Core during Cycle 7 charge	96
A- 8	Test 3 on East Branch Core during Cycle 8 charge	97
A- 9	Test 3 on East Branch Core during Cycle 9 charge	97
A- 10	Test 3 on East Branch Core during Cycle 11 charge	98
A- 11	Test 3 on East Branch Core during Cycle 14 charge	98
A- 12	Test 3 on East Branch Core during Cycle 14 charge	99
A- 13	Test 3 on East Branch Core during Cycle 15 discharge.....	99

A- 14	Test 3 on East Branch Core during Cycle 15 discharge.....	100
A- 15	Test 3 on East Branch Core during Cycle 16 discharge.....	100
A- 16	Test 3 on East Branch Core during Cycle 16 discharge.....	101
A- 17	Test 3 on East Branch Core during Cycle 18 discharge.....	101
A- 18	Test 3 on East Branch Core during Cycle 18 discharge.....	102
A- 19	Test 3 on East Branch Core during Cycle 20 discharge.....	102
A- 20	Test 3 on East Branch Core during Cycle 20 discharge.....	103
A- 21	Test 3 on East Branch Core during Cycle 24 discharge.....	103
A- 22	Test 3 on East Branch Core during Cycle 25 charge	104
A- 23	Test 3 on East Branch Core during Cycle 25 discharge.....	105
A- 24	Test 3 on East Branch Core during Cycle 27 discharge.....	106
A- 25	Test 3 on East Branch Core during Cycle 27 discharge.....	107
A- 26	Test 1 on Sand with Clay during Cycle 1 charge	108
A- 27	Test 1 on Sand with Clay during Cycle 1 discharge.....	108
A- 28	Test 1 on Sand with Clay during Cycle 1 discharge.....	109
A- 29	Test 1 on Sand with Clay during Cycle 2 charge	109
A- 30	Test 1 on Sand with Clay during Cycle 2 discharge.....	110
A- 31	Test 1 on Sand with Clay during Cycle 3 charge	110
A- 32	Test 1 on Sand with Clay during Cycle 4 charge	111
A- 33	Test 1 on Sand with Clay during Cycle 4 discharge.....	111
A- 34	Test 1 on Sand with Clay during Cycle 5 discharge.....	112
A- 35	Test 1 on Sand with Clay during Cycle 5 discharge.....	112

A- 36	Test 1 on Sand with Clay during Cycle 6 charge	113
A- 37	Test 1 on Sand with Clay during Cycle 6 discharge.....	113
A- 38	Test 1 on Sand with Clay during Cycle 8 charge	114
A- 39	Test 1 on Sand with Clay during Cycle 8 charge	115
A- 40	Test 1 on Sand with Clay during Cycle 8 charge	116
A- 41	Test 1 on Sand with Clay during Cycle 9 charge	117
A- 42	Test 1 on Sand with Clay during Cycle 9 discharge.....	118
A- 43	Test 1 on Sand with Clay during Cycle 9 discharge.....	119
A- 44	Test 1 on Sand with Clay during Cycle 9 discharge.....	120
A- 45	Test 1 on Sand with Clay during Cycle 10 charge	121
A- 46	Test 1 on Sand with Clay during Cycle 10 discharge.....	122
A- 47	Test 1 on Sand with Clay during Cycle 10 discharge.....	123
A- 48	Test 1 on Sand with Clay during Cycle 10 discharge.....	124
A- 49	Test 1 on Sand with Clay during Cycle 11 charge	125
A- 50	Test 1 on Sand with Clay during Cycle 11 discharge.....	126
A- 51	Test 1 on Sand with Clay during Cycle 11 discharge.....	127
A- 52	Test 1 on Sand with Clay during Cycle 11 discharge.....	128
A- 53	Test 1 on Teton Core during Cycle 1 charge	128
A- 54	Test 1 on Teton Core during Cycle 1 charge	129
A- 55	Test 1 on Teton Core during Cycle 1 discharge	129
A- 56	Test 1 on Teton Core during Cycle 2 charge	130
A- 57	Test 1 on Teton Core during Cycle 2 discharge	130

A- 58	Test 1 on Teton Core during Cycle 3 charge	131
A- 59	Test 1 on Teton Core during Cycle 3 discharge	131
A- 60	Test 1 on Teton Core during Cycle 4 charge	132
A- 61	Test 1 on Teton Core during Cycle 4 discharge	132
A- 62	Test 1 on Teton Core during Cycle 5 charge	133
A- 63	Test 1 on Teton Core during Cycle 5 discharge	133
A- 64	Test 1 on Teton Core during Cycle 6 charge	134
A- 65	Test 1 on Teton Core during Cycle 6 discharge	134
A- 66	Test 1 on Teton Core during Cycle 7 charge	135
A- 67	Test 1 on Teton Core during Cycle 7 discharge	135
A- 68	Test 1 on Teton Core during Cycle 8 charge	136
A- 69	Test 1 on Teton Core during Cycle 8 discharge	136
A- 70	Test 1 on Teton Core during Cycle 9 charge	137
A- 71	Test 1 on Teton Core during Cycle 9 discharge	137
A- 72	Test 1 on Teton Core during Cycle 11 charge	138
A- 73	Test 1 on Teton Core during Cycle 11 discharge	138
A- 74	Test 1 on Teton Core during Cycle 12 charge	139
A- 75	Test 1 on Teton Core during Cycle 12 discharge	139
A- 76	Test 1 on Teton Core during Cycle 13 charge	140
A- 77	Test 1 on Teton Core during Cycle 13 discharge	140
A- 78	Test 1 on Teton Core during Cycle 14 charge	141
A- 79	Test 1 on Teton Core during Cycle 14 discharge	141

A- 80	Test 1 on Teton Core during Cycle 15 charge	142
A- 81	Test 1 on Teton Core during Cycle 15 discharge	142
A- 82	Test 1 on Teton Core during Cycle 16 charge	143
A- 83	Test 1 on Teton Core during Cycle 16 discharge	143
A- 84	Test 1 on Teton Core during Cycle 17 charge	144
A- 85	Test 1 on Teton Core during Cycle 17 discharge	144
A- 86	Test 1 on Teton Core during Cycle 17 discharge	145
A- 87	Test 1 on Teton Core during Cycle 17 discharge	145
A- 88	Test 1 on Teton Core during Cycle 18 charge	146
A- 89	Test 1 on Teton Core during Cycle 18 discharge	147
A- 90	Test 1 on Teton Core during Cycle 18 discharge	148
A- 91	Test 2 on Teton Core during Cycle 1 charge	149
A- 92	Test 2 on Teton Core during Cycle 1 charge	150
A- 93	Test 2 on Teton Core during Cycle 1 discharge	151
A- 94	Test 2 on Teton Core during Cycle 2 charge	152
A- 95	Test 2 on Teton Core during Cycle 2 charge	153
A- 96	Test 2 on Teton Core during Cycle 2 discharge	154
A- 97	Test 2 on Teton Core during Cycle 2 discharge	155
A- 98	Test 2 on Teton Core during Cycle 2 discharge	155
A- 99	Test 2 on Teton Core during Cycle 2 discharge	156
A- 100	Test 3 on Teton Core with constant downward gradient.....	156
A- 101	Test 3 on Teton Core with constant downward gradient.....	157

A- 102	Test 3 on Teton Core with constant downward gradient.....	157
A- 103	Test 3 on Teton Core with constant downward gradient.....	158
A- 104	Test 3 on Teton Core with constant downward gradient.....	159
A- 105	Test 3 on Teton Core with constant downward gradient.....	160
A- 106	Test 3 on Teton Core with constant downward gradient.....	161
A- 107	Test 3 on Teton Core with constant downward gradient.....	161
A- 108	Test 3 on Teton Core with constant downward gradient.....	162
A- 109	Test 3 on Teton Core with constant downward gradient.....	162
A- 110	Test 3 on Teton Core with constant downward gradient.....	163
A- 111	Test 3 on Teton Core with constant downward gradient.....	164
A- 112	Test 3 on Teton Core with constant downward gradient.....	165

Chapter 1

INTRODUCTION

Many earthen dams and levees have been built throughout the United States and the world for many years. Several previously unforeseen problems have occurred due to the increased hydraulic pressures and gradients that dam and levee construction imposes on open or soil-filled solution voids such as karst formations or jointed bedrock. Karst formations are formed by the dissolution of soluble bedrock such as limestone, dolomite and gypsum resulting in channels and caves. Along with jointed bedrock these different types of voids are generally what this paper is referring to when speaking of the soil-filled or open voids. It was previously thought that the major concern when constructing a dam on the karst or fractured bedrock is that the dam may not be able to hold as much water as was desired, but not much thought or concern was taken as to the need for prevention of internal erosion using filters or other methods (Schaefer 2009). The higher gradients and pressures along with the low total confining stress of the soil in the voids can lead to internal erosion, creating a negative effect on the integrity of a dam when constructed over these open or soil-filled voids. Many dams that are built on these karst formations have had serious problems due to erosion into the voids found underneath the structures. Some examples of this type of erosion occurring today are East Branch Dam in Pennsylvania, Center Hill Dam in Tennessee, and Wolf Creek Dam in Kentucky. More information on these dams can be found in the literature review portion of this paper.

Often voids in the foundation tend to be filled with soil. However, due to the higher gradients that dams and levees create along with the low total confining stress and low strength of the soil, the soil-filled voids can easily be eroded since these soils generally have never before seen this intensity of pressures and gradients previously. These now open voids provide an exit point and conduit for more soil to follow. If these voids are not protected by some form of filter or by simply grouting in the void, then erosion could potentially continue unimpeded, likely creating a very dangerous and even life threatening situation. Not only is this situation very dangerous but it could be very costly to repair. There have been instances where dams were experiencing this type erosion into open voids and millions were spent in an attempt to repair the problem only to have to return to fix the same problem several years down the road. It is important that we gain a better understanding of the effects these voids can have on different types of soil and the effect they can have on the integrity of earth filled dams and levees where these high pressures and gradients are created in such a localized area.

Research Outline

The objective of this research is to gain a better understanding of the effects that these increased hydraulic gradients and pressures have on various types of soil when they are located in areas with high amounts of soil defects such as dissolution of carbonate bedrock or fractured bedrock. By using different soil types, confining stresses, varying heads, defect sizes, and cyclic effects, we can see on a small scale what

effects these variables will have on the soil. It is important to understand how different soils will perform so that we can better predict what will happen in the field. This information can then be used to aid in the risk assessment of dams and levees. The research and laboratory modeling consisted of the following items:

1. Design and Construction of a testing apparatus where soils can be tested under a variety of stresses, hydraulic loading conditions, and defect aperture sizes to mimic what is seen in the field.
2. Collection of relevant data during testing using a variety of sensors and data loggers along with pictures and visual interpretation of the erosion.
3. Analyzing the data collected to develop conclusions in regards to the mechanisms of erosion and how the different variables affect the erodibility of the soils tested.

Chapter 2

REVIEW OF RELATED LITERATURE

2.1 Introduction

Little laboratory testing has been performed directly in regard to internal erosion of soil when in contact with open voids such as those often found in solutioned limestone or cracked bedrock. As such, much of this literature review deals with topics that are related to the mechanisms associated with this phenomenon. The following are related topics and the limited testing that has been done in regards to this type of erosion:

- Sinkholes
- Internal erosion
- Karst problems
- Open Void Test Cells (previous laboratory work)
- Case histories

2.2 Sinkholes

Tharp (1999)

This paper discusses the various mechanisms that lead to failure of a soil void located over a cavern which over time can create a sinkhole. Failures can occur due to mechanisms with the soil either in compression or tension. Soil located above a bedrock void can and most likely will erode over time creating the void in the soil

discussed in the paper. Soil located along the wall of this void has the potential to shear due to the tangential stresses that exist, but the soil also has the tendency to soften along the wall of the void and slough off prior to shearing so signs of shearing are generally not going to be present.

When trying to understand sinkhole occurrence, one very important factor to consider is the role that pore water pressure has, especially the transient pore pressure, since the steady state pore pressure gradients generally do not play a large role in the sloughing and failure of the void wall. The three main scenarios that are discussed where transient pore pressures would lead to sloughing of the void wall are:

1. Rapid drawdown of the water table,
2. High pore pressure gradient across the wetting front, and
3. Transport and exsolution of air in partially saturated soil.

The two main factors affecting the formation of sinkholes during rapid drawdown of the water table are the loss of buoyant forces and the development of high pore pressure gradients. Oftentimes these high pore pressure gradients will cause sloughing, making the void propagate upwards very quickly. If the drawdown of the water table were to happen slowly, we would not see the development of the high pore pressure gradients, leaving the loss of buoyant forces as the primary factor for sloughing.

The next scenario regarding the high pore pressure gradient across the wetting front is important when the permeability contrast is high, creating a very large head drop across the wetting front. This is due to the lower hydraulic conductivity of

unsaturated soil. This is similar to the rapid drawdown which creates high pore pressure gradients across the void walls leading to sloughing.

The last scenario happens over time and does not appear to have as big of an effect as the other two. As water travels from the surface down through the soil the pore pressures increase compresses what air that is present in the soil into solution. The pore pressure in the void is generally less than the pore pressure in the soil; therefore, as the water nears the void the dissolved air will exsolve, expanding in the soil structure and disrupt the soil along the walls of the void.

Waltham, Bell, & Culshaw (2005)

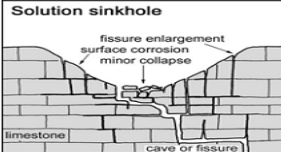
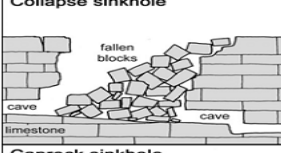
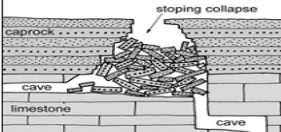

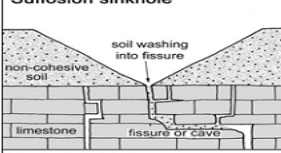
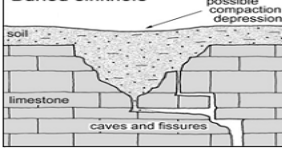
This book discusses different types of sinkholes and how they relate to karst topography. Dolines, crown holes, and karstic depressions are all categorized as sinkholes throughout the book. In general there are three main types of sinkholes which are broken into six subcategories as follows: solution sinkholes; cover-collapse sinkholes subcategorized as collapse, caprock, and dropout sinkholes; and cover-subsidence sinkholes subcategorized as suffusion and buried sinkholes.

Table 1 displays these six subcategories and gives a detailed description of each.

The book also details the affects that engineering works have on inducing sinkholes. The two main factors that induce subsidence sinkholes are water table decline and increase in imposed drainage. Water table decline is not relevant if the water table is already below the rock/soil interface, although this can change due to rainwater or irrigation raising the location of the water table above this interface. When

the water table declines again, a rapid drawdown can occur, greatly increasing the sinkhole development. The construction of dams and reservoir impoundments greatly increase the drainage at a specific location. These increased seepage or through-flows of water can scour the already existing voids, enlarging them. The enlargement in turn will increase the velocity through these voids, leading to further internal erosion and possibly end in an occurrence of a suffosion or a dropout sinkhole. This scouring is especially important in regards to a carbonate rock since you will have both scour and dissolution of the rock.

Table 1. Six subcategories of sinkholes with cross section and information (Waltham et al. 2005)

	<p><i>Formation process</i> <i>Host rock types</i> <i>Formation speed</i> <i>Typical max size</i> <i>Engineering hazard</i> <i>Other names in use</i></p>	<p>Dissolutional lowering of surface Limestone, dolomite, gypsum, salt Stable landforms evolving over >20,000 years Up to 1,000 m across and 100 m deep Fissure and cave drains must exist beneath floor Dissolution s/h, cockpit, doline</p>
	<p><i>Formation process</i> <i>Host rock types</i> <i>Formation speed</i> <i>Typical max size</i> <i>Engineering hazard</i> <i>Other names in use</i></p>	<p>Rock roof failure into underlying cave Limestone, dolomite, gypsum, basalt Extremely rare, rapid failure events, into old cave Up to 300 m across and 100 m deep Unstable breakdown floor; failure of loaded cave roof Cave collapse s/h, cenote</p>
	<p><i>Formation process</i> <i>Host rock types</i> <i>Formation speed</i> <i>Typical max size</i> <i>Engineering hazard</i> <i>Other names in use</i></p>	<p>Failure of insoluble rock into cave in soluble rock below Any rock overlying limestone, dolomite, gypsum Rare failure events, evolve over >10,000 years Up to 300 m across and 100 m deep Unstable breakdown floor Subjacent collapse s/h, interstratal karst</p>
	<p><i>Formation process</i> <i>Host rock types</i> <i>Formation speed</i> <i>Typical max size</i> <i>Engineering hazard</i> <i>Other names in use</i></p>	<p>Soil collapse into soil void formed over bedrock fissure Cohesive soil overlying limestone, dolomite, gypsum In minutes, into soil void evolved over months or years Up to 50 m across and 10 m deep The main threat of instant failure in soil-covered karst Subsidence s/h, cover collapse s/h, alluvial s/h</p>
	<p><i>Formation process</i> <i>Host rock types</i> <i>Formation speed</i> <i>Typical max size</i> <i>Engineering hazard</i> <i>Other names in use</i></p>	<p>Down-washing of soil into fissures in bedrock Non-cohesive soil over limestone, dolomite, gypsum Subsiding over months or years Up to 50 m across and 10 m deep Slow destructive subsidence over years Subsidence s/h, cover subsidence s/h, alluvial s/h</p>
	<p><i>Formation process</i> <i>Host rock types</i> <i>Formation speed</i> <i>Typical max size</i> <i>Engineering hazard</i> <i>Other names in use</i></p>	<p>Sinkhole in rock, soil-filled after environmental change Rockhead depression in limestone, dolomite, gypsum Stable features of geology, evolved over >10,000 years Up to 300 m across and 100 m deep Local subsidence on soft fill surrounded by stable rock Filled s/h, compaction s/h, paleosinkhole</p>

As mentioned before, rapid drawdown and seepage through an open void prove to be of great concern in regards to sinkhole occurrence and is important when choosing a location for the construction of dams.

2.3 Internal Erosion

ICOLD (2012)

This report describes internal erosion as “the process by which soil particles become detached and are carried downstream by water flowing through soil or bedrock.” Internal erosion occurs when necessary hydraulic and mechanical conditions are met. The hydraulic condition is reached when the seepage velocity through an embankment is high enough to produce sufficient energy to detach and carry the soil particles downstream.

This paper addresses the following initiating mechanisms of internal erosion: concentrated leak erosion, backward erosion, contact erosion, and suffusion. One condition needed for internal erosion to occur consists of a soil that can sustain a channel that serves as an exit point for the soil particles to travel. If the crack or channel through which the soil particles are traveling were to collapse or develop an effective filter, the mechanical condition would be frustrated and further internal erosion would be impeded.

This report does not discuss at length erosion directly into an open defect, joint, or crack. It briefly mentions that erosion will continue as long as the crack or defect is large enough to allow for all the soil particles to pass through. Solutioned rock or

cracked bedrock will often provide a supported exit tunnel and, when the critical gradient condition is met, internal erosion can occur. There is no standard method for analyzing erosion into an open crack or void but Fell et al. (2008) suggest using the criteria found in Table 2 shown below.

Table 2. Continuing erosion criteria into an open defect (Fell et al. 2008)

Erosion Condition	Comparison of Soil Gradation to Joint/Defect Opening Size (JOS)
Continuing erosion (CE)	$JOS_{CE} = D_{95}$ surrounding soil

Notes: JOS_{CE} = Joint/defect opening size that would allow continuing erosion of the surrounding soil.

D_{95} should be based on the average soil grading after re-grading on 4.75mm particle size.

2.4 Karst Problems

Johnson (2008)

This article discusses the problems that gypsum rock, which is easily eroded by solutioning, has in regards to dam construction in the United States. Gypsum is highly soluble and easily forms caves, sinkholes, disappearing streams and other karst features. Gypsum is prevalent throughout the United States as shown in Figure 1. In the eastern United States much of this gypsum is found below the ground surface due to the higher amounts of precipitation dissolving the upper portions of the gypsum. In the west much of the gypsum formations can be found near the ground surface due to the much dryer conditions.

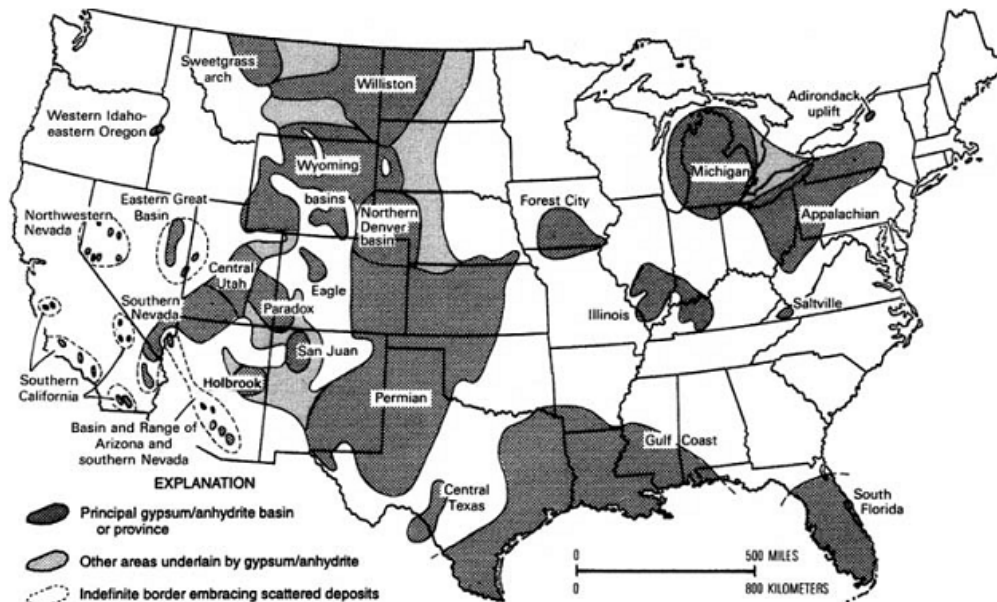


Figure 1. Deposits of gypsum and anhydrite (Johnson 2008)

When dams are constructed over these gypsum-karst areas the high hydraulic gradient that the dam creates can readily dissolve the gypsum rock as much as 1 cm/year according to some mathematical models (Dreybrodt et al. 2002). Many voids in the gypsum can be filled with clay or other types of soil and the hydraulic gradient created by dams or dikes can weaken and erode these soil filled voids making an exit point for more soil to follow (Figure 2 and Figure 3). The presence of this gypsum rock led to the abandonment of the Upper Mangum Dam site in southwest Oklahoma. Coring and pressure testing was done at the Upper Mangum Dam site and it was determined that open cavities and other karst features were too prevalent to justify the construction of a dam at this location.



Figure 2. Gypsum-karst located at abandoned Upper Mangum Dam filled with soil (Johnson 2008)

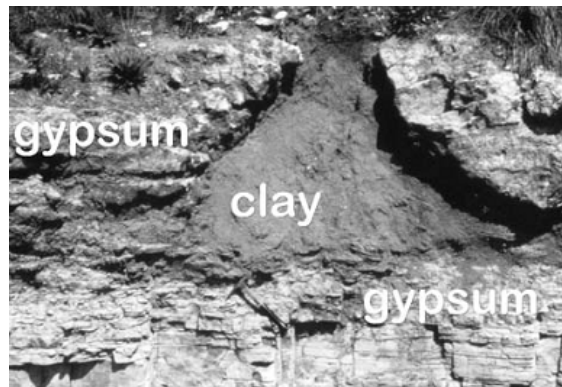


Figure 3. Gypsum-karst located at abandoned Upper Mangum Dam (Johnson 2008)

Other dams discussed in the Johnson paper that are affected by gypsum karst topography are: the failure and reconstruction of Quail Creek Dike in southwest Utah, Horsetooth Reservoir and Carter Lake Reservoir in north-central Colorado, and Anchor dam in northwest Wyoming. All of these dams or dikes are experiencing seepage through these open voids created by the dissolution of the gypsum rock. Quail Creek Dike actually failed due to the seepage through the open voids and was rebuilt at a cost of US \$12 million (Johnson 2008).

2.5 Open Void Test Cell (previous laboratory work)

Lei, Jiang, & Yu (2002)

This article discusses a large-scale model experiment conducted in China to determine the mechanisms of karst collapse. The model and experiments were not discussed in length, but rather the paper focused on the mechanisms and risk assessment of karst collapse discovered from the experiment. The experiment model itself was 3.0 m in height, and 2.0 m in both width and length. The upper portion consists of a 1.5 m-high soil zone with the lower portion consisting of pipes to simulate the openings in soluble rock. This model is presented in Figure 4 and Figure 5.



Figure 4. Photo of apparatus (Lei et al. 2002)

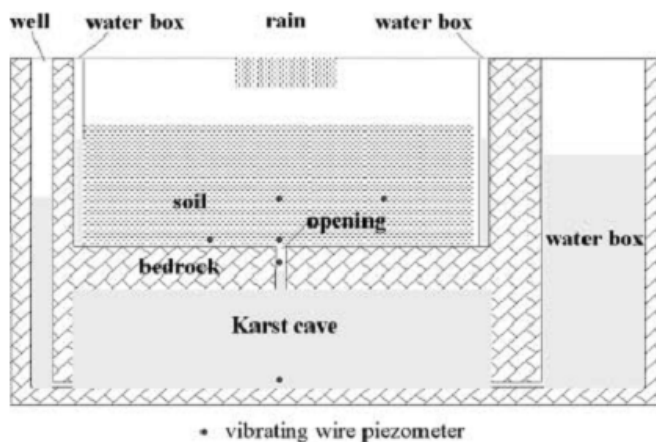


Figure 5. Sketch of apparatus (Lei et al. 2002)

It was determined that three critical conditions of sinkhole development in the surrounding provinces in China are: change in pressure in the karst opening, critical velocity in karst voids as water levels decline, and the critical drawdown in wells. The mechanism of soil failure found using the model experiment is seepage deformation or piping. As the water level in the karst void decreases, a negative pressure can develop leading to higher gradients at the void. It was determined that this pressure in the karst opening was the key parameter leading to sinkhole formation. Monitoring this pressure at key locations throughout the area of concern can help in the prediction and prevention of the destructive and sometimes deadly cover-collapse sinkholes.

2.6 Case History

Greene, Crock, Moskovitz, & Premozic (2010) - East Branch Dam:

This article is an ideal example of internal erosion occurring in association with bedrock voids at East Branch Dam in Pennsylvania. East Branch Dam is a rolled earth-filled embankment dam that is 1,725 ft. long and 184 ft. tall located along the East

Branch Clarion River in northwestern Pennsylvania. Construction of East Branch Dam was started in June of 1948 with first filling of the reservoir occurring in 1952.

Problems occurred during construction where the contractor had difficulty reaching the compaction requirements along the right abutment due to the short turning radius of the compactors and excessive lift thickness. Another issue for concern is the fact that the dam is constructed directly on top of highly fractured bedrock without any type of filter to protect it. Valley stress relief features exist along the abutments and along the valley floor and present themselves as highly fractured and open vertical joints. A typical cross section of this dam is shown in Figure 6 with the rock at the bottom being where many open cracks and joints exist. The fine-grained impervious core was placed directly against the cracked rock along the right abutment, without any surface treatment or filter, leading to erosion of the embankment soils.

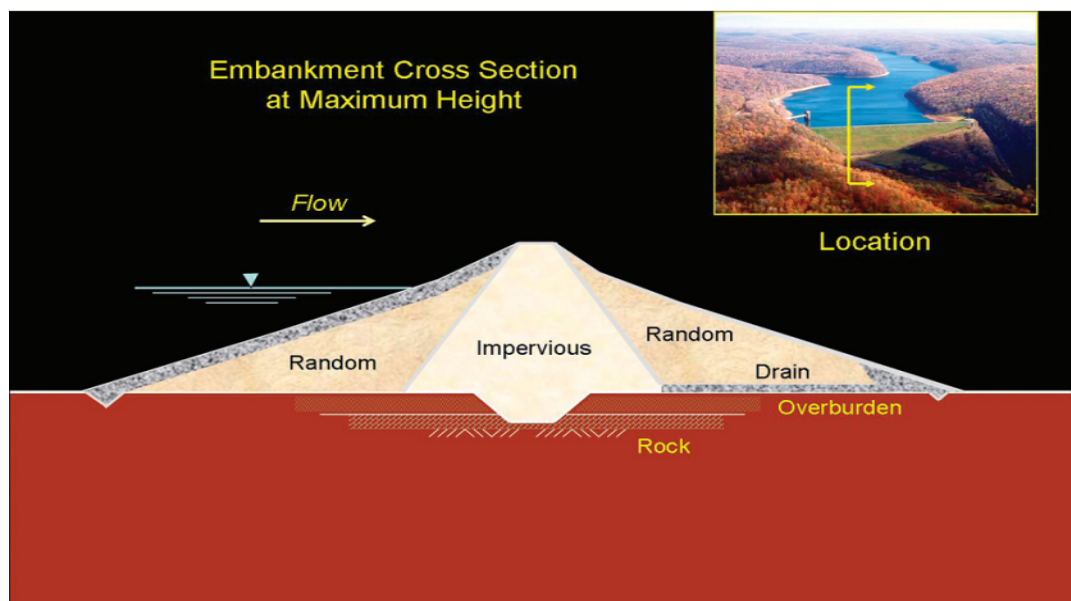


Figure 6. Typical cross section of embankment dam (Greene et al. 2010)

In 1957 this dam was observed to have muddy water flowing out of the rock toe of the dam. Soon after this observation was made holes were drilled in the embankment itself without finding any seepage or voids, but when holes were core drilled along the abutment large voids were discovered. After drilling the holes in the abutment it was noted that water could be heard flowing through the embankment which most likely would lead to void collapse within the embankment if not treated. Measures were quickly taken to rectify this problem such as the lowering of the reservoir and grouting of the voids along with compaction grouting to help compact the soil along the foundation and embankment.

Some of the dam features and design that may have led to this significant internal erosion are as follows: poor foundation treatment, geometry of the cutoff, construction practices, construction of a haul road, and presence of springs. Foundation treatment is one of the features that are looked at in this study. Samples from East Branch Dam were obtained and tests were run using the impervious core soil. When fine-grained soil is in direct contact without any type of filter with some type of void, such as the highly fractured bedrock found under East Branch, then seepage can readily erode the embankment soil.

Rice (2007) and Knight & Roman (2009) Wolf Creek Dam

Wolf Creek Dam was finished in 1952 and is a combination homogeneous earth fill embankment and concrete gravity dam. In a matter of only a few years after construction karstic voids found underneath the dam lead to internal erosion of the foundation. Signs of internal erosion were observed in 1968 presenting itself in the

form of large sinkholes and muddy water occurring downstream of the dam. A grouting program was quickly put into place in the '60s along with the installation of a seepage barrier which was built in the '70s. The grouting program was credited with saving the dam, but the seepage barrier was determined to be largely ineffective. Since that time more seepage problems have occurred, which are possibly caused by:

1. Erosion of the soil infill in the karstic voids around the boundaries of the seepage barrier.
2. Further solutioning of the limestone and carbonate rocks.
3. Erosion of the soil into and through these solution voids.

The higher gradients that exist at Wolf Creek Dam have created new or opened existing pathways in the karst formations. These now open voids provide an exit allowing for piping and further progression of internal erosion. These soil defects can cause serious problems which can be very dangerous to any people living downstream of any such dam and can also be very costly to repair. Another, more complete seepage barrier is currently being built at Wolf Creek to repair the seepage problems it is again facing at a cost estimated at \$584 million. It is important that we gain a better understanding of the effects these voids can have on the integrity of earth filled dams and levees especially in cases where these high pressures and gradients are created in localized areas.

USACE (2008) Center Hill Dam

Construction on Center Hill Dam was completed in 1951 and is a combination homogeneous earth fill embankment and concrete gravity dam. It is located in

Tennessee along the Caney Fork River which is a major tributary to the Cumberland River. Center Hill Dam was built around the same time, in the same geology, and with similar design philosophy as Wolf Creek Dam, so when problems started to occur at Wolf Creek Dam in 1967 concerns that similar problems were happening at Center Hill Dam arose. Similar to Wolf Creek Dam, Center Hill Dam was constructed on a site of soluble limestone and karst topography. This is seen in the numerous caves, springs, and sinks in the surrounding area. This limestone foundation contains numerous vertical cracks due to valley stress relief and solutioning. Because of the geology at this site numerous seepage problems have occurred throughout the lifespan of Center Hill Dam.

Center Hill Dam is constructed using well-compacted clay. As the voids in the foundation are slowly cleared out due to the increased pressures created by the dam, internal erosion occurs, creating a pathway for further erosion to occur. At first these conduits could be very small but over time the soil in the void along with the limestone itself has slowly eroded causing higher flow volumes and greater flow velocities to occur, thus increasing the rate of erosion. As the piping propagates upstream it eventually gets back to the embankment itself, affecting the hydraulic and structural integrity of the dam.

Over the years several different studies and grouting programs have been completed to help mitigate the seepage problems. The first grouting program was put into place soon after first filling when seepage developed along the left abutment. A single line 3500 ft. grout curtain was put into place along the left abutment. In 1983

more grout was pumped only into the main section of the embankment despite significant seepage occurring again in the left abutment. Seepage continued to increase over the years and another grout curtain was constructed in 1993. Despite all these efforts significant seepage continues along with the appearance of cover-collapse sinkholes occurring downstream of the grout curtains (Figure 7). In 2006 the Nashville District Corps of Engineers received approval for major rehabilitation of Center Hill Dam. This rehabilitation project will consist of grouting and an installation of a concrete barrier wall to impede further seepage through the karst features (Figure 8).



Figure 7. Left rim sinkholes at Center Hill Dam (Brimm 2010)

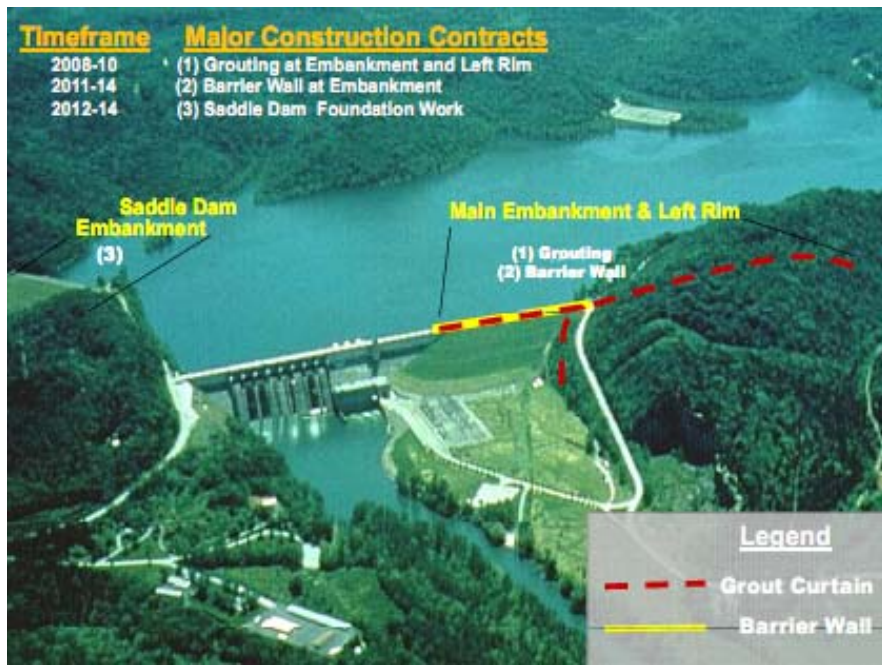


Figure 8. Location of the two main construction projects on Center Hill Dam (Brimm 2010)

Chapter 3

FOUNDATION VOID EROSION TEST CELL

3.1 Testing Apparatus

A foundation void erosion test cell was designed and constructed at Utah State University for the purpose of modeling seepage erosion through an open foundation void such as a bedrock joint or solutioned rock. The apparatus consisted of two main cells: an upper 4-ft. (1.22 m) wide, 4-ft. (1.22 m) tall, 6-in. (0.15 m) deep cell and a lower 4-ft. (1.22 m) wide, 2-ft. (0.61 m) tall, and 6-in. (.15 m) deep cell. The entire upper and lower sections were sealed using 1.5-in. (38.1 mm) thick sheets of Plexiglas, allowing for viewing of soil sample during erosion. The testing apparatus framing was constructed of 0.5-in. (12.7 mm) steel plates supported with 0.25-in. (6.35 mm) steel angles. Rectangular tube steel (2in. x 2in. x ¼in.) was used to reinforce the face of the apparatus and to reduce Plexiglas deflection due to water pressure. The steel components were all welded together, with the exception of the lid and rectangular tube steel braces, forming the frame of the structure. Holes were drilled into the steel frame allowing the ½ in. thick steel lid, Plexiglas, and rectangular braces to bolt onto the frame making it more easily accessible during teardown. A schematic of the apparatus can be seen in Figure 9 and a photo of the testing apparatus is shown in Figure 10.

The foundation void test cell has an adjustable gap connecting the upper cell with the lower cell. The crack aperture ranges from as small as 0.02 in. (0.5mm) up to 15 in. (381 mm). The gap is adjusted by loosening two bolts found underneath each of

the adjustable plates. The space in the larger upper cell was used for compaction of the different soils, placing them adjacent to the gap. The lower cell was left empty representing an open cavity. The gap between the two cells provided an exit point for soil to erode from the upper cell to the lower cell.

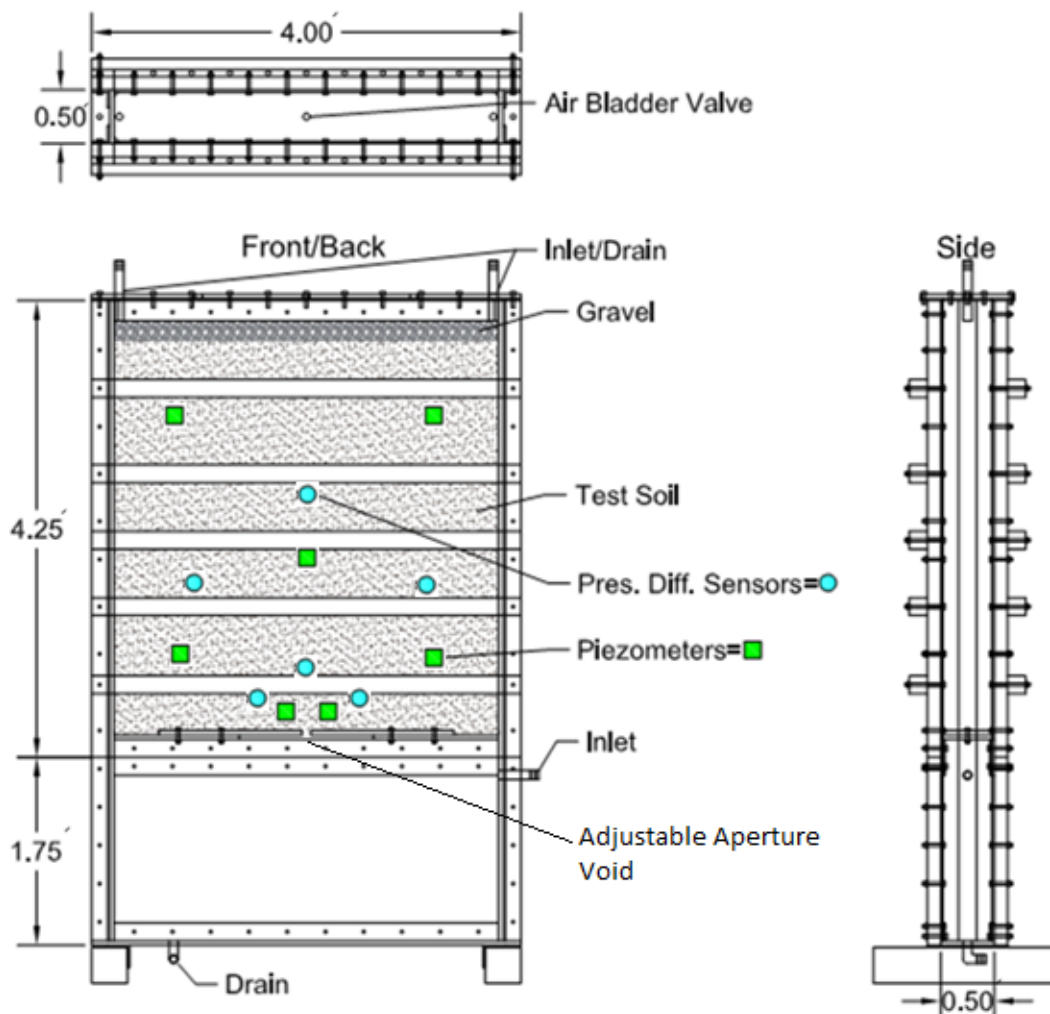


Figure 9. Schematic drawing of foundation void erosion test cell

Plumbing for the foundation void erosion test cell was connected to both the upper and lower cells allowing for seepage to occur either in the upward or downward directions. Both directions of flow were necessary in order to simulate different

scenarios of seepage erosion such as water table fluctuations due to rainfall or dewatering and downward seepage which can occur due to reservoir seepage. Two tests, the Teton shell material test and Test #3 on the Teton core material, were conducted where the only seepage flow allowed came in from the top of the apparatus flowing downward, while all the remaining tests were run with flow going in both directions. By doing this we were able to simulate seepage erosion under different scenarios, such as those described previously, that exist in the field.



Figure 10. Photo of foundation void test cell

A variety of instrumentation was used to help simulate the different scenarios described above. To keep the inlet pressure from rising too high, a Type B Cash Valve pressure regulator with a range of 2 to 20 psi was used. An air bladder was placed on top of the soil sample to simulate various overburden pressures on the soil. Below the air bladder is a 6+ in. (152.4 mm) thick gravel layer containing a perforated pipe which was connected to the two inlets in the upper cell. The perforated pipe helped to prevent the incoming water from jetting into the soil by dispersing it more evenly over the sample area. Differential pressure transducers, piezometers, a flow meter, and a data logger were also used during testing and are described in more detail in the proceeding section.

3.2 Data Collection

Data was collected during each test using several different types of sensors and equipment described hereafter in more detail. Six Validyne DP15 variable reluctance differential pressure transducers were used to measure the difference in pressure between the location of the sensor in Figure 11 and the lower reservoir. Six Honeywell 24PC Series piezometers were used for the Teton Dam shell and East Branch Dam core tests. Piezometer 7 and 8 were later added for the Teton Dam core and the sand-kaolinite tests. Flow through the sample is measured using an Octave flow meter.

Data was collected and stored using a Campbell Scientific CR1000 data logger. The data from each of the different sensors and flow meter were gathered and stored every 3 minutes of each test. Figure 9 and Figure 11 show the location and number

assigned to each of the different pressure sensors. The front and back of the apparatus was constructed of clear Plexiglas as shown in Figure 10. This allowed for visual observation and tracking of erosion and settlement that occurred during testing. Strings and/or spaghetti noodles were also placed in the soil against the Plexiglas during compaction at about 6 in. (152.4 mm) intervals as markers within the soil to track the deflection in the soil during testing.

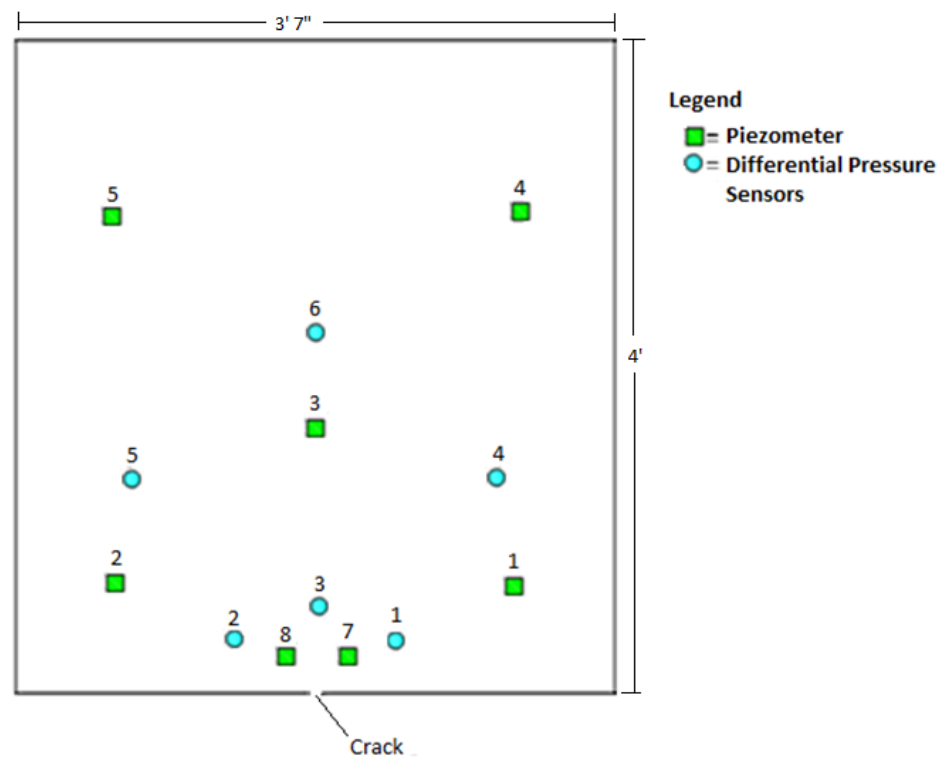


Figure 11. Sensor number and location

3.3 Procedure Setup

The various soils that were used in this experiment were tested for maximum density and optimum moisture content (ASTM D1557-12) and Atterberg limits (ASTM D4318-10). The soil properties obtained are summarized in Table 3. Using this

information we were able to control the level of compaction in the soils obtain compaction levels greater than 90% relative compaction according to ASTM D1557-12 (Modified Proctor test).

In preparation for testing, the soil was dried and placed into a ball mill for approximately 30 min. After the soil was broken down, water was added until the optimum water content was achieved. The soil was then carefully placed into the upper cell of the foundation void testing apparatus in 3/4 in. (19.1 mm) lifts and compacting using a 5 lb. hammer dropped approximately 24 in. (610 mm) 90 times per lift section. Successive lifts were used to fill the box to a depth of 3 ft. (.91 m) using a compaction energy of about 57600 lb-ft/ft³ per lift (compared to the 56000 lb-ft/ft³ per lift of energy used in the modified proctor test). This value was achieved using Equation 3.1:

$$E = (B*L*W*H)/V \quad (3.1)$$

where E is the compaction energy, B is the blows/lift, L is the number of lifts, W is weight of the hammer, H is the height of the drops, and V is the volume of the box.

Once the soil layer was compacted, a gravel layer was added to fill the testing apparatus up to the top. The gravel was added to allow for the placement of a perforated pipe which allowed for water entering the top of the cell to disperse evenly over the soil sample, preventing jetting of the soil from occurring. The air bladder was then placed on top of the gravel and the top of the cell was then sealed using a 0.5-in. (1.27 mm) thick steel lid which was bolted down making the apparatus water tight.

Once this was accomplished the plumbing was then connected making the test ready to begin.

Table 3. Soil properties

Soil	Soil Description	Dry Unit Weight (pcf)	Optimum Water Content (%)	PL	LL	PI
Teton Dam Shell of Embankment	Sandy-Gravel (GM)	135**	5.3	NA	NA	NA
East Branch Dam Core of Embankment	Silty-Clay (CL-ML)	133**	9.5	18	22	4
Quartz Sand-Kaolinite Sample	Sandy-Clay (SC)	126**	14	NA	NA	NA
Teton Dam Core of Embankment	Clayey-Silt (ML)	121**	14	-	26	4

**95% of maximum density as determined by ASTM D1557-12

Depending on the test the soil would then be saturated in two steps. The first step is saturating the soil with carbon dioxide (CO₂), displacing the oxygen. This is done because CO₂ more readily dissolves in water than oxygen making saturation of the sample easier. By placing a vacuum at the top and slowly adding water through the bottom the sample over time becomes nearly saturated. The carbon dioxide and saturation process was only used on the Teton Dam shell seepage test since full saturation was within the scope of that particular seepage test. Because the other tests were intermittently filled and then drained, CO₂ would only help during the first filling of the test and not for the subsequent cycles, therefore it was not used.

After the sample was saturated the pressure regulator was set at the desired inflow pressure and flow was initiated either from bottom to top or vice versa,

depending on the desired hydraulic loading conditions for the particular test. If flow was from top to bottom, the sample would be left running until significant erosion had occurred. If flow was from bottom up, cycles of loading were performed on the sample. This was done by again setting the pressure regulator to the desired pressure and allowing the water to charge the sample from the bottom. The pore pressures in the soil increased over time as the gradient continued to move through the soil until a state of equilibrium is reached, where the pore pressures in the soil stop increasing and level off. Once the sensor readings within the soil sample reached equilibrium, the flow was shut off and the sample was allowed to drain. Again the sensor readings were allowed to reach equilibrium and the drain was closed and flow was initiated again from the bottom. This was repeated until significant erosion had occurred.

Chapter 4

ANALYSIS OF RESULTS

The purpose for each laboratory test performed was to look at the localized effects of soil migration due to an open void defect. The soils tested were: 1) the Teton Dam shell of embankment, 2) East Branch Dam core of embankment, 3) a mix of 65 percent by weight medium-coarse quartz sand with 35 percent by weight kaolinite clay, and 4) Teton Dam core of embankment. Piezometric pressures were applied to the soil to create a gradient across the system while piezometers and differential pressure sensors at different locations in the soil sample measured the head and pressure changes during testing. The piezometric pressure was used to mimic 1) seepage flow created by steady reservoir loading and 2) cyclic events caused by lowering or rising of groundwater levels generally caused by change in seasons, precipitation, and reservoir loading.

Six different tests were completed as summarized in Table 4. Teton Dam shell of embankment test was performed using a constant downward gradient thereby mimicking the flow through an embankment into a void. East Branch Dam core of embankment test was performed with cyclic loading using a water pressure charge and discharge cycle acting from the lower cell thus mimicking the fluctuations in the bedrock voids due either to reservoir fluctuations or other groundwater recharge. Sand with clay test, Teton Dam core of embankment test #1, and Teton Dam core of embankment test #2 were performed using similar cyclic loading conditions as East Branch Dam core of embankment test. Teton Dam core of embankment test #3 was performed using

similar constant downward flow loading conditions as Teton Dam shell of embankment test. Discussions of each of the tests and test results are presented in the following sections.

Table 4. Summary of tests

Soil Tested	Loading Conditions	# of Days Tested	Size of Gap (in.)
Teton Dam Shell of Embankment	Constant Downward Gradient	23	2
East Branch Dam Core of Embankment	Charge and Discharge Cycles	25	1
Sand with Clay	Charge and Discharge Cycles	11	1
Teton Dam Core of Embankment Test #1	Charge and Discharge Cycles	14	1
Teton Dam Core of Embankment Test #2	Charge and Discharge Cycles	2	2
Teton Dam Core of Embankment Test #3	Constant Downward Gradient	48	1

4.1 Teton Dam Shell of Embankment Soil

The first soil that was tested was the Teton Dam shell of embankment. This test was performed by applying water pressure to the top of the cell to create a constant downward gradient toward the void at the base of the sample. The gradient was shut off twice during the test to allow the soil to “relax”. A water pressure of 7 to 10 psi was applied to the top of the sample allowing seepage to flow from the top of the soil down through the soil and out a 2 in. (50.8 mm) gap at the base of the soil cell. This test was designed to mimic flow through the embankment in the void.

In preparation for this test, the soil was ball milled and passed through a 2 in. (50.8 mm) sieve since the larger cobbles and boulder would not easily fit into the soil sample section of the apparatus. Once the soil was ready, it was mixed with water to optimum water content for compaction of 5 percent by weight. The soil was then compacted to a dry unit weight of 122.5 pcf (1962 kg/m³) (91 percent relative compaction according to ASTM D1557-12). After placement of the soil, the gravel, perforated pipe, air bladder, and lid were then installed. The bladder above the soil was pressurized with air to 21.5 psi to create an overburden in the soil. To help the soil reach a high level of saturation, the sample was flushed with CO₂. Figure 12 shows the soil right before initiating the saturation.



Figure 12. Teton Shell before saturation

De-aired water was slowly added through the bottom reservoir at a pressure of 2 psi while a vacuum was applied to the highest point of the apparatus. Figure 13 shows the sample after soil saturation. Once the sample was saturated, flow to the top of the apparatus was turned on and the drain at the bottom was opened, allowing a downward seepage through the sample.



Figure 13. Teton Shell after saturation

This being our first soil to be tested in this apparatus there was some learning to be had. During the initiation of the test we discovered that we had problems with our pressure regulator. The regulator was set at 11 psi, but when the test was turned on the pressure shot up to as high as 50 psi. Because of such a high pressure there was a significant deflection occurring in the Plexiglas. Due to the deflection in the Plexiglas, the soil settled significantly immediately after the initiation of flow, as shown in Figure 14 and Figure 15.



Figure 14. Teton Shell immediately following the start of flow



Figure 15. Teton Shell immediately following the start of flow

After this initial movement the soil settled and no further movement due to deflection occurred, so it was decided to allow the test to proceed. After the necessary adjustments were made to the regulator, the test was left to run at 7 to 13 psi creating a gradient ranging from 5 to 9 across the sample.

The Teton shell test was left running for 23 days with the water being shut off at day 11 and again at day 14. Each time the water was only shut off for about 30 minutes and then flow was turned back on. This was done each time the lower reservoir became

clear indicating that no visible erosion was occurring. Each time the water was turned back on after being shut off, large amounts of sediment were carried out through the void and erosion was allowed to continue indicating a surge of erosion. Over time the soil continued to erode and, because of the cohesionless nature of this soil, a zone of suffusion was being formed. This zone of suffusion is described as a preferential seepage pathway where the finer fraction of the soil gradation has been removed. This can be seen in Figure 16 and Figure 17. Figure 18 shows the soil eroded during the test which consists primarily of the finer fraction the sample.



Figure 16. Teton Shell at end of test



Figure 17. Teton Shell at end of test

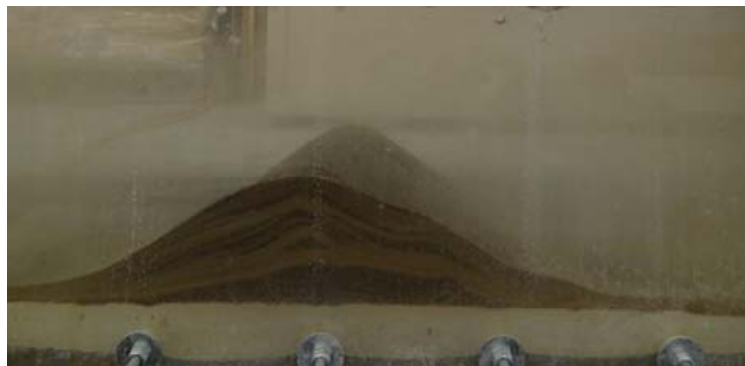


Figure 18. Eroded soil in lower reservoir

Another interesting point in this test is the fact that you can see the natural soil filter being formed around the void. The larger rocks in the gradation were large enough to form a bridge over the void which allowed the progressively smaller rocks and gravel to be caught behind it. This process continued where larger soil particles would catch smaller ones and proceeded back to the finer sand and silts. This filter can be seen in Figure 19. The filter prevented the removal of soil particles through the filter, thus preventing further erosion along that particular pathway.



Figure 19. Natural soil filter around open void

Throughout this entire test, the flow rate increased linearly with time as the void and channels continued to develop. Figure 20 shows this change in flow over time. Quick drops in the flow occurred at about 120 and 420 hours into the test and are attributed to preferential flow paths being blocked off due to collapse as the soil shifts and settles. When this movement occurs the water has to find other pathways, temporarily slowing the flow. As these soil shifts occur movements of the water pressure are seen in the soil sample. Figure 21 presents the pressure readings from Piezometers 1 through 5 over time. The increase in pressure of Piezometer 3 following the first water shutoff is an indication that a pathway between that sensor and the void was blocked due to collapse of a pathway as the soil relaxed, thus causing the water to find easier paths through the soil.

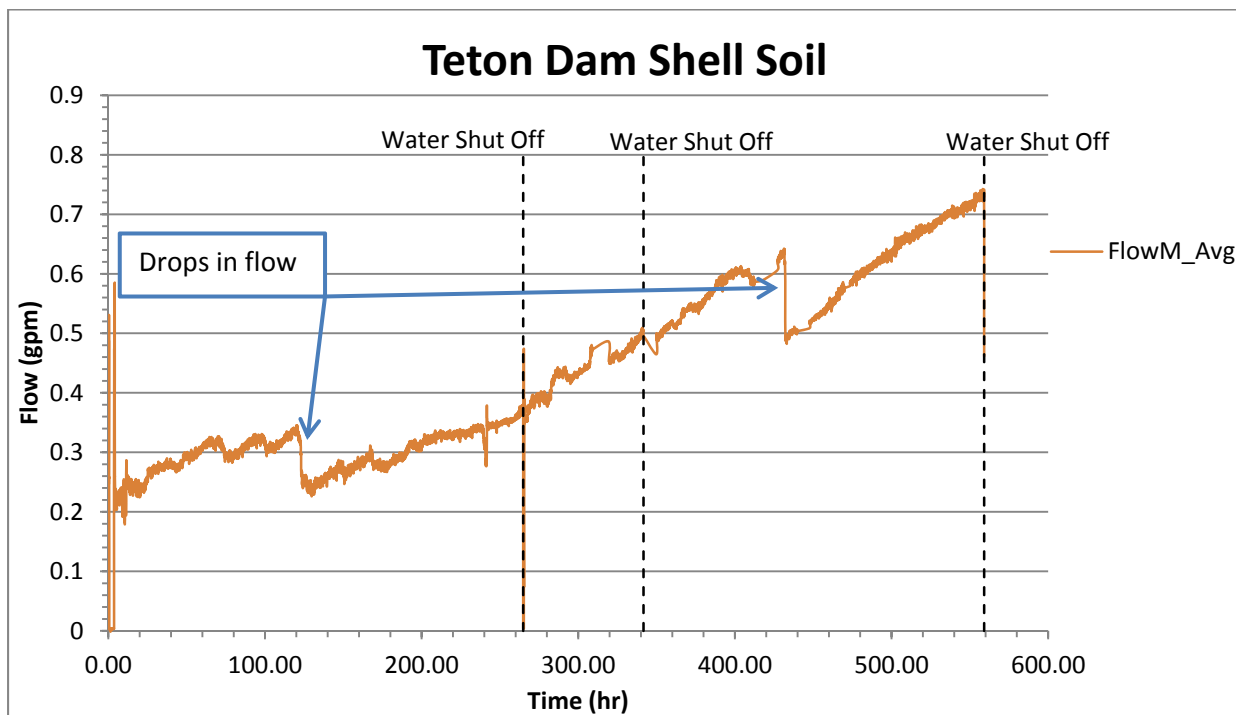


Figure 20. Flow vs. Time of Teton Shell test

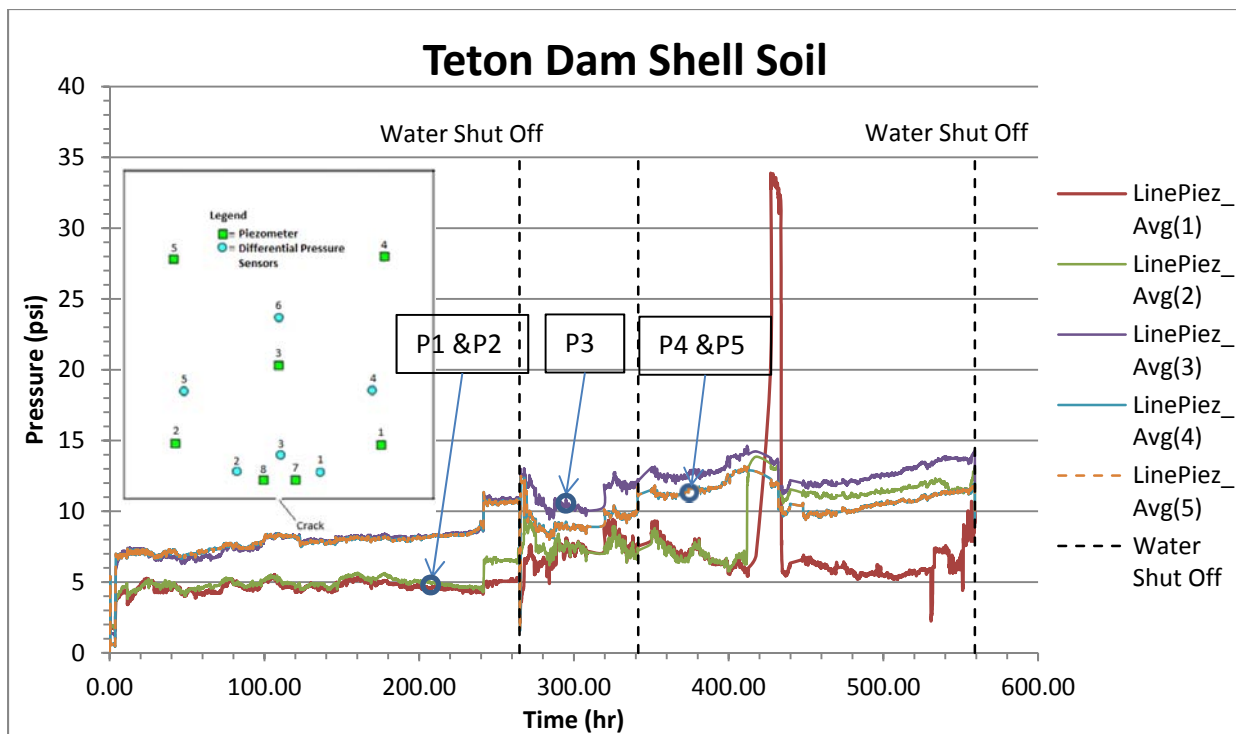


Figure 21. Pressure vs. Time of Teton Shell test

Because the flow continued to increase throughout the test, it appears that this soil would have continued to erode until either a complete soil filter is formed across all seepage pathways, preventing further erosion, or complete failure of soil occurred resulting in a sinkhole similar to the suffusion sinkhole in

Table 1. As the gradient continued to act across the sample, erosion may have continued until all the fines are washed out of the soil or a complete filter was formed around the entire gap. Fluctuations in flow have potential to disrupt filters and preferential flow paths, thus allowing erosion to continue deteriorating the soil structure. Erosion due to a constant gradient can be slow, but even after only 23 days more than 5 inches of settlement movement could be observed.

4.2 East Branch Dam Core of Embankment Soil

The next soil to be tested was the East Branch Dam core of embankment soil. This test was the first to be performed using a water pressure charge and discharge cycle acting from the bottom reservoir (through the void). Each charge and discharge cycle was maintained until an equilibrium condition was reached (i.e. pore pressure sensors all reached a steady level). This loading sequence is designed to model groundwater fluctuations in the bedrock voids due either to reservoir fluctuations or other groundwater recharge.

This soil was also ball milled and a water content of 9.5 percent by weight was added to the soil prior to compaction. The void in the apparatus was set to 1 in. (25.4 mm) and soil was compacted achieving a dry unit weight of 125 pcf (2002 kg/m³) (94 percent relative compaction according to ASTM D1557-12). As discussed earlier, the soil was not saturated prior to testing. The bladder pressure was set to 21.5 psi creating the overburden pressure on the soil.

Design modifications of the apparatus were performed to prevent overpressuring the cell and Plexiglas deflection. Steps were taken to fix the regulator making it capable of being set to a specific pressure, which for this test and the following tests the water charging pressure was 7.5 psi. Larger steel beams along with two additional steel beams were installed across the face of the Plexiglas to reduce the deflection, making any settlement due to deflection negligible in the test. Figure 22 and Figure 23 show the sample after compaction. Note that the yellow marker strings and the red

lines on the Plexiglas (indicating the original location of the marker strings) indicate no significant movement of the soil at this time.



Figure 22. East Branch Core before initial saturation



Figure 23. East Branch Core before initial saturation

To start the test, the lower reservoir was filled with water and 7.5 psi of water pressure was applied, giving the sample an upward hydraulic gradient and a differential head of about 14.1 feet between the void and the top of the sample. The valves on top of the cell were open during the entire test. This pressure was fixed in the lower

reservoir for 24 hours before being shut off. After the 24 hours of charging the water was then shut off and allowed to drain out of the lower reservoir. This fast change in flow and rapid drawdown allowed for the development of high pore pressure gradients acting across the soils surrounding the void and, coupled with the loss of buoyant forces, created a scenario where the formation of sinkholes is expected. One cycle of loading, consisted of applying the pressure in the lower reservoir, allowing the sensors to reach equilibrium, and then letting the sample drain until the sensors essentially reached equilibrium (or zero differential head). This entire test consisted of 27 cycles. Table 5 shows the schedule of each of the cycles along with the visual interpretation of what was occurring in the soil.

Table 5. Hydraulic loading cycles for East Branch Dam test

Cycle	Date and Times of Charge:				Date and Times of Discharge:				Visual Interpretation:		
1	1/28/2013	11:45am	-	1/29/2013	11:45am	1/29/2013	11:48am	-	1/29/2013	4:30pm	Horizontal erosion ↓ Formation of void Continued horizontal erosion ↓ Visible upward erosion Continued erosion ↓ Increase in void size and stoping rate Continued erosion ↓ Drastic increase in stoping rate Rapid Stopping ↓ Failure
2	1/29/2013	4:33pm	-	1/30/2013	4:30PM	1/30/2013	4:33pm	-	1/30/2013	9:03pm	
3	1/30/2013	9:06pm	-	2/1/2013	9:30am	2/1/2013	9:33am	-	2/1/2013	1:15pm	
4	2/1/2013	1:18am	-	2/2/2013	12:39pm	2/2/2013	12:42pm	-	2/3/2013	10:42pm	
5	2/3/2013	10:45pm	-	2/4/2013	1:48pm	2/4/2013	1:51pm	-	2/4/2013	5:09pm	
6	2/4/2013	5:12pm	-	2/5/2013	1:45pm	2/5/2013	1:48pm	-	2/5/2013	5:06pm	
7	2/5/2013	5:09pm	-	2/6/2013	11:24am	2/6/2013	11:27am	-	2/6/2013	3:09pm	
8	2/6/2013	3:12pm	-	2/7/2013	9:45am	2/7/2013	9:48am	-	2/7/2013	1:30pm	
9	2/7/2013	1:33pm	-	2/8/2013	9:36am	2/8/2013	9:39am	-	2/8/2013	2:15pm	
10	2/8/2013	2:18pm	-	2/9/2013	10:00am	2/9/2013	10:03am	-	2/11/2013	8:57am	
11	2/11/2013	9:00am	-	2/11/2013	12:03pm	2/11/2013	12:06pm	-	2/11/2013	5:06pm	
12	2/11/2013	5:09pm	-	2/11/2013	10:51pm	2/11/2013	10:54pm	-	2/12/2013	9:12am	
13	2/12/2013	9:15am	-	2/12/2013	12:54pm	2/12/2013	12:57pm	-	2/12/2013	5:00pm	
14	2/12/2013	5:03pm	-	2/12/2013	9:18pm	2/12/2013	9:21pm	-	2/13/2013	9:15am	
15	2/13/2013	9:18am	-	2/13/2013	12:27pm	2/13/2013	12:30pm	-	2/13/2013	5:06pm	
16	2/13/2013	5:09pm	-	2/14/2013	9:30am	2/14/2013	9:33am	-	2/14/2013	1:57pm	
17	2/14/2013	2:00pm	-	2/14/2013	9:03pm	2/14/2013	9:06pm	-	2/15/2013	9:48am	
18	2/15/2013	9:51am	-	2/15/2013	12:09pm	2/15/2013	12:12pm	-	2/15/2013	5:03pm	
19	2/15/2013	5:06pm	-	2/16/2013	7:09pm	2/16/2013	7:12pm	-	2/18/2013	9:33am	
20	2/18/2013	9:36am	-	2/18/2013	12:33pm	2/18/2013	12:36pm	-	2/18/2013	4:48pm	
21	2/18/2013	4:51pm	-	2/19/2013	9:42am	2/19/2013	9:45am	-	2/19/2013	12:03pm	
22	2/19/2013	12:06pm	-	2/19/2013	1:57pm	2/19/2013	2:00pm	-	2/19/2013	5:03pm	
23	2/19/2013	5:06pm	-	2/20/2013	9:42am	2/20/2013	9:45am	-	2/20/2013	1:12pm	
24	2/20/2013	1:15pm	-	2/20/2013	2:18pm	2/20/2013	2:21pm	-	2/20/2013	5:15pm	
25	2/20/2013	5:18pm	-	2/20/2013	9:00pm	2/20/2013	9:03pm	-	2/21/2013	10:21am	
26	2/21/2013	10:24am	-	2/21/2013	12:06pm	2/21/2013	12:09pm	-	2/21/2013	3:54pm	
27	2/21/2013	3:57pm	-	2/21/2013	5:21pm	2/21/2013	5:24pm	-	2/22/2013	9:15am	

At the end of cycle 1 and beginning of cycle 2 horizontal erosion could be seen along the bottom of the sample as seen in Figure 24. The horizontal erosion was quickly followed by a small amount of erosion above the void at the base of the sample. This erosion above the void and horizontal erosion continued until about cycle 11 when visible upward erosion directly above the void was noted. This upward erosion can be seen in Figure 25. The rate of upward erosion, or stoping, increased dramatically at cycles 20 and 21, as shown in Figure 26, reaching a height of about 8 inches and a width of about 1.5 to 2 inches. The stoping continued, and even increased in rate, at cycle 24 where the void continued to open up, reaching a width of 2 or more inches. Once the void reached about 2 inches the soil quickly failed with the stoping propagating upward in a matter of hours to more than double its height as shown in Figure 27 and Figure 28.



Figure 24. Horizontal Erosion

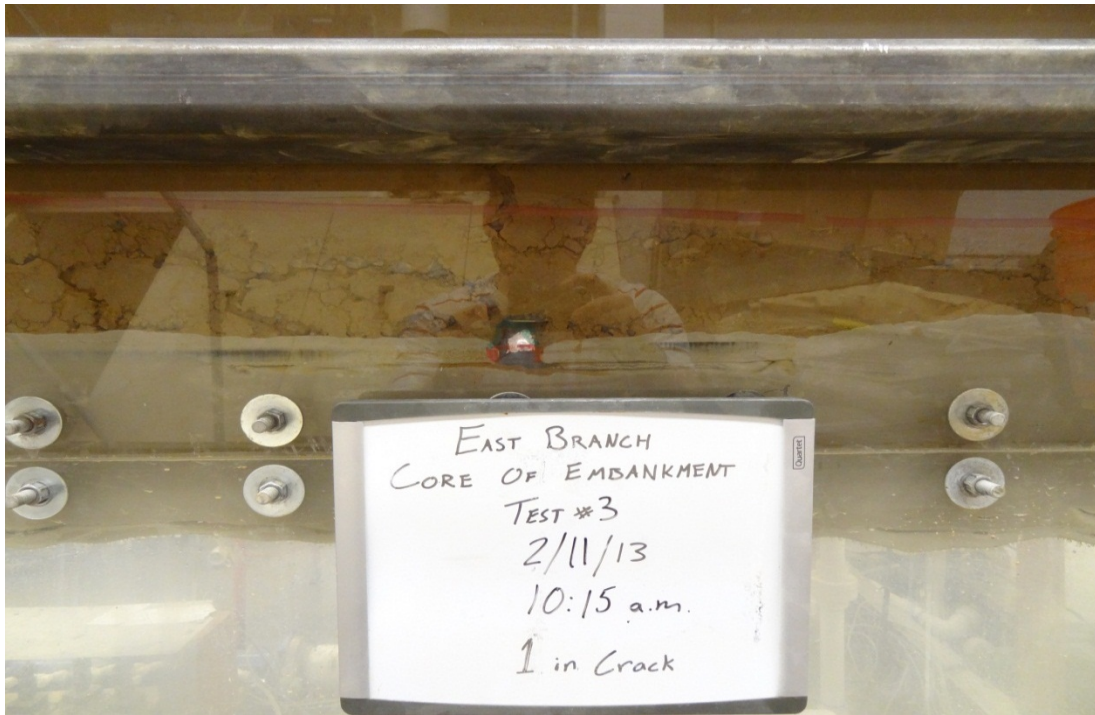


Figure 25. Initial upward erosion

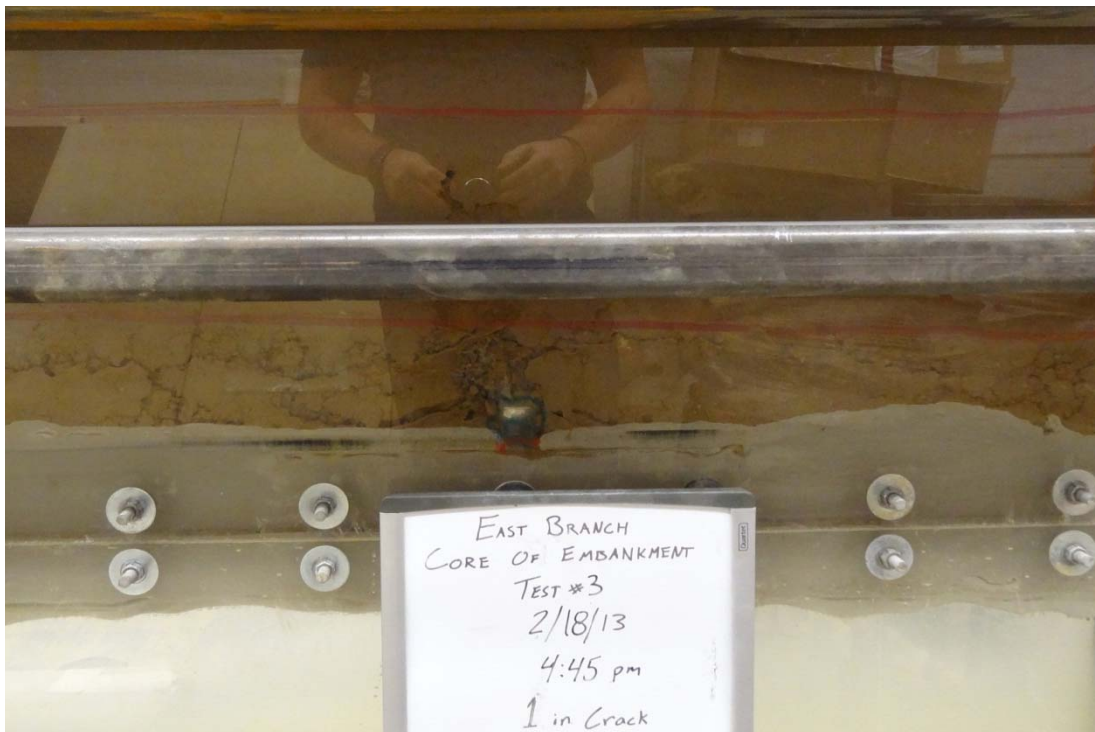


Figure 26. Increased void size and stopping rate



Figure 27. Opening of void and drastic increase in stopping rate

Figure 29 and Figure 30 present plots of the pressure versus time for piezometers 2 and 3 during different cycles of the test. As the soil continues to erode between these piezometers and the void, the pressures at which equilibrium is reached (level-off pressures) continue to rise and the time to reach equilibrium decreases with each successive cycle. These figures show the progression of the hydraulic behavior until failure of the soil occurred.



Figure 28. Drastic stoping and failure

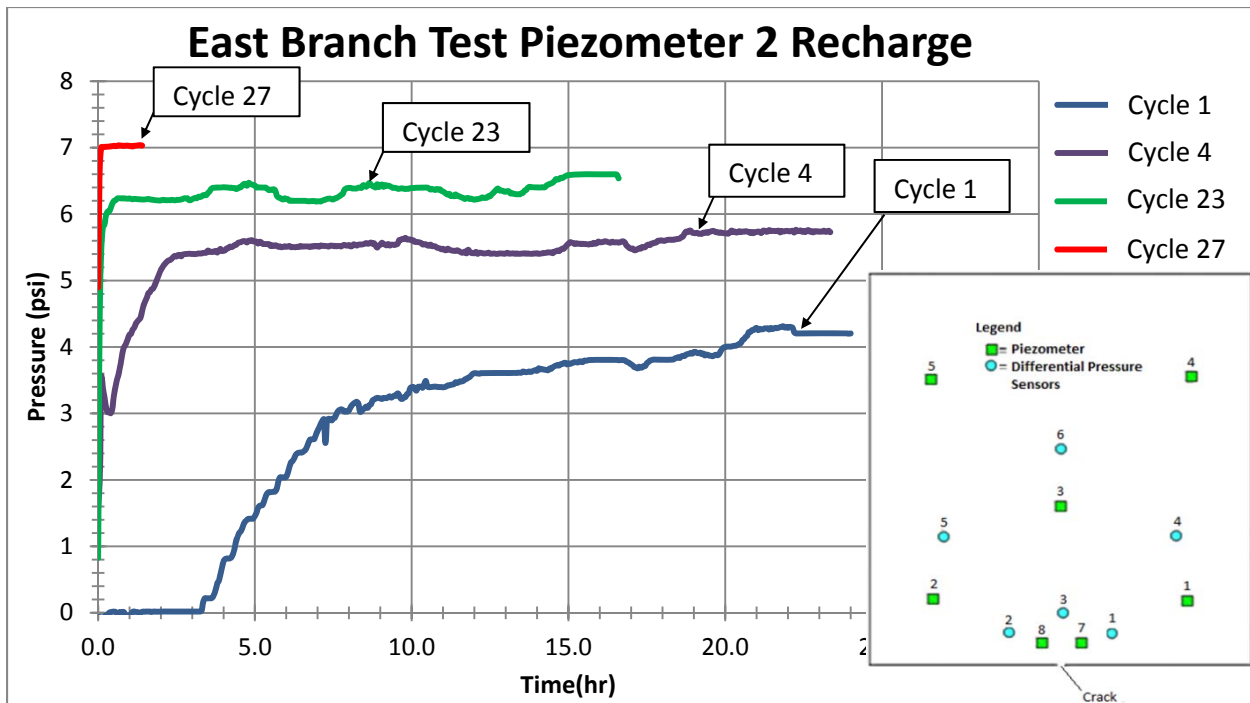


Figure 29. Pressure vs. Time of sensor #2

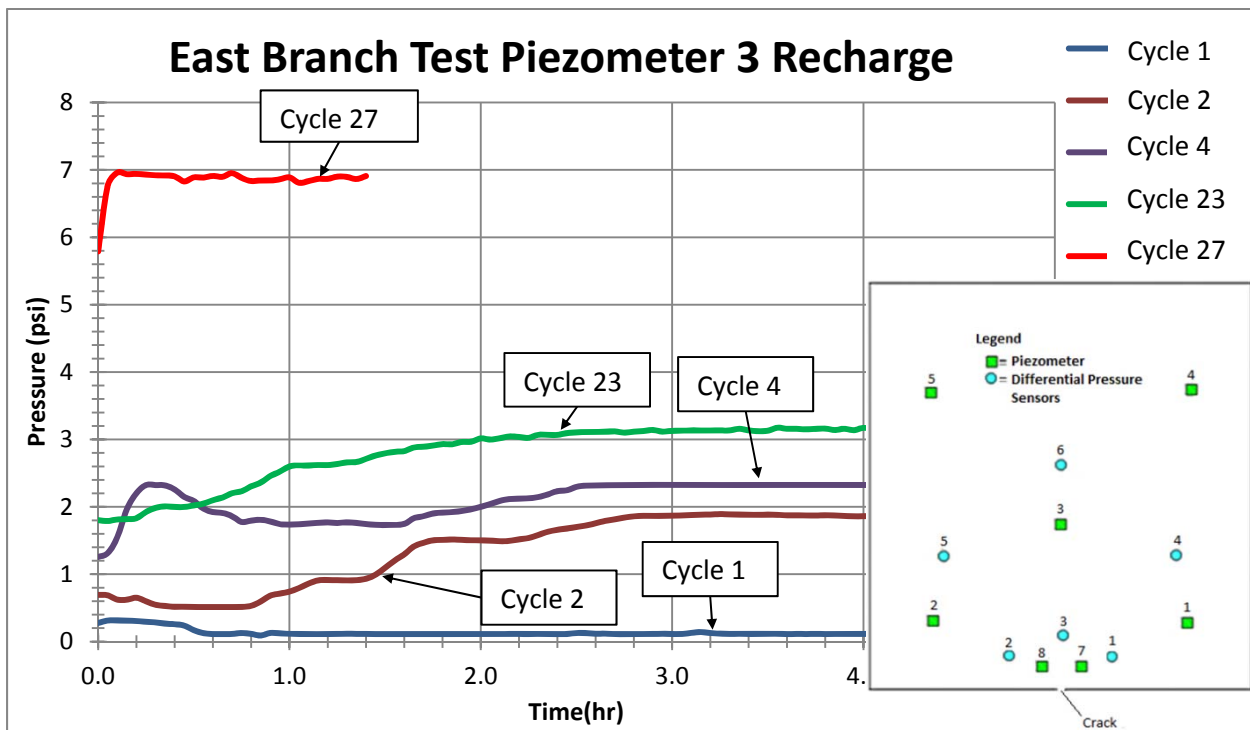


Figure 30. Pressure vs. Time of sensor #3

The data in Figure 29 and Figure 30 indicate the level-off pressure, or the pressure at which the cell reaches equilibrium with the load of each cycle, slowly increased after each cycle. From cycle 1 to 8, the data plots progressed between the traces for cycles 1 and 23 shown in Figures 26 and 27. After about 8 cycles (cycles 9-26) the pressure plots all approximately followed the Cycle 23 line (green line) with the only real change occurring at Cycle 27 where the pressure matched that of the inlet pressure, indicating the void opened up and no head loss was occurring between the lower reservoir and that particular sensor.

During this test a number of mechanisms are believed to have contributed to the internal erosion and failure of the soil structure. The sample initially started stoping early on, likely due to tensile failure in the soft soil as an arch formed over the void. Once the initial arch formed little additional erosion occurred until the later stages of the test. With the continued erosion and opening of the void, a point was reached where arching played a little part in preventing the soil from falling. Erosion was occurring during both the charge and discharge cycles with most of the erosion occurring during discharge. At each cycle, whether it was charge or discharge, erosion was observed in the form of small plate-like pieces and clouds of fine silt in the lower void. It seems that during much of the middle cycles where little movement could be seen, the soil structure was slowly being broken down and small channels were being created throughout the soil (although these channels were not observed the pore pressure data supports their existence). Since there was an unfiltered exit point, the soil particles were slowly broken off and carried away through the crack at the initiation of

each cycle. With the combination of an unfiltered exit point and the soil structure being able to support a small open channel, localized piping occurred. The channels seemed to propagate more rapidly in the horizontal direction than in the vertical direction due to the anisotropy of the soil, with a higher permeability in the horizontal direction. The void had little visible movement in the vertical direction for much of the test. Because erosion was still occurring during each cycle and the rapid progression of the void in the vertical direction, it is assumed that even though it could not be seen from the outside that channels in the vertical direction were formed.

Most of the erosion in this test took place during the discharge portion of each cycle; this is thought to be due to a number of factors. One large contribution is caused by rapid drawdown of the water. As water pressure was applied within the void, the water pressure helped to support the void. These pressures help support the soils around the void in two ways. First, they balance the water pressures within the soil so that the hydraulic gradient works outward in a direction it cannot erode the soil (soil is filtered by the adjacent soil). Upon release of the pressure, the gradients are reversed making the soil susceptible to piping erosion. Second, the water pressure acts as a confining stress for the soil, giving the soil around the perimeter of the void resistance to shearing due to the compressive ring stresses around the void. The release of these pressures leaves the soil in an unconfined state, thus susceptible to compression failure. These mechanisms are discussed in detail below. These two mechanisms likely explain why most of the erosion is occurring during the discharge portion of the cycle.

While the reversal of gradient may be sufficient to initiate piping erosion, it is believed this effect is enhanced by the effects of differential hydraulic conductivity in the soils around the void. During the loading phase of the cycles a small air bubble could not be completely removed and remained at the top of the void. Thus, while water was forced into the sides of the void air was being forced into the roof of the void, resulting in partial saturation of the soils above the void and thus lower hydraulic conductivity in this zone as shown in Figure 31. With the release of pressure in the void and the reversal of gradients, pressures above the unsaturated zone would be inhibited from dissipation by the low hydraulic conductivity zone; resulting in a prolonged time period for the high gradient to work on eroding the soil. This may explain the upward propagation of the stope observed in this test.

Evidence of the low hydraulic conductivity zone effect was observed in the pore pressure measurements. Figure 32 presents a plot of the pressures measured in Piezometers 1, 2, and 3 (located to the right, left, and above the void, respectively) during Cycle 19 of the test. It is noted that, while the pressures in the piezometers to the sides of the void (1 and 2) were initially higher than the piezometer above (3), the dissipation of the pressures to the sides of the void occurred much faster than the pressure above. This is assumed to be due to the low hydraulic conductivity zone theorized above. Figure 33 is a similar plot of the pressures during Cycle 24; during which rapid upward stoping occurred during discharge. At the start of the discharge the behavior is similar to that of Cycle 19. However, approximately 7 hours into the discharge the pressure in Piezometer 3 rapidly drops. As the stoping moved upwards

during the discharge portion of Cycle 25 the zone of low permeability between Piezometer 3 and the void eroded and collapsed into the void allowing the gradient to rapidly decrease and start behaving like the gradients between Piezometers 1 and 2 and the void. Thus, not only does the data in Figure 32 and Figure 33 support the low hydraulic conductivity theory, but it also graphically illustrates the erosive effects of the maintained high hydraulic gradient.

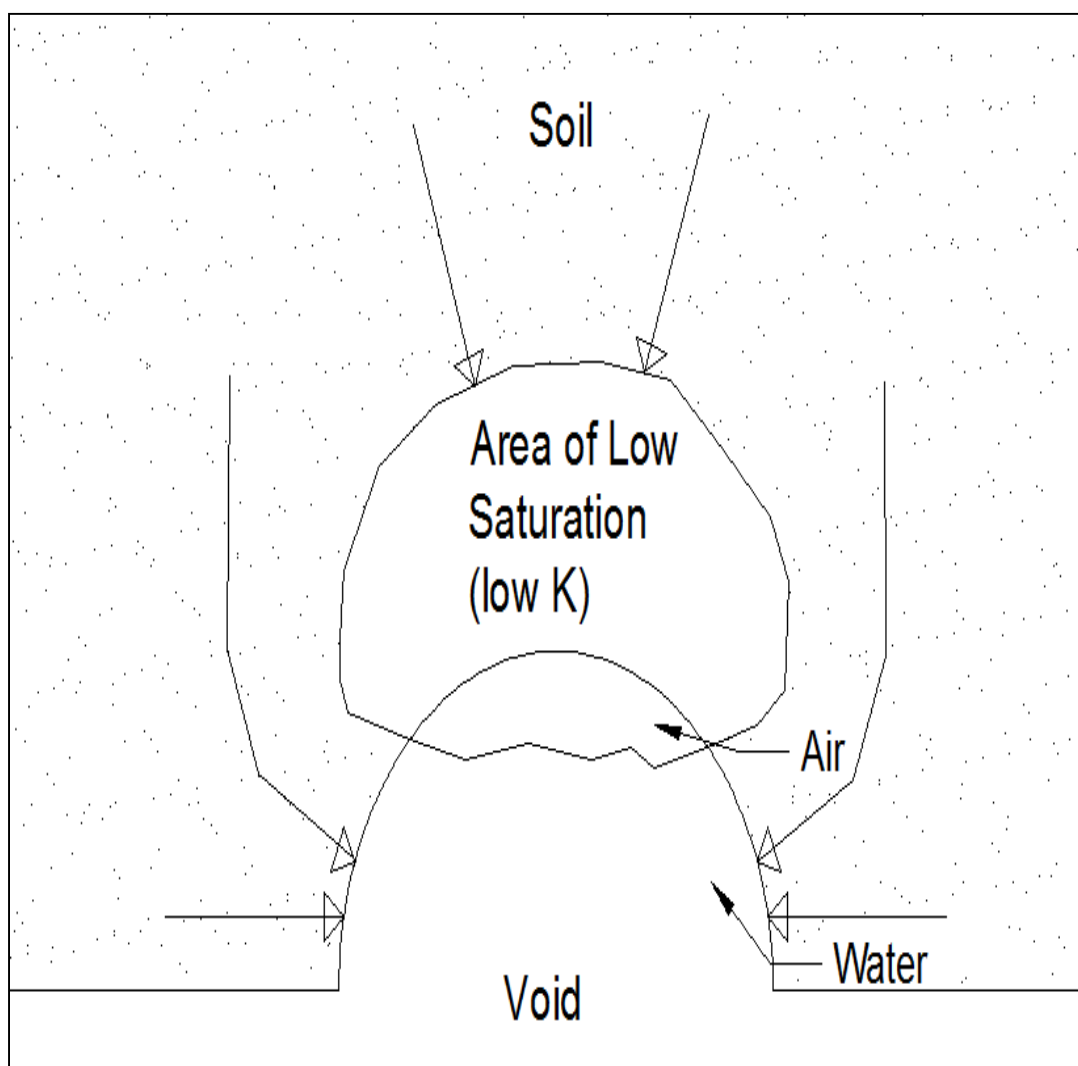


Figure 31. Low permeable zone

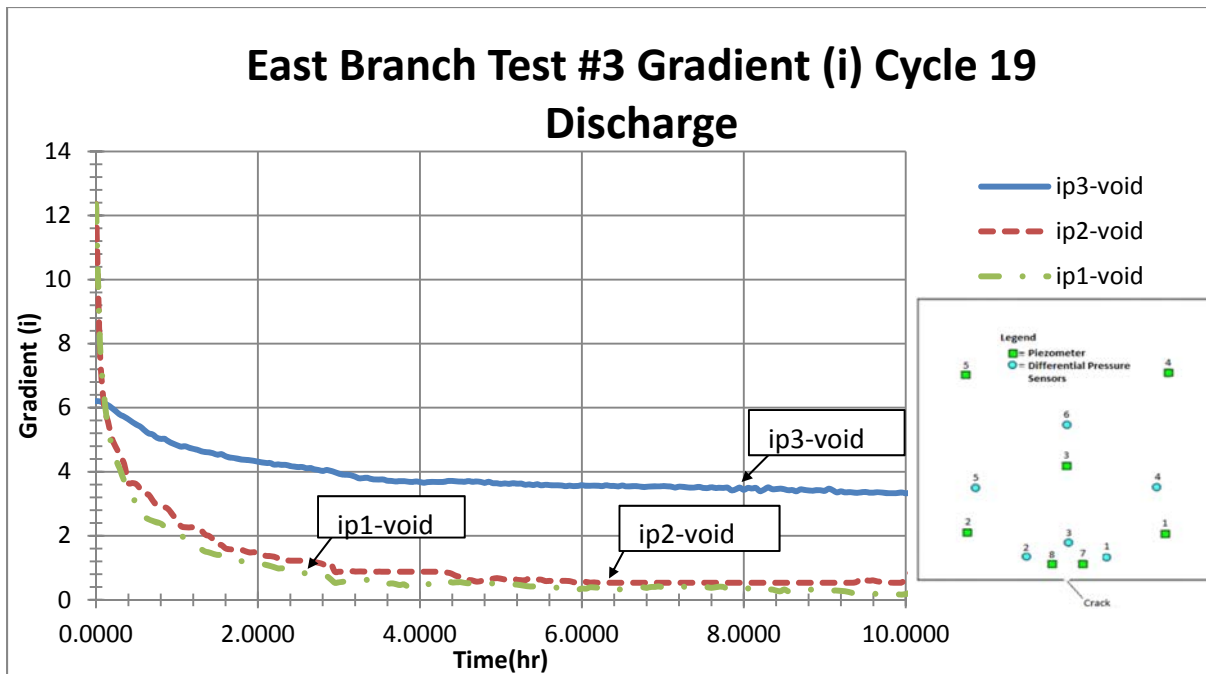


Figure 32. Calculated gradients between piezometers 1, 2, and 3 and the void during discharge of cycle 19

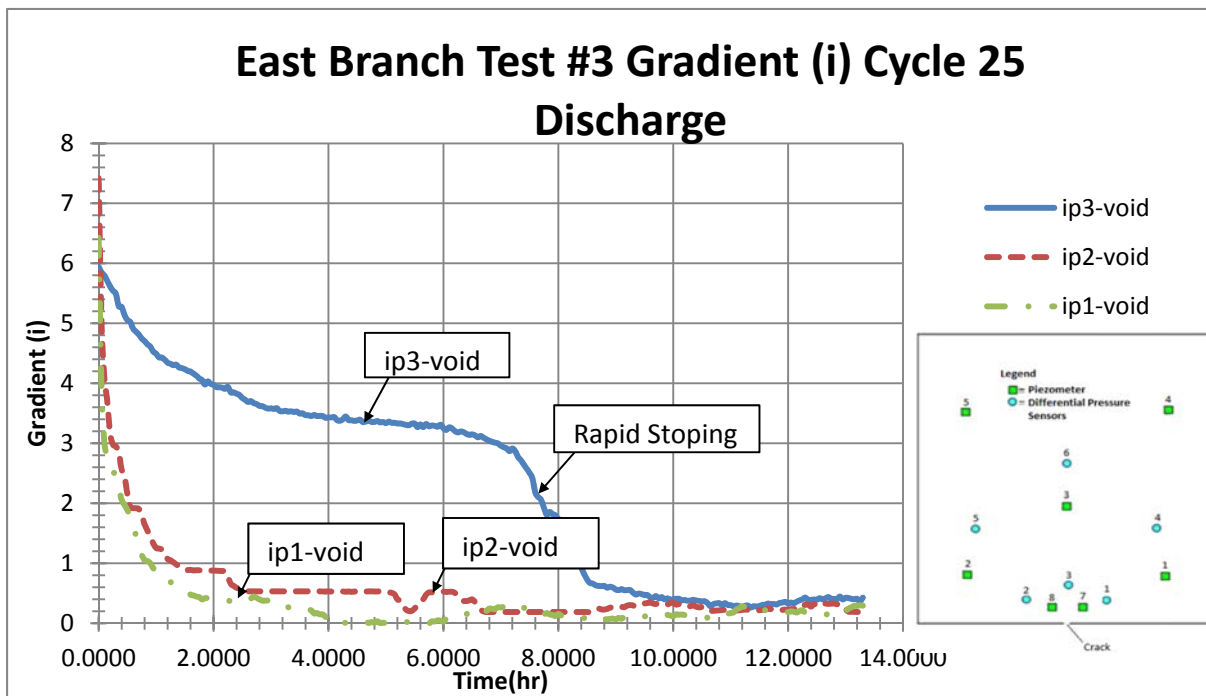


Figure 33. Calculated gradients between piezometers 1, 2, and 3 and the void during discharge of cycle 25

Figure 34 presents the level-off heads that developed in each of the pressure sensors during the charging portion of each stage during the test (note that Piezometers 7 and 8 were not yet installed at the time of this test). The level-off head is the head that was obtained in each sensor when equilibrium was achieved for the respective stage. Figure 34 shows how the various sensors reacted as the various stages of erosion occurred within the sample. It is interesting to note that when upward erosion was the primary erosion mode (cycles 3 through 11) the most affected sensors were Piezometer 3 and Differential Sensor 6; both of which are located vertically above the void. To help interpret the data from the pore pressure sensors, finite element analyses were performed using Rocscience Slide 6.0 to produce contours of total head and evaluate the hydraulic gradients in the vicinity of the void. The model is set up using a constant pressure head for a boundary at the top and zero pressure head at the boundary of the void. The pore pressures measured by the sensors were input in their respective locations as known head values for the various cycles. Figure 35 and Figure 36 present the contours of total head resulting from the analyses performed for cycles 10 and 20 of the test. Figure 35 shows how the head dropped through the sample when the void was small and approximately semi-circular in cross section. As the erosion progressed so did the size of the void. Figure 36 presents the head contours during the later cycles of the test. For the analysis in Figure 36 zero pressure values were set within the void area to describe the outline of the void. Figure 35 shows that in the early stages of the test there is a fairly uniform head drop around the void, albeit with higher gradients above the void compared to the sides. As the void enlarges higher head drops and

therefore higher gradients develop above the void. This supports the theory that a zone of low saturation and decreased permeability forms above the void resulting in higher head loss over a short distance. As the test progressed, the void continued to open up contributing to these higher gradients at the top of the void which helped to drastically increase rate of erosion resulting in the fast upward propagation in the void.

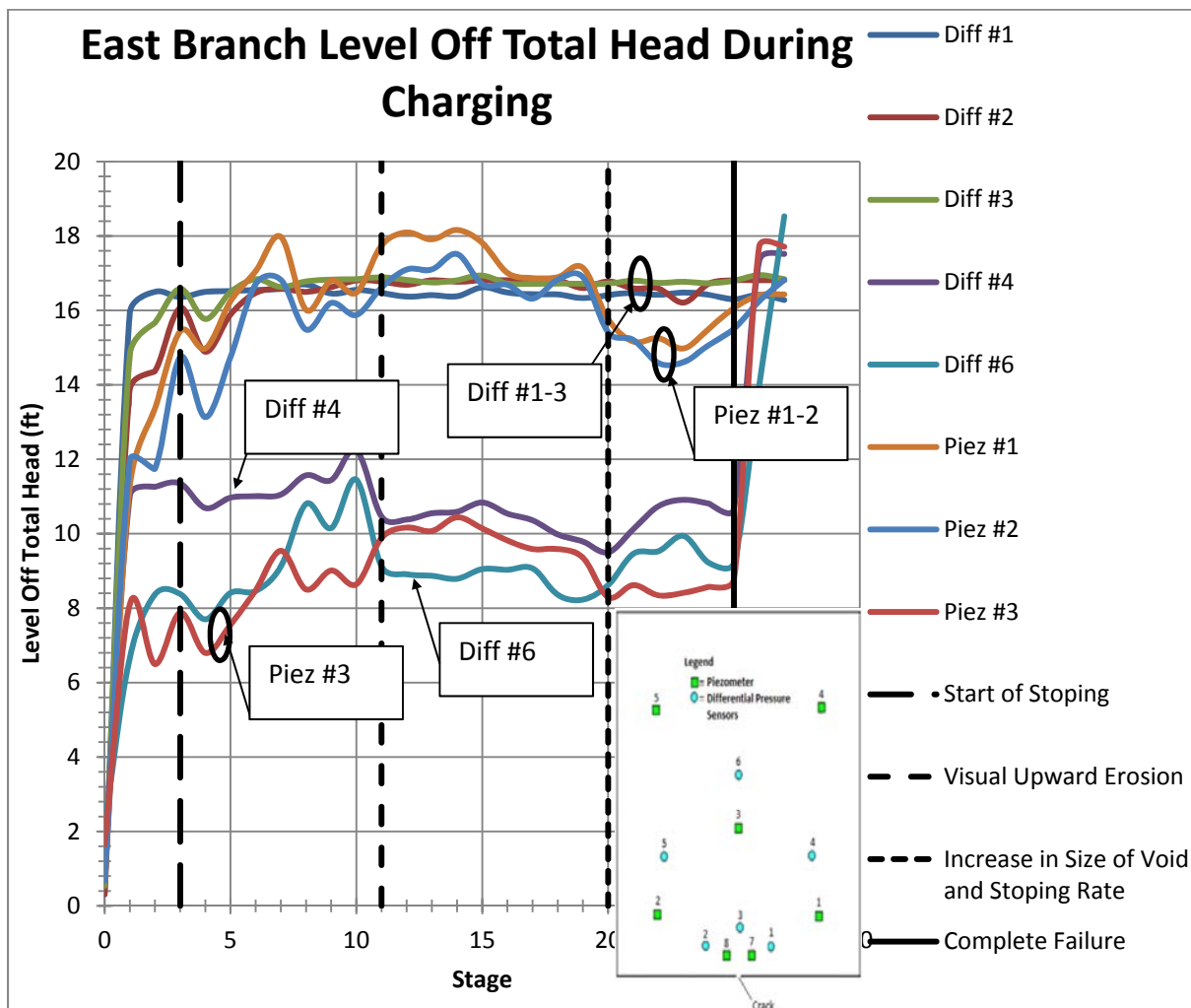


Figure 34. Total head that each sensor reached during charging of the East Branch soil

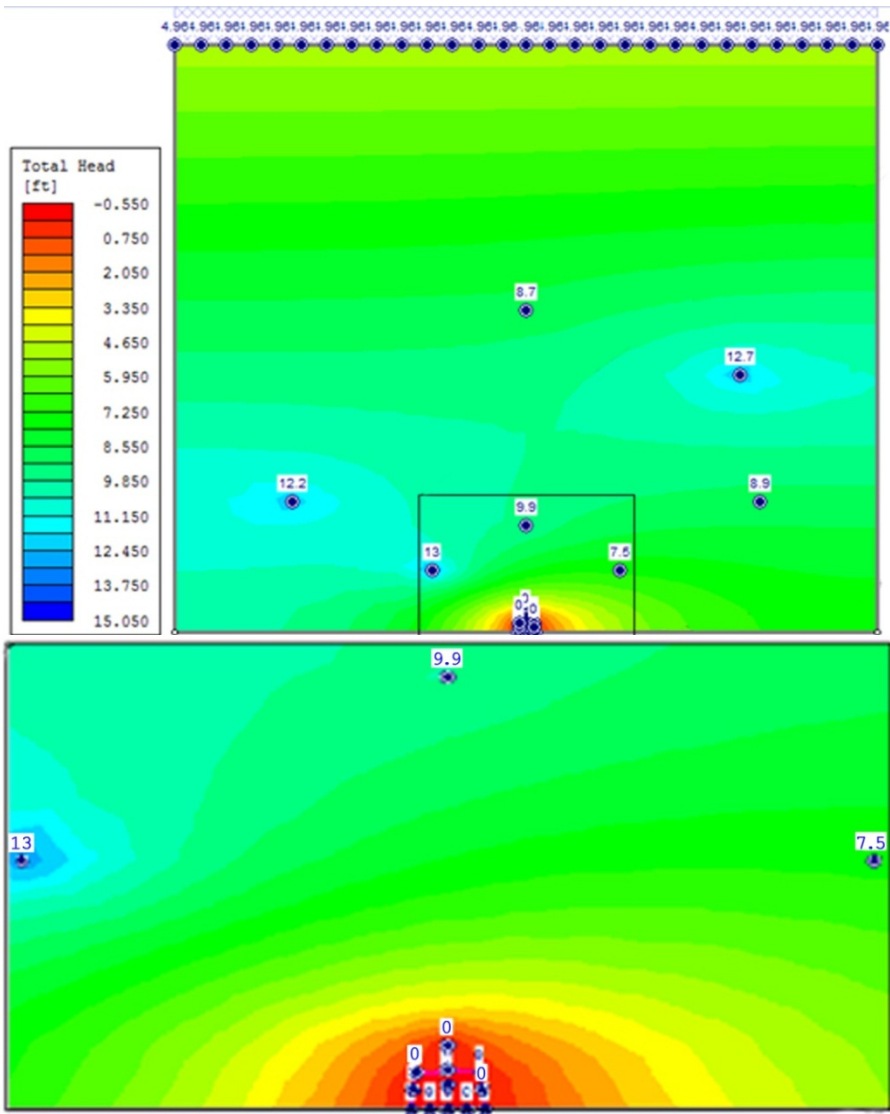


Figure 35. E. B. Cycle 10 Slide 6.0 analysis showing discharge total head drops around the void

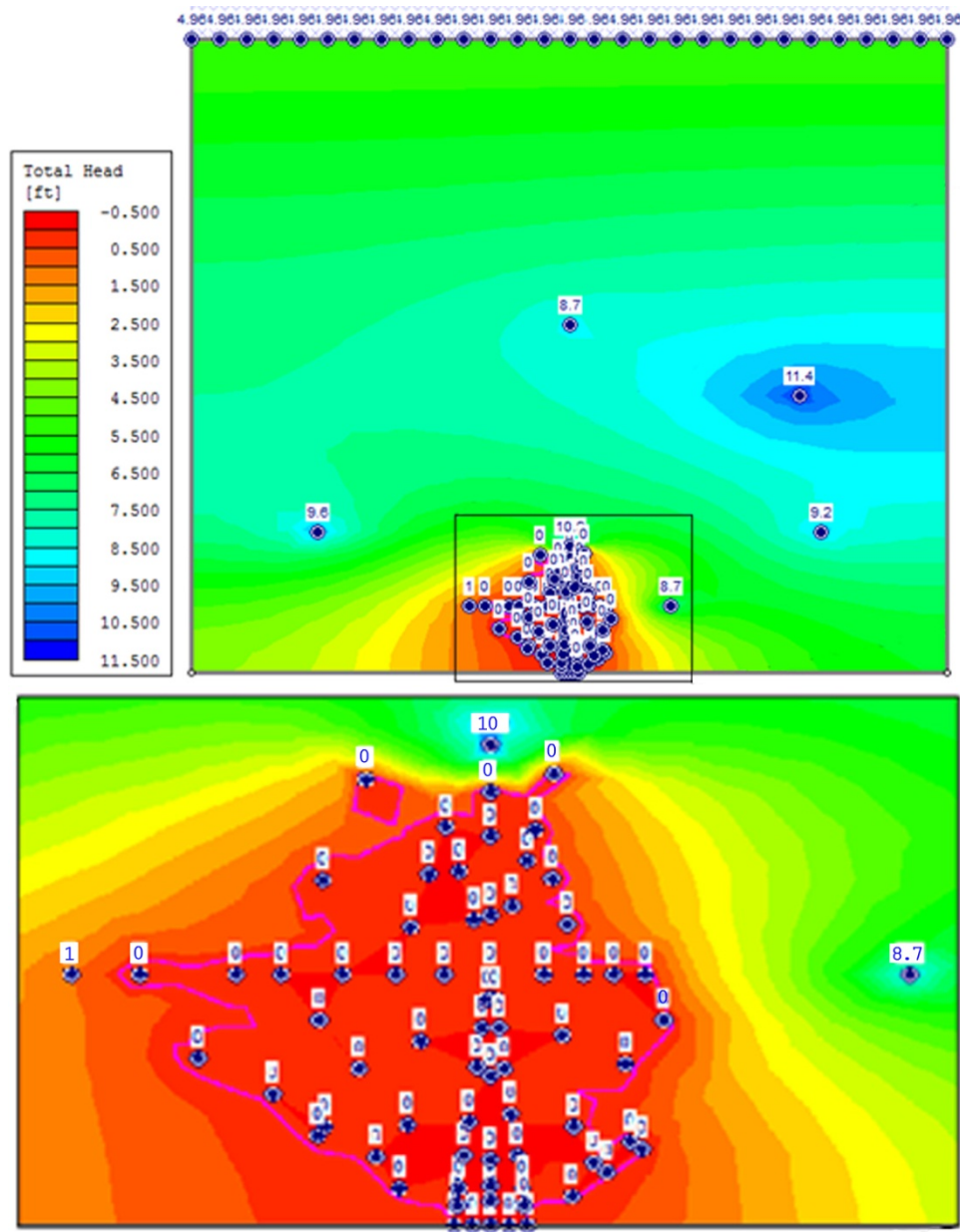


Figure 36. E. B. Cycle 20 Slide 6.0 analysis showing discharge total head drops around the void

The second mechanism associated with enlargement of the void is the loss of confining stress on the walls of the void and cyclic loading of the soil on the perimeter of the void. Figure 37a illustrates the principle stresses acting on a soil element at the top

of the void. In Figure 37b, the water pressure is essentially zero and thus the soils at the edge of the void are undergoing unconfined compression with the major principal stress tangent to the wall of the void (the tangential stress). Because there is no water pressure to counteract the soil forces, the effective compressive stress in the tangential direction is at a maximum. In Figure 37b, the water pressure acts as a principal stress in a direction perpendicular to the wall of the void. The water pressure also acts to expand the void, thereby decreasing the compressive tangential stresses. If the water pressure is high enough, there can be a switch in the principal stresses with the water pressure becoming the major principal stress and the tangential stress becoming the minor. If the water pressure were to further increase the effective tangential stress could become negative (tension) and the soils adjacent to the void would be susceptible to hydraulic fracture.

The stresses at the location of the soil element shown in Figure 35 can be estimated with a form of the Kirsch solution (Brady and Brown 2006) as presented in the following equation:

$$\sigma_{tan} = 3\sigma_h - \sigma_v - u \quad (1)$$

where σ_{tan} is the tangential stress at the top of the void, σ_h is the horizontal stress in the soil, σ_v is the vertical stress in the soil, an u is the water pressure in the void. The stress, σ_v , can be assumed to be equal to the imposed vertical stress (21.5 psi in this test) and the pore pressure, u , can be assumed to be the water pressure used during charging (7.5 psi) during the charge cycle and 0 during the discharge cycle. The horizontal stress can be estimated with the equation:

$$\sigma_h = K_o \sigma_v \quad (2)$$

where K_o is the lateral earth coefficient. K_o is difficult to estimate in this situation due to the lateral stresses imposed during compaction but, for the purposes of this discussion, can be assumed somewhere between the values of 0.5 and 1.0. Using Equations 1 and 2, the assumed K_o values, and the stress values discussed above, the calculated values of the principal stresses on the soil element shown in Figure 35 are presented in Table 6. The calculated values are somewhat approximate; they do illustrate how the principal stresses at the top of the void vary through the loading cycles. If the K_o value is assumed to be 0.5 the major and minor principal stresses switch directions between the cycles. If the K_o value is assumed to be 1.0 the major and minor principal stresses do not switch directions but the tangential stress does undergo significant variation in magnitude and stress ratio. The actual value for K_o is likely between these two values.

Table 6. Calculated stresses at top of void in Figure 35.

Loading Condition	Water Pressure	Vertical Stress, σ_v	Assumed K_o	Calculated Horizontal Stress, σ_h	Calculated Tangential Stress, σ_{tan}	Normal Stress, σ_{norm}
Charging	7.5 psi	21.5 psi	0.5	10.7 psi	3.2 psi	7.5
			1.0	21.5 psi	35.5 psi	7.5
Discharge	0	21.5 psi	0.5	10.7 psi	10.7 psi	0
			1.0	21.5 psi	43.0 psi	0

The cycling of principal stresses illustrated by the calculations presented in Table 6 are believed to be partially responsible to the observed erosion behavior associated with the enlargement of the void. As the stresses cycle, shear planes are believed to

initiate at the surface of the void at acute angles from the void surface (likely close to $45 - \phi/2$). With repeated cycles, several of these shear planes (oriented in opposite directions) may coalesce, forming the chip-shaped soil particles that were observed during the test.

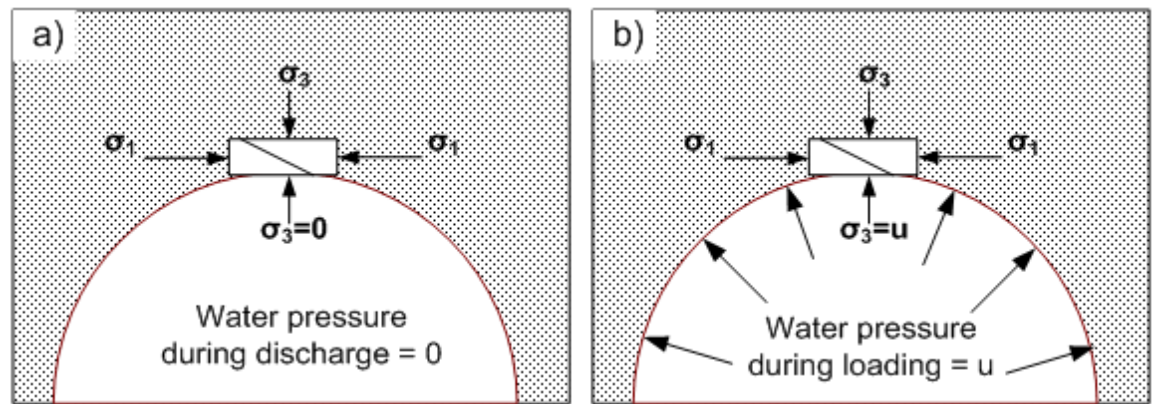


Figure 37. Changes in stress in the soils around the void a) during discharge, and b) during charging.

4.3 Sand with Clay Soil

A mixture of 65 percent by weight medium to coarse poorly graded sand and 35 percent kaolinite clay was created and tested in the foundation void erosion test cell. This soil was put under similar loads as was the East Branch sample. A crack width of 1 in. (25.4 mm) was used with a lower reservoir pressure of 7.5 psi and an overburden pressure of 21.5 psi. Water was added to the soil mixture before compaction giving it water content by weight of 14 percent. The soil was compacted achieving a dry unit weight of 118 pcf (1890 kg/m³) (94 percent relative compaction according to ASTM D1557-12).

Table 7. Hydraulic loading cycles for Sand-Kaolinite test

Sand-Kaolinite Soil											
Cycle	Date and Times of Charge:				Date and Times of Discharge:				Visual Interpretation:		
1	3/2/2013	6:45 PM	-	3/3/2013	7:21 PM	3/3/2013	7:21 PM	-	3/4/2013	3:57 PM	No Major Erosion ↓ Opening of Void ↓ Increased Stopping Rate ↓ Drastic increase in Stopping Rate ↓ Failure
2	3/4/2013	3:57 PM	-	3/5/2013	2:09 PM	3/5/2013	2:09 PM	-	3/6/2013	12:18 PM	
3	3/6/2013	12:18 PM	-	3/7/2013	9:40 AM	3/7/2013	9:40 AM	-	3/7/2013	2:54 PM	
4	3/7/2013	2:54 PM	-	3/7/2013	8:59 PM	3/7/2013	8:59 PM	-	3/8/2013	9:38 AM	
5	3/8/2013	9:38 AM	-	3/8/2013	12:30 PM	3/8/2013	12:30 PM	-	3/9/2013	9:50 AM	
6	3/9/2013	9:50 AM	-	3/9/2013	1:45 PM	3/9/2013	1:45 PM	-	3/10/2013	7:58 PM	
7	3/10/2013	7:58 PM	-	3/10/2013	9:00 PM	3/10/2013	9:00 PM	-	3/10/2013	10:15 PM	
8	3/10/2013	10:15 PM	-	3/11/2013	8:49 AM	3/11/2013	8:49 AM	-	3/11/2013	12:10 PM	
9	3/11/2013	12:10 PM	-	3/11/2013	2:27 PM	3/11/2013	2:27 PM	-	3/11/2013	4:48 PM	
10	3/11/2013	4:48 PM	-	3/11/2013	8:54 PM	3/11/2013	8:54 PM	-	3/11/2013	10:34 PM	
11	3/11/2013	10:34 PM	-	3/11/2013	12:03 AM	3/11/2013	12:03 AM	-	3/12/2013	10:40 AM	

The sand-clay test was run for a total of 11 cycles of water pressure being applied to the lower reservoir followed by rapid drawdown until complete failure occurring after 11 days. A summary of the cycles with a brief account of the soil behavior is presented in Table 7. Compared to the East Branch test, the erosion in this test occurred over a shorter amount of time and with significantly fewer cycles. This test failed more quickly due to the fact that the sand has lower cohesive strength than the East Branch sample.

The vertical stoping that occurred in the East Branch Test did not occur in this test. However, the test results were similar in that erosion started out slowly and then hit a critical point where failure progressed fairly rapidly. In the East branch test, a shaft formed in the vertical direction with very steep sides, while in this test as the void propagated upwards, the confining pressure would decrease and, coupled with the soil softening, the walls would collapse and erosion would occur at the angle of repose of

the sand creating a fan like void. The sand-clay test had a slow start and then hit a point after 8 days of testing where the void increased in size and upward propagation of erosion continued rapidly until complete failure of the test which occurred 3 days later as shown in Figure 38 through Figure 42.

During each part of the cycle, whether it is charging or drainage of the sample, erosion could be observed to deposit eroded soil into the lower cell. Similar to East Branch, more erosion was noted during the discharge portion of each cycle. Again, this is due to the loss of water pressure and high hydraulic gradients. During discharge, it was common to see chunks break off as well as finer particles being washed out into the lower cell.

In contrast, hardly any finer particles were seen being washed into the lower cell during recharge. It was much more common during recharge to see erosion in the form of plate like chunks breaking off of the wall of the void occurring immediately following the application of water pressure into the lower cell. This was interpreted to be due to a combination of factors. During discharge the soil along the void wall experienced increased tangential stresses and, as a result, small cracks or shear surfaces may have formed. When the cycle is switched there is straining of the soil that likely lead to the coalescing of shear planes and formation of small platy soil masses. Water pressure entering these small cracks the soil may also tend to break off the platy chunks along the wall of the void. This also happens during the discharge of the sample, but in addition to the hydraulic gradients you also lose the confining pressure of the water, greatly increasing the rate of erosion.



Figure 38. Test after 8 days



Figure 39. Test after 9 days



Figure 40. Test after 10 days



Figure 41. Test after 11 days

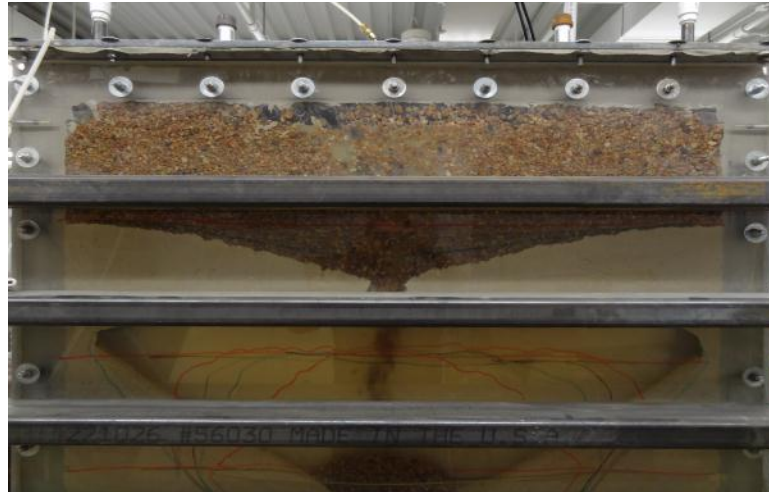


Figure 42. Complete failure of sample

Figure 43 graphs the level off total head for each cycle of the test. A similar trend to the East Branch sample can be observed. As the void continued to enlarge over time the total head reached during each charge of the cycle continued to increase. Pressures for each sensor seemed to reach an initial level off peak at about cycle 3, but as the erosion and stoping increased the level off total heads also continued to increase. Piezometers 1 and 2 had a slight drop at cycles 6 and 7 which may have been due to soil around those sensors shifting making it more difficult for the higher head to be reached during the charging portion of the cycle. Piezometers 3, 7, and 8, which are located directly above the void, showed drastic increases in the level off total head as the soil eroded upward. A relatively constant head during charging was reached up to a point where the soil structure breaks down and erosion occurs at an accelerated rate. Over time, the pressure gradients continue to increase until complete failure of the sample occurred and pressure heads for all sensors converged. It is interesting to note that the

level off total head for Piezometer 3 started to increase prior to Piezometer 1 or 2. This shows that we see a faster vertical propagation of the void than horizontal.

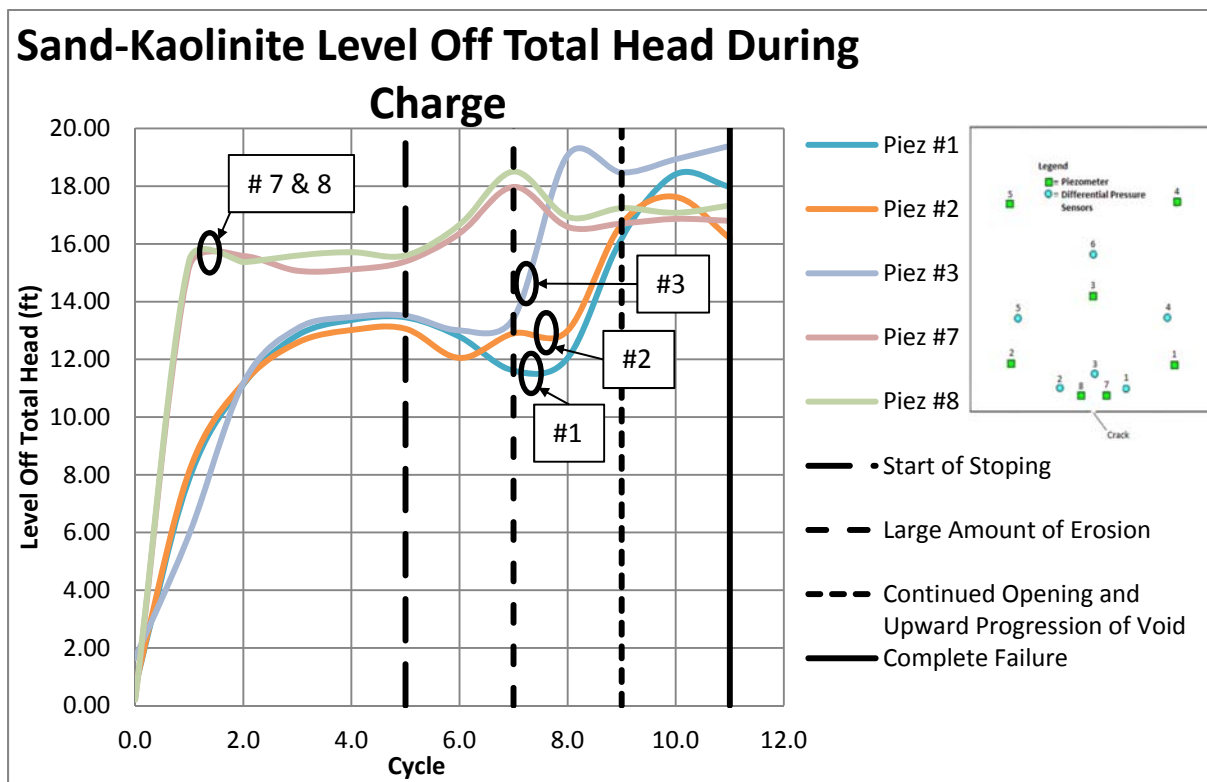


Figure 43. Total head that each sensor reached during charging of the Sand-Kaolinite soil

Similar to the East Branch test, when the measured pressures are input into the finite element analysis, the initial gradients are fairly uniform around the void as can be seen in Figure 44 (Cycle 4). Over time we see the gradients above the void increase as shown in Figure 45 (Cycle 6). This is again thought to be due to an air pocket forming at the top of void as shown in Figure 47. The same process as before is occurring where this pocket of air creates a low permeable zone in the surrounding soil. This lower permeable zone in turn creates a higher gradient across the top of the void, as is seen in the finite element models (Figure 44-45), which are the cause of higher erosion rates in

the vertical direction. This is why erosion in the vertical direction begins to increase over time as this pocket develops and why failure can occur relatively quickly. The fan-like shape of the void and rate of erosion is likely due to the higher erodibility of the soil once the width increases past a certain arching limit. As the void continues to move upward the soil along the side walls of the void continued to see side erosion due to the soil softening at these locations and the angle of repose of the soil with low cohesive strength.

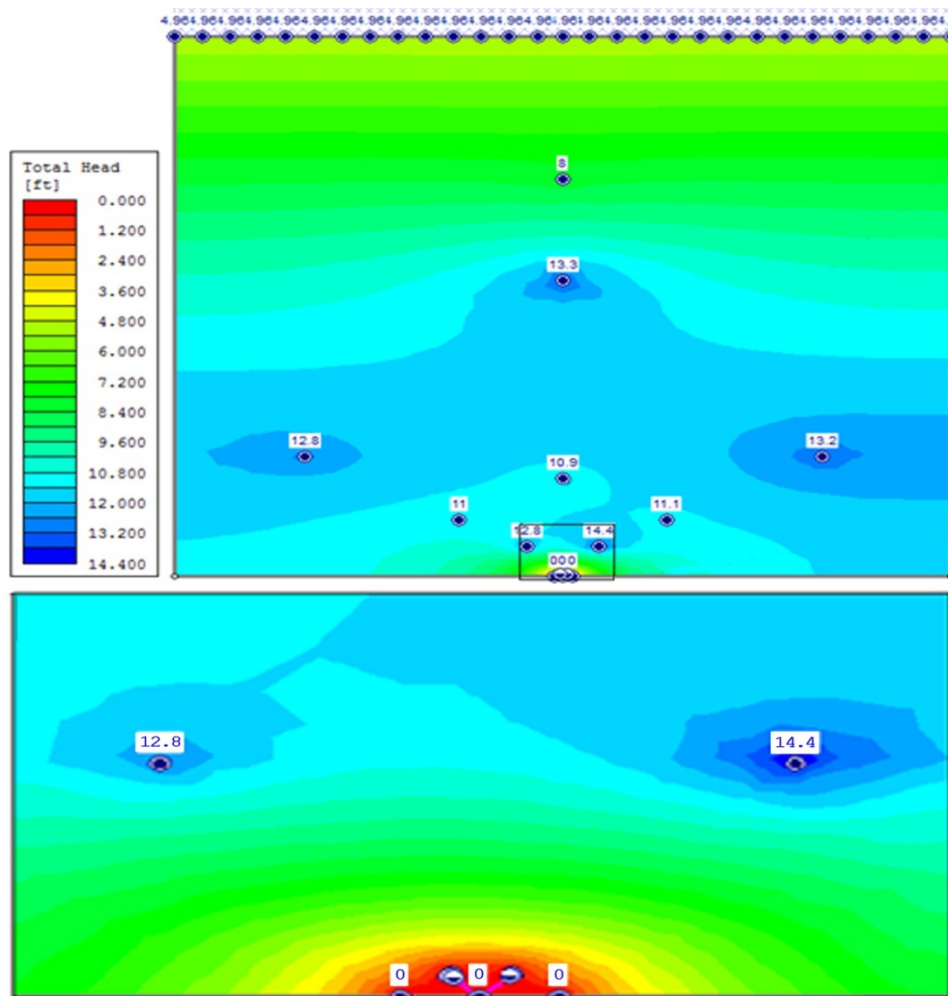


Figure 44. Sand-Kaolinite Cycle 4 Slide 6.0 analysis showing discharge total head drops around the void

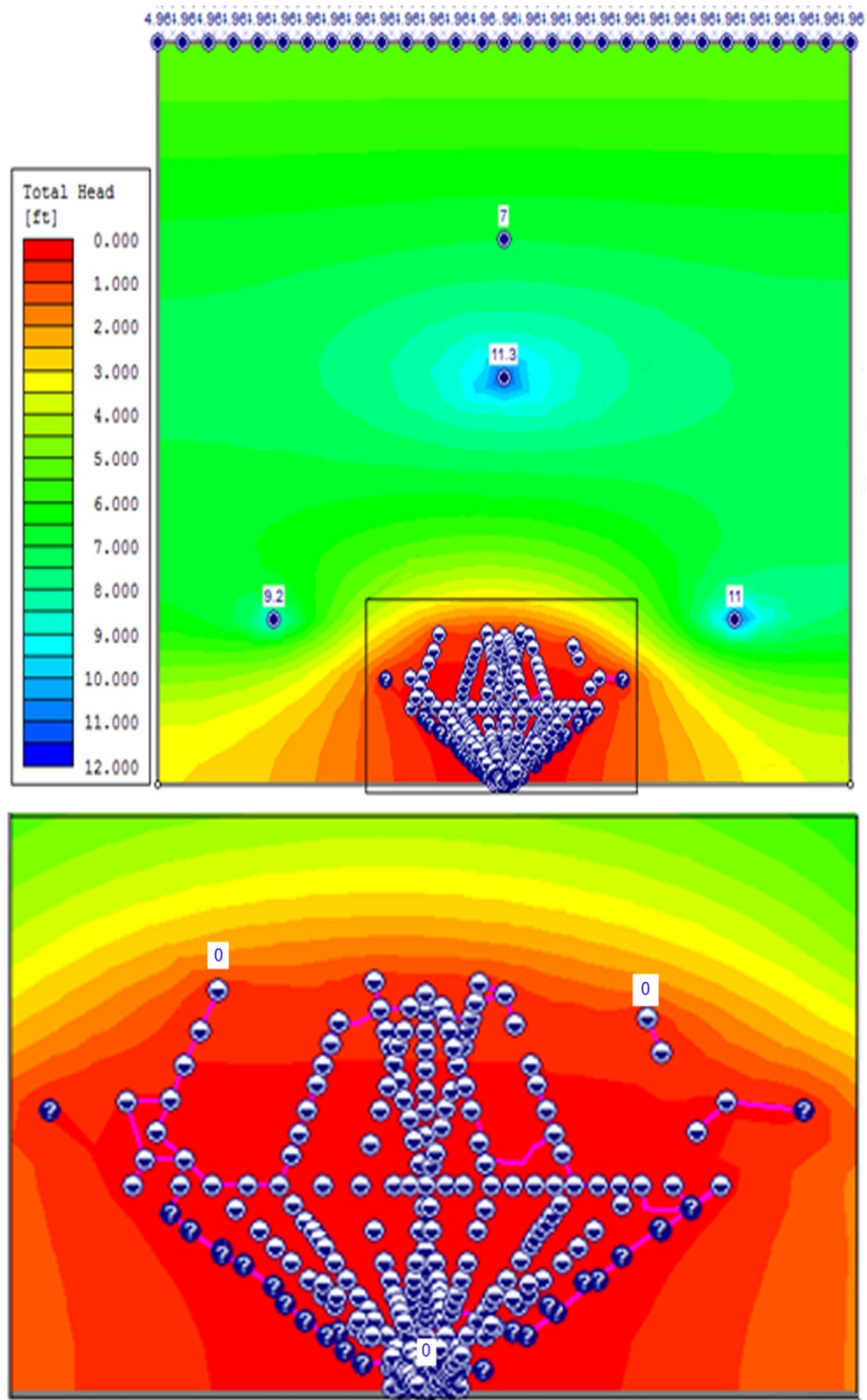


Figure 45. Sand-Kaolinite Cycle 6 Slide 6.0 analysis showing discharge total head drops around the void

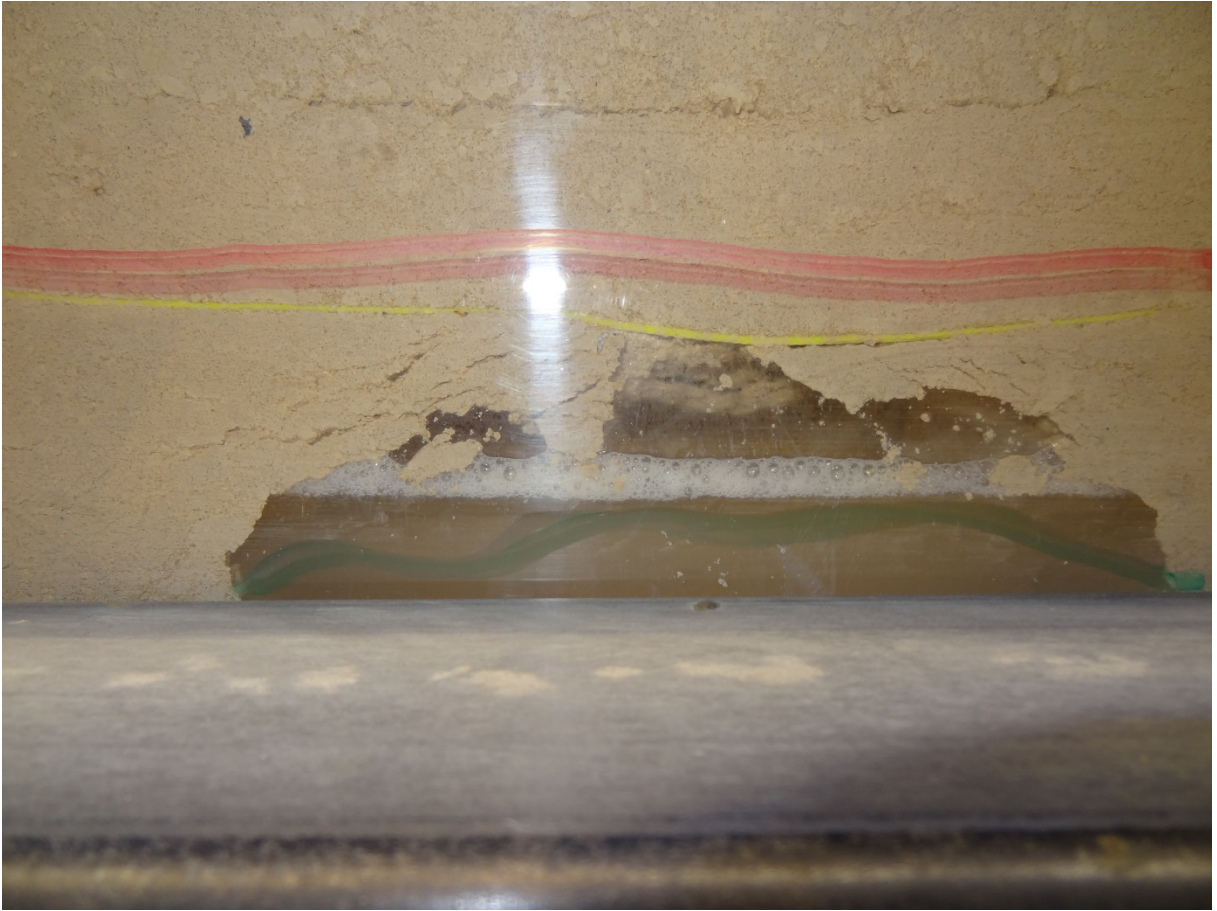


Figure 46. Air pocket during cycle 6 of Sand-Kaolinite test

4.4 Teton Dam Core of Embankment Soil Test #1

The Teton Dam core soil was the next to be tested. This soil was put under similar loads as were the previous tests. A crack width of 1 in. (25.4 mm) was used with a lower reservoir pressure of 7.5 psi and an overburden pressure of 21.5 psi. Water was added to the soil mixture giving it water content by weight of 14 percent. The soil was compacted achieving a dry unit weight of 114 pcf (1826 kg/m³) (94 percent relative compaction according to ASTM D1557-12).

Table 8. Hydraulic loading cycles for Teton Dam Core test #1

Teton Dam Core of Embankment Test #1											
Cycle	Date and Times of Charge:				Date and Times of Discharge:				Visual Interpretation:		
1	3/22/2013	2:56 PM	-	3/23/2013	3:22 PM	3/23/2013	3:22 PM	-	3/24/2013	3:24 PM	No Major Erosion Initiation of Stopping ↓ Slight Increase in Stopping ↓ Opening of Void ↓ Very Rapid vertical erosion Failure
2	3/24/2013	3:24 PM	-	3/25/2013	4:55 PM	3/25/2013	4:55 PM	-	3/26/2013	10:16 AM	
3	3/26/2013	10:16 AM	-	3/26/2013	1:25 PM	3/26/2013	1:25 PM	-	3/26/2013	4:45 PM	
4	3/26/2013	4:45 PM	-	3/26/2013	9:38 PM	3/26/2013	9:38 PM	-	3/27/2013	9:45 AM	
5	3/27/2013	9:45 AM	-	3/27/2013	1:00 PM	3/27/2013	1:00 PM	-	3/27/2013	5:00 PM	
6	3/27/2013	5:00 PM	-	3/27/2013	10:13 PM	3/27/2013	10:13 PM	-	3/28/2013	9:20 AM	
7	3/28/2013	9:20 AM	-	3/28/2013	1:35 PM	3/28/2013	1:35 PM	-	3/28/2013	5:42 PM	
8	3/28/2013	5:42 PM	-	3/28/2013	9:35 PM	3/28/2013	9:35 PM	-	3/29/2013	9:20 AM	
9	3/29/2013	9:20 AM	-	3/29/2013	12:50 PM	3/29/2013	12:50 PM	-	3/29/2013	4:00 PM	
10	3/29/2013	4:00 PM	-	3/30/2013	10:00 AM	3/30/2013	10:00 AM	-	3/30/2013	8:00 PM	
11	3/30/2013	8:00 PM	-	4/1/2013	9:34 AM	4/1/2013	9:34 AM	-	4/1/2013	1:36 PM	
12	4/1/2013	1:36 PM	-	4/1/2013	5:34 PM	4/1/2013	5:34 PM	-	4/2/2013	9:16 AM	
13	4/2/2013	9:16 AM	-	4/2/2013	1:15 PM	4/2/2013	1:15 PM	-	4/2/2013	5:25 PM	
14	4/2/2013	5:25 PM	-	4/2/2013	10:27 PM	4/2/2013	10:27 PM	-	4/3/2013	9:40 AM	
15	4/3/2013	9:40 AM	-	4/3/2013	1:58 PM	4/3/2013	1:58 PM	-	4/3/2013	5:58 PM	
16	4/3/2013	5:58 PM	-	4/3/2013	10:09 PM	4/3/2013	10:09 PM	-	4/4/2013	9:14 AM	
17	4/4/2013	9:14 AM	-	4/4/2013	1:12 PM	4/4/2013	1:12 PM	-	4/4/2013	5:23 PM	
18	4/4/2013	5:23 PM	-	4/4/2013	6:24 PM	4/4/2013	6:24 PM	-	4/4/2013	7:20 PM	

This Teton Dam core test #1 had a total of 18 cycles occurring over a time frame of two weeks. Details of the cycles and a brief synopsis of the erosion progression are presented in Table 8. This test demonstrated how fast an erosion stope can develop after a slow start to the erosion process. During cycle 2 the first signs of stopping were noted as seen in Figure 48. A slight increase in stopping occurred during Cycle 5, but little movement could be seen until Cycles 11 and 12. After 12 days and 14 cycles little erosion had occurred with stopping only just starting to appear as can be seen in Figure 48. Figures 49 through 51 show the sample only two days later with complete failure having occurred. These figures show how, after many cycles of slow erosion progression, a 4 in. (102 mm) high void can propagate upward 2 ft. (0.61 m) or more in a matter of hours and just 1 cycle. This test had very rapid vertical stopping with an initial void width ranging from 2-4 inches and extending to a height of 1 to 2 feet before the

side walls collapsed, leading to that fan-like shape similar to than seen in the sand-kaolinite test. This shaft is outlined in Figure 50.

The level off total heads for each cycle through the duration of the test are presented in Figure 52. These total heads show a steady increase of the level-off total head at each sensor with a slight slope increase in the lower sensors (Piezometers 7, 8, and Differential Pressure Sensors 1-3) until that critical point is reached where the soil structure breaks down and fails altogether. In this test erosion early on was minimal and thus the level off total heads did no change drastically until the rate of erosion increased significantly. Figures 49 and 50 show the progression of this void started out almost completely vertical. Figure 50 shows this vertical shaft that progressed upward several feet in a matter of minutes before the side walls failed, widening the void.



Figure 47. Day 2 Cycle 2 of Teton Core Test #1



Figure 48. Day 12 Cycle 13 of Teton Core Test #1



Figure 49. Day 14 Cycle 17 of Teton Core Test #1 (Time – 9:10 a.m.)



Figure 50. Day 14 Cycle 17 of Teton Core Test #1 (Time – 1:22 p.m.)



Figure 51. Day 14 Cycle 18 of Teton Core Test #1 (Time – 7:20 p.m.)

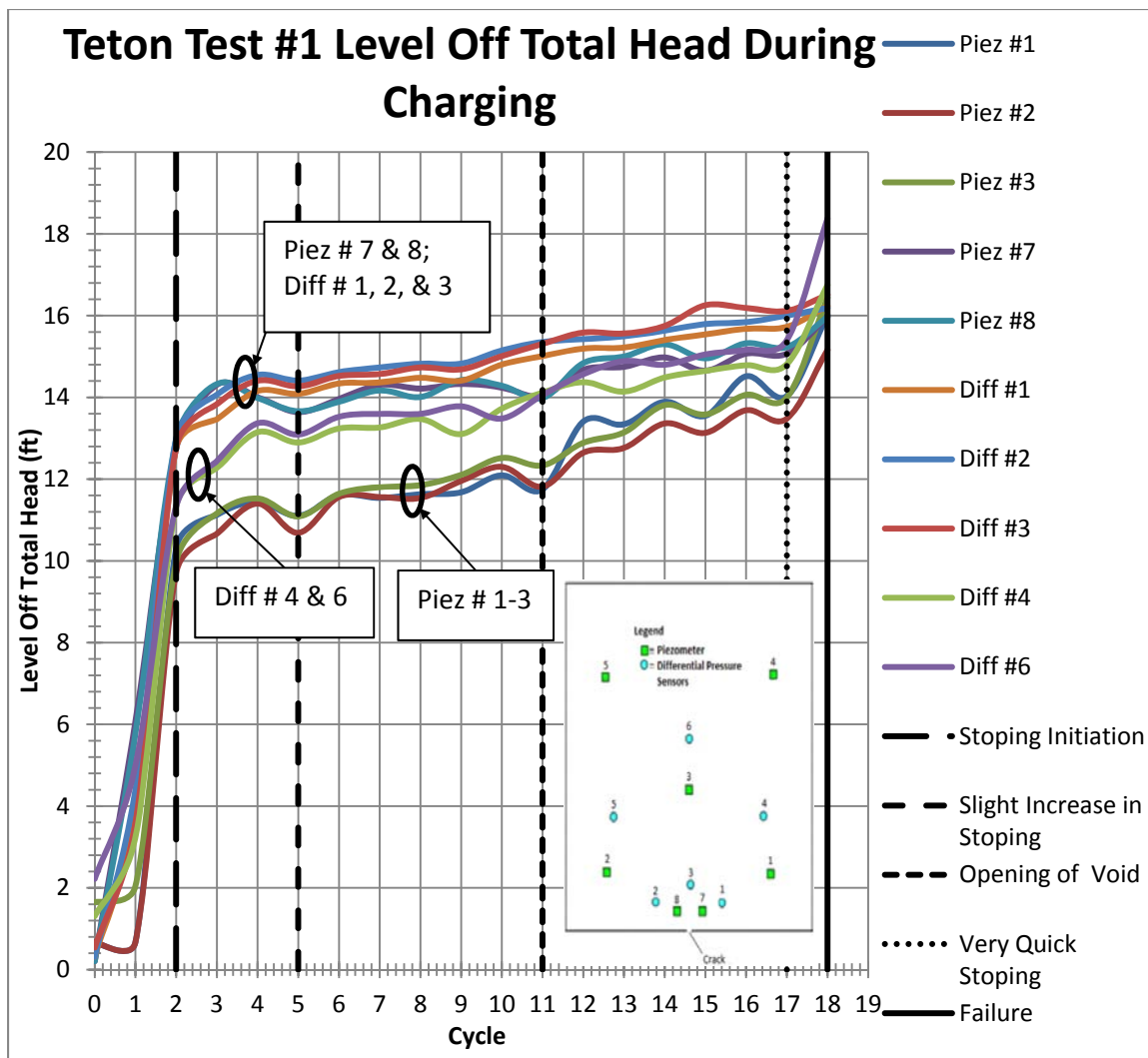


Figure 52. Total head that each sensor reached during charging of the Teton Core test #1 soil

Finite element seepage models were performed similar to those performed in the previous tests. The results of these analyses indicate that with the development of the void there was an area above the void of much higher gradients than on the sides. The soil was not able to support these gradients leading to a failure in the soil structure with the quick vertical propagation of an open shaft. The gradients and a photo during cycle 8, 14, and 17 are presented in Figure 53 through 58, respectively.

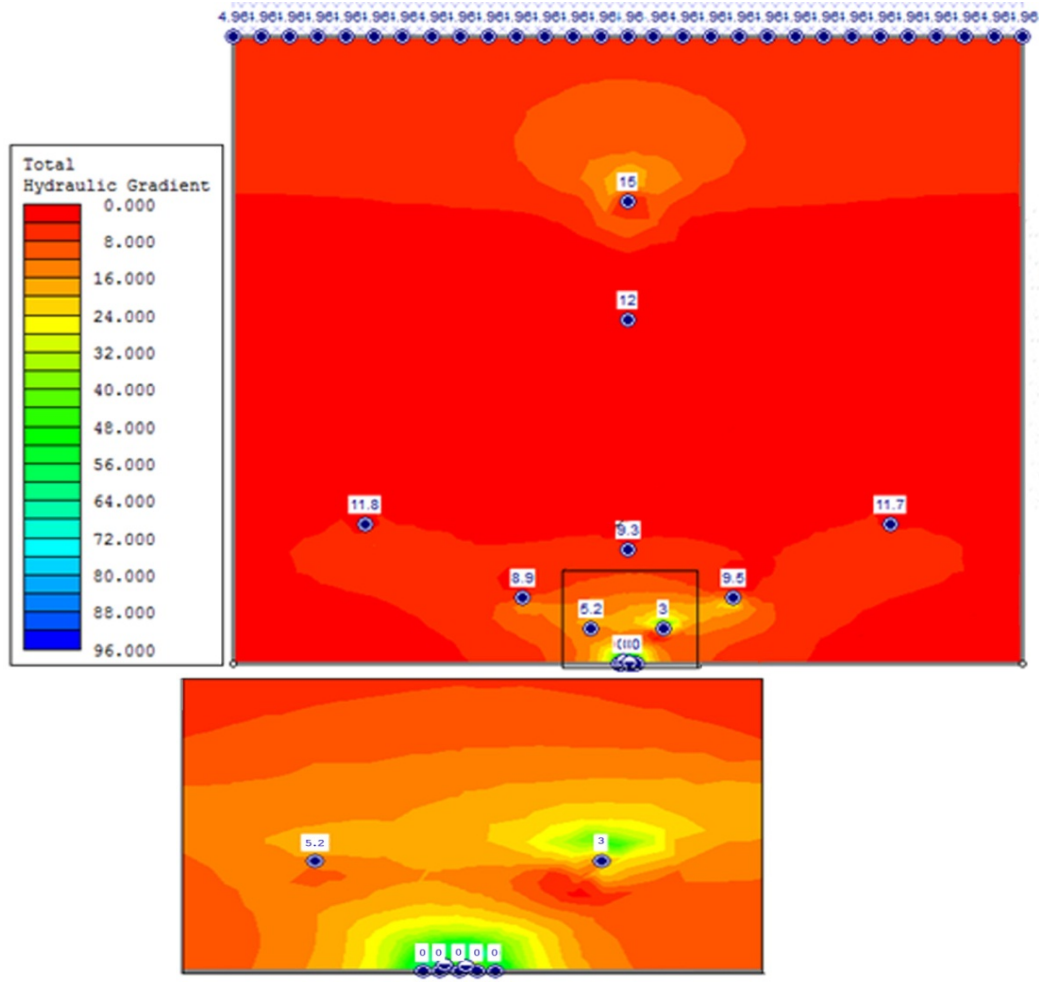


Figure 53. Teton Dam Core test #1 Cycle 8 Slide 6.0 analysis showing discharge gradients around the void



Figure 54. Teton Dam Core test #1 Cycle 8

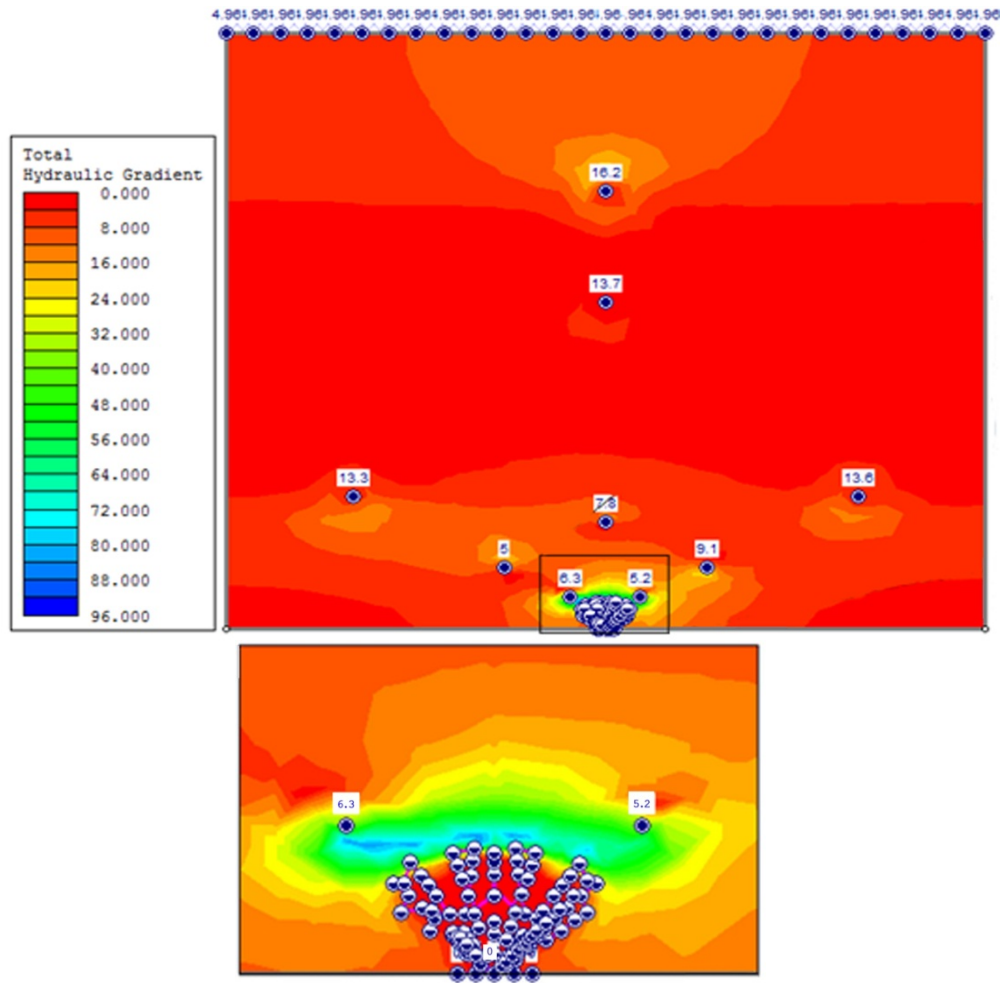


Figure 55. Teton Dam Core test #1 Cycle 14 Slide 6.0 analysis showing discharge gradients around the void



Figure 56. Teton Dam Core test #1 Cycle 14

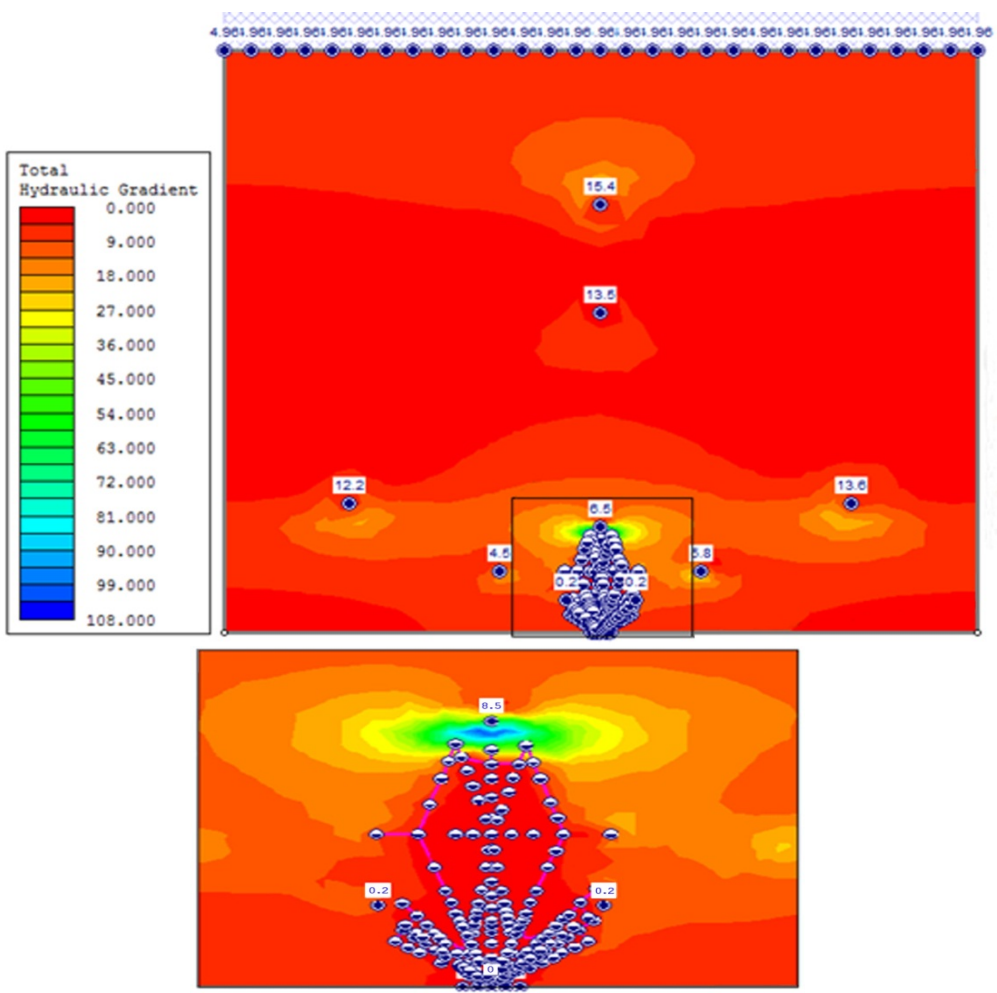


Figure 57. Teton Dam Core test #1 Cycle 17 Slide 6.0 analysis showing discharge gradients around the void



Figure 58. Teton Dam Core test #1 Cycle 17

Another possible explanation for the quick moving vertical opening of the void is hydraulic fracturing of the soil. Hydraulic fractures can occur if the water pressure exceeds the total stress of the soil. Generally, the crack will propagate parallel to the greatest principle stress and perpendicular to the least principle stress. Thus, if the water pressure in the void were to exceed the total stress soil above the void, a hydraulic fracture could propagate off of the top of the void and continue to a point where the soil stresses are again greater than the water pressure. A schematic illustration of this phenomenon is presented in Figure 59. A hydraulic fracture may open a preferential flow path for water to flow, greatly increasing the rate of erosion that is occurring in the vertical direction.

The soils stress calculations presented in Section 4.2 did not indicate that hydraulic fractures were likely to originate from a semi-circular void under the stress conditions imposed in this test (which are the same as the test on East Branch material). However, minor perturbations in the soil consistency and the shape of the void could lead to negative stress concentrations in the soil that may allow for the initiation of a hydraulic fracture. Thus, while neither the observations during the test nor the pore pressure data provide direct evidence of hydraulic fracture, it is presented herein as a possible mechanism to be considered in the initiation and propagation of vertical slope formation.

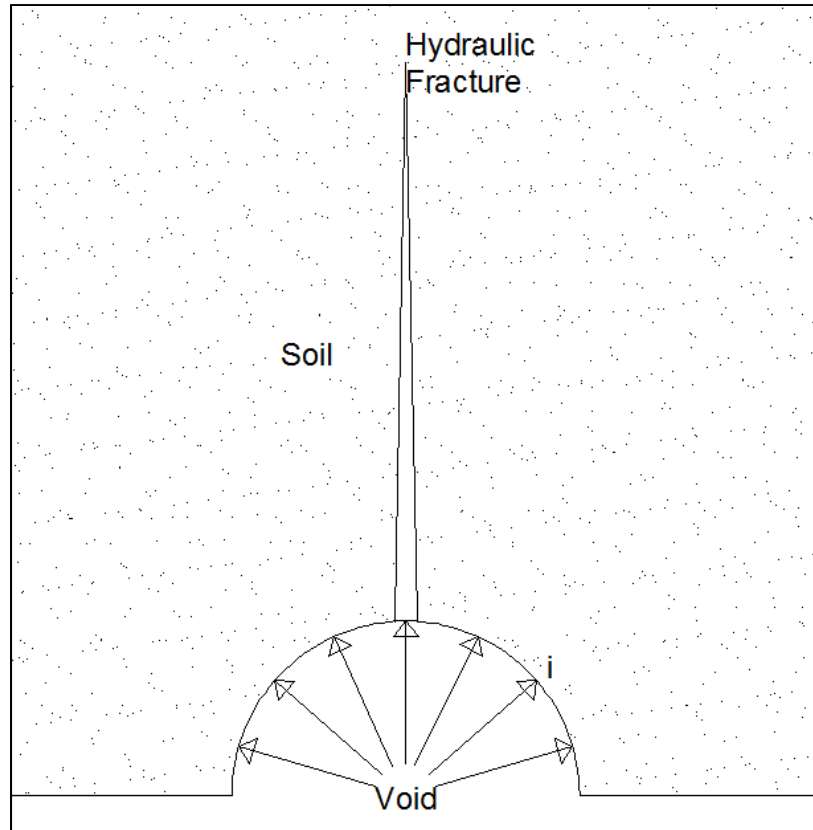


Figure 59. Hydraulic fracturing of soil matrix

4.5 Teton Dam Core of Embankment Soil Test #2

The Teton Dam core or embankment soil was again tested in the foundation void erosion test cell with the all the same parameters as presented in the previous test except for the size of the void. This soil was put under the same loads as was the previous tests. A crack width of 2 in. (50.8 mm) was used with a lower reservoir pressure of 7.5 psi and an overburden pressure of 21.5 psi. Water was added to the soil mixture giving it water content by weight of 14 percent. The soil was compacted achieving a dry unit weight of 113 pcf (1810 kg/m³) (93 percent relative compaction according to ASTM D1557-12).

Table 9. Hydraulic loading cycles for Teton Dam Core test #2

Teton Dam Core of Embankment Test #2											
Cycle	Date and Times of Charge:					Date and Times of Discharge:				Visual Interpretation:	
1	4/10/2013	2:03 AM	-	4/10/2013	10:45 PM	4/10/2013	10:45 PM	-	4/11/2013	2:25 PM	Initiation of Stopping
2	4/11/2013	2:25 PM	-	4/12/2013	11:15 AM	4/12/2013	11:15 AM	-	4/12/2013	2:50 PM	Major Erosion & Failure

With the larger void it was expected that the rate of erosion in this test would proceed very quickly. When the void in the previous Teton Dam test reached a width of about 2 to 3 in. (50.8-76.2 mm) the void propagated upward very quickly so by opening the void to this critical width it was expected that fallout will occur in a much shorter time frame.

As per expectations the Teton Dam test #2 failed in only 2 cycles occurring over a time period of only 2 days. Details of the cycles are presented in Table 9. After the first cycle only a small void had eroded in the soil. When the drain was opened for the end of the second cycle the soil gave way and quickly eroded into the lower reservoir. The erosion occurred over a period of about two hours. The failure progression is presented in Figures 60, 61, and 62. This fast rate of erosion is likely due to the size of the void exceeding the arching capacity of the soil. The test was ended when the soil eroded back to the sides of the apparatus. With the opening of the initial void the soil most likely saw similar high gradients acting across the wall of the void during drawdown and, in combination with the large void opening, led to the fast progression of the erosion. The test occurred so quickly that the data was unusable for a finite element analysis comparison.



Figure 60. Teton Core test #2 end of cycle 1



Figure 61. Teton Core test #2 after charge and just before drainage of cycle 2



Figure 62. Teton Core test #2 one hour after start of drainage of cycle 2



Figure 63. Teton Core test #2 at failure 2.5 hours after start of drainage of cycle 2

4.6 Teton Dam Core of Embankment Soil Test #3

The Teton Dam core of embankment soil was again tested in the foundation void erosion test cell; this time with the all the same parameters as the Teton Dam shell of embankment test except for the size of the void. For this test a 1 in. (25.4 mm) gap was used and an overburden pressure of 21.5 psi. Water was added to the soil mixture giving it water content by weight of about 14 percent. The soil was compacted achieving a dry unit weight of 114 pcf (1826 kg/m³) (94 percent relative compaction according to ASTM D1557-12).

This test was performed by applying water pressure to the top of the cell to create a constant downward gradient toward the void at the base of the sample. The gradient was shut off once during the test to allow the soil to “relax.” A water pressure of 12 psi was applied to the top of the sample allowing seepage to flow from the top of the soil down through the soil and out a 1 in. (50.8 mm) gap at the base of the soil cell. This test was designed to mimic seepage flow through the embankment into the foundation. Once the sample was ready the flow was turned on and the drain at the bottom was open allowing a downward seepage through the sample.

The Teton Core Test #3 was left running for 48 days with the water being shut off at day 13. The water was shut off for about 2 hours and then flow was turned back on. This was done due to leaking occurring in the lid of the apparatus. Over time the soil continued to erode and numerous channels, both internally (unable to be viewed from outside the cell) and against the Plexiglas, developed up through the soil. No stopping was noted, so the main failure mechanism in this test was backward erosion or piping.

As these channels propagated back up through the soil the flow increased through these channels. Figures 64 through 66 show the test before and after the development of the channels. The channels are traced with red marker on the Plexiglas to make them easier to follow in the photos.

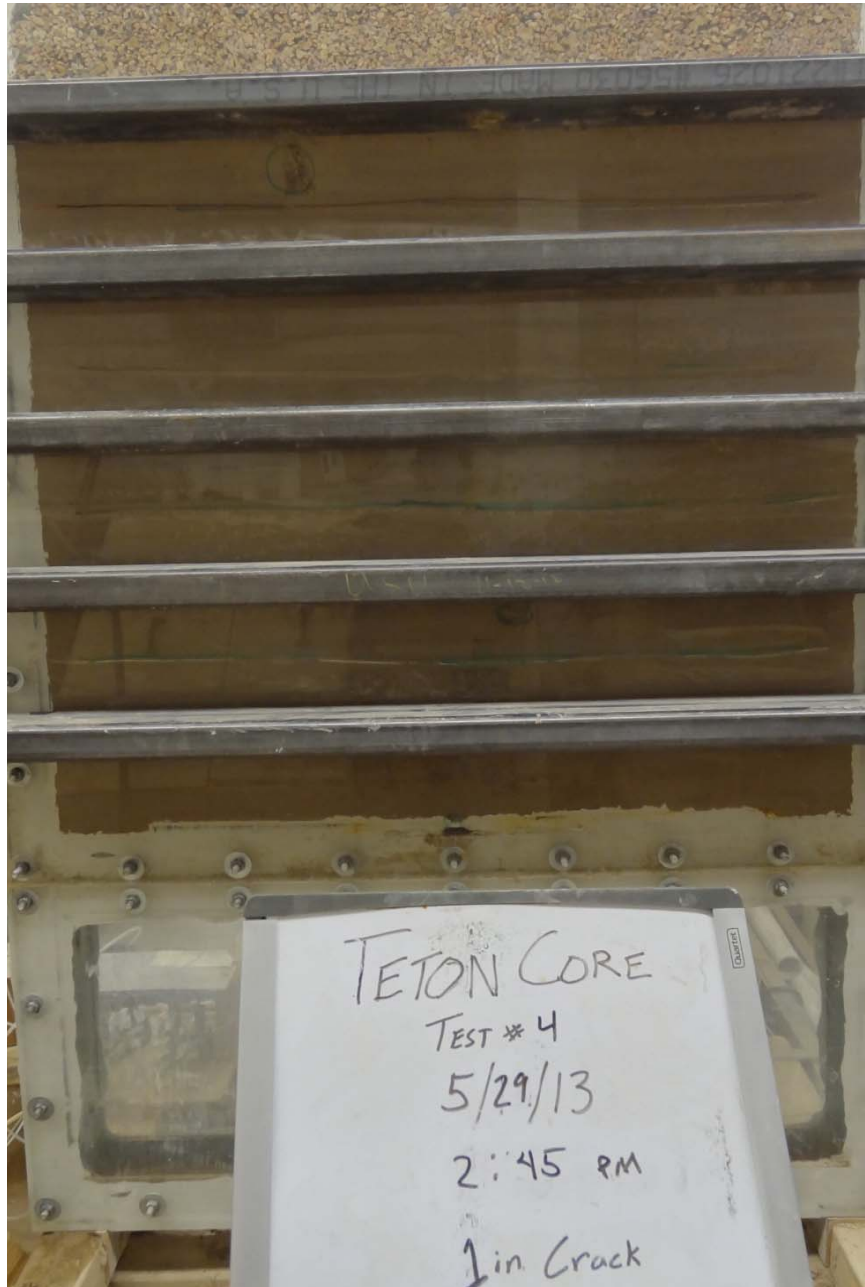


Figure 64. Teton Core test #3 before start of test



Figure 65. Teton Core test #3 35 days after start of test (visible channels marked in red)



Figure 66. Teton Core test #3 43 days after start of test (visible channels marked in red)

This test demonstrated a different failure mechanism for the soil due to a different seepage regime. Piping initiated at the void opening due to the concentration of flow into the void resulting in high hydraulic gradients. As piping channels worked backward into soil mass they represent pathways of least resistance, causing flow to again concentrate into the heads of the pipes. As the pipes work toward the water source, they collect more flow which, if the velocity is great enough, can enlarge the pipes through concentrated leak erosion along the pipe walls. In a dam, the pipe channels could eventually progress back to the reservoir and increase in size to eventually lead to failure if not mitigated.

Chapter 5

SUMMARY AND CONCLUSIONS

Laboratory models were performed to assess the potential for soil erosion to occur when an open void (such as a bedrock joint or solution void) is found adjacent to a soil layer. Results of these laboratory tests show that over time, unless a filter is present or the void is filled or plugged, upward propagation of erosion will continue resulting in the opening of a sinkhole at the surface or a pipe through the dam. This soil erosion occurred in all the samples tested forming large voids leading to the collapse of the soil structure or piping channels that reduced the soil mass's resistance to seepage and may eventually lead to development of a piping channel through the embankment. This erosion may take time to initiate, but, once a critical stage in the progression is attained, could suddenly propagate very quickly; leading to the failure of the soil and failure of any structure that may be found on top of these bedrock features.

Tests were run with a constant downward gradient to simulate seepage from the reservoir, through the embankment, and into the foundation void. Tests with this loading condition were run on the predominantly granular Teton Dam Shell material and the predominantly fine grained Teton Dam Core material. In both tests the erosion occurred due to the backward erosion piping mechanism. In the Teton Dam Shell material the erosion was controlled by the formation of natural filters that prevented rapid erosion of the cohesionless soil. In the Teton Dam Core material the numerous piping channels formed simultaneously and increased in length and width as the piping progressed. In both cases, the flow through the test cell increased steadily throughout

the tests as the piping channels developed indicating a gradual progression of the erosion toward an incident or failure.

Tests were also run with cyclic hydraulic loading from the void at the base of the apparatus. These tests were designed to model cycles of pressure in the bedrock caused by reservoir fluctuations or seasonal groundwater fluctuation. Tests with this loading condition were run on East Branch Dam Embankment material, Teton Dam Core material, and a manufactured soil consisting of medium-coarse sand mixed with the minimum amount of kaolinite clay to make it behave cohesively. The internal erosion in these tests occurred quite differently than those with constant downward gradient; forming an upward progressing stope that only widened once it reached a critical height. The development of the stope started slowly, often requiring many cycles before significant upward migration began to occur. However, once a critical width of the stope developed it progressed upward rapidly often reaching a critical height in a few cycles. Once a critical height of the stope was achieved, the walls of the stope became unstable and, aided by the seepage forces during the drainage cycle, were able to collapse back to an angle of repose.

The behavior in two of the tests performed with cyclic hydraulic loading differed somewhat from the progression described above. In the test with the manufactured soil, the cohesion of the soils was so low that the stope was not able to form to a significant height before the side collapsed to the angle of repose. In one of the tests on Teton Dam material the gap was set to a width of 2 inches rather than the 1-inch gap used in the other tests. The 2-inch width was apparently close enough to the critical

width of the stope that it progressed upward rapidly from the start of the test, resulting in failure in just a few cycles.

Several mechanisms were identified that contribute to the erosion progression during cyclic loading. First, the development of high gradients during the discharge portion of the hydraulic cycles. These gradients were enhanced above the void by lower hydraulic conductivities caused by partially saturated soils in this region. Second, the cycling of the principle stresses in the soils surrounding the void are thought to enhance the erosion by developing shear planes in the soils at the edge of the void that coalesce to dislodge chip-like particles of soil from the walls of the void. Third, the formation of a vertical hydraulic fracture from the top of the void may enhance the upward propagation of the stope. While no evidence of hydraulic fracture was observed, this is believed to be a mechanism that could occur in certain circumstances (i.e. high water pressure with relatively low overburden pressures).

The distinctly different modes of erosion propagation that were observed for the two types of hydraulic loading have significant implications on the assessment and monitoring of dam safety. The mechanism observed with the constant downward hydraulic gradient loading was observed to progress at a constant rate in both the granular and cohesive soils. With this type of progression there is a much higher likelihood of detecting the development of the internal erosion before it develops into a critical condition. Conversely, the progression pattern of the erosion caused by cyclic hydraulic loading from the void is not likely to manifest detectable changes to the pore pressure or seepage regime in the dam or foundation until the erosion has reached the

point of rapid propagation. Thus, making intervention of this failure mechanism much less likely or effective.

REFERENCES

- Brady, B.G.H., and Brown, E.T. (2006). *Rock mechanics for underground mining* (Third Edition), Chapman and Hall, London.
- Brimm, R. (2010). *Presentation: Marshall University*.
<http://www.marshall.edu/cegas/geohazards/2010pdf/presentations/Session4/3_GeoHzd_CH_RBrimm.pdf> (Feb. 8, 2013).
- Dreybrodt, W., Romanov, D., and Gabrovsek, F. (2002). "Karstification below dam sites: a model of increasing leakage from reservoirs." *Environ. Geology* 42, 518-524.
- Fell, R., Foster, M., Davidson, R., Cyganiewicz, J., Sills, G., and Vroman, N. (2008). "Unified method for estimating probabilities of failure of embankment dams by internal erosion and piping." University of New South Wales, Sydney.
- Greene, B. H., Crock, J., Moskovitz, L., and Premozic, J. W. (2010, August). Evaluation of Seepage, Internal Erosion, and Remedial Alternatives for East Branch Dam, Elk County, Pennsylvania. *Environ. & Engineering Geosci.*, XVI(3), 229-243.
- ICOLD (2012). "Internal Erosion of Existing Dams, Levees, and Dikes, and their Foundations." *International Commission on Large Dams Bulletin 1XX*, Draft of May 21, 2012.
- Johnson, K. S. (2008). "Gypsum-karst problems in constructing dams in the USA." *Environ. Geology* 53, 945-950.
- Knight, M. A., and Roman, W. M. (2009). "Characterization of geologic features affecting seepage through carbonate dam foundations." *USSD Conference*, Nashville, TN, 601-618.
- Lei, M., Jiang, X., and Yu, L. (2002). "New advances in karst collapse research in China." *Environ. Geology* 42, 462-468.
- Rice, J. D. (2007). "A Study on the Long-Term Performance of Seepage Barriers in Dams." Virginia Polytechnic Institute and State University, Blacksburg.
- Schaefer, J. A. (2009). "Risk Evaluation of Dams on Karst Foundations." *USSD Conference*, Nashville, TN, 541-579.
- Tharp, T. M. (1999). Mechanics of upward propagation of cover-collapse sinkholes. *Engrg. Geology* 52, 23-33.

USACE. (2008, June). "A history of karst seepage - Center Hill Dam rehab." *Intl. Water Power and Dam Construction*, 60(6), 24-28.

Waltham, T., Bell, F., and Culshaw, M. (2005). *Sinkholes and subsidence - Karst and cavernous rocks in engineering and construction*. Praxis Publishing, Chichester.

APPENDIX

East Branch Test Pictures:

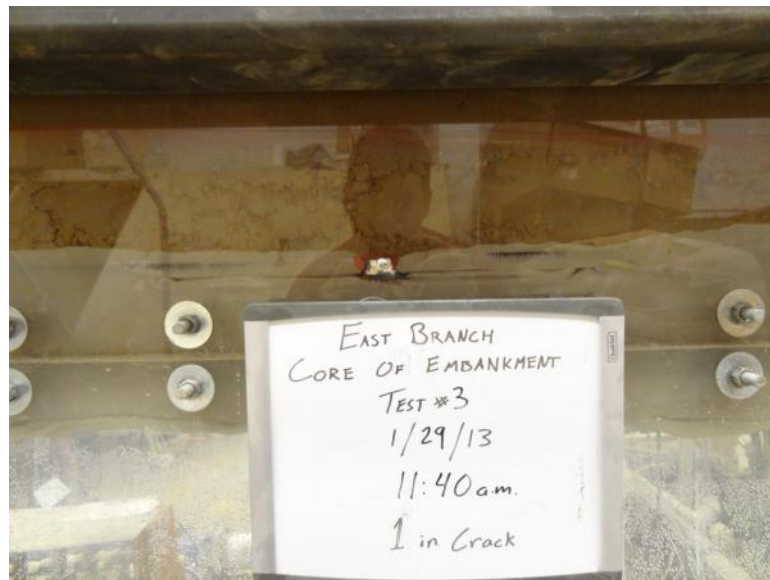


Figure A- 1. Test 3 on East Branch Core during Cycle 1 charge



Figure A- 2. Test 3 on East Branch Core during Cycle 2 charge



Figure A- 3. Test 3 on East Branch Core during Cycle 3 charge



Figure A- 4. Test 3 on East Branch Core during Cycle 4 charge



Figure A- 5. Test 3 on East Branch Core during Cycle 5 charge



Figure A- 6. Test 3 on East Branch Core during Cycle 6 charge



Figure A- 7. Test 3 on East Branch Core during Cycle 7 charge



Figure A- 8. Test 3 on East Branch Core during Cycle 8 charge



Figure A- 9. Test 3 on East Branch Core during Cycle 9 charge



Figure A- 10. Test 3 on East Branch Core during Cycle 11 charge



Figure A- 11. Test 3 on East Branch Core during Cycle 14 charge

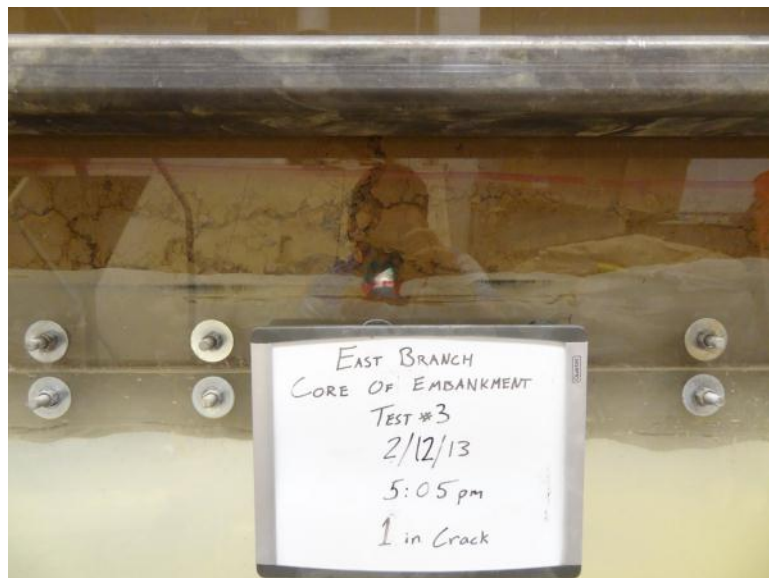


Figure A- 12. Test 3 on East Branch Core during Cycle 14 charge



Figure A- 13. Test 3 on East Branch Core during Cycle 15 discharge

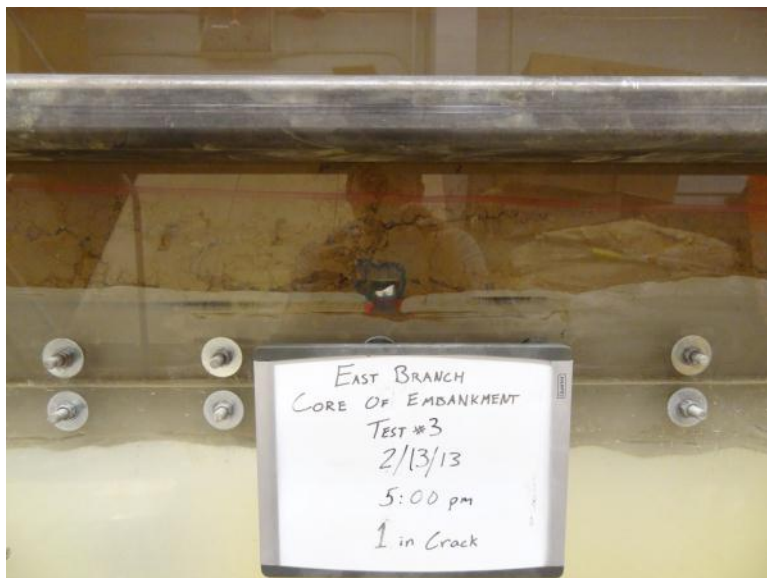


Figure A- 14. Test 3 on East Branch Core during Cycle 15 discharge



Figure A- 15. Test 3 on East Branch Core during Cycle 16 discharge



Figure A- 16. Test 3 on East Branch Core during Cycle 16 discharge



Figure A- 17. Test 3 on East Branch Core during Cycle 18 discharge



Figure A- 18. Test 3 on East Branch Core during Cycle 18 discharge



Figure A- 19. Test 3 on East Branch Core during Cycle 20 discharge



Figure A- 20. Test 3 on East Branch Core during Cycle 20 discharge



Figure A- 21. Test 3 on East Branch Core during Cycle 24 discharge



Figure A- 22. Test 3 on East Branch Core during Cycle 25 charge



Figure A- 23. Test 3 on East Branch Core during Cycle 25 discharge



Figure A- 24. Test 3 on East Branch Core during Cycle 27 discharge



Figure A- 25. Test 3 on East Branch Core during Cycle 27 discharge

Sand-Kaolinite Test Pictures:



Figure A- 26. Test 1 on Sand with Clay during Cycle 1 charge



Figure A- 27. Test 1 on Sand with Clay during Cycle 1 discharge

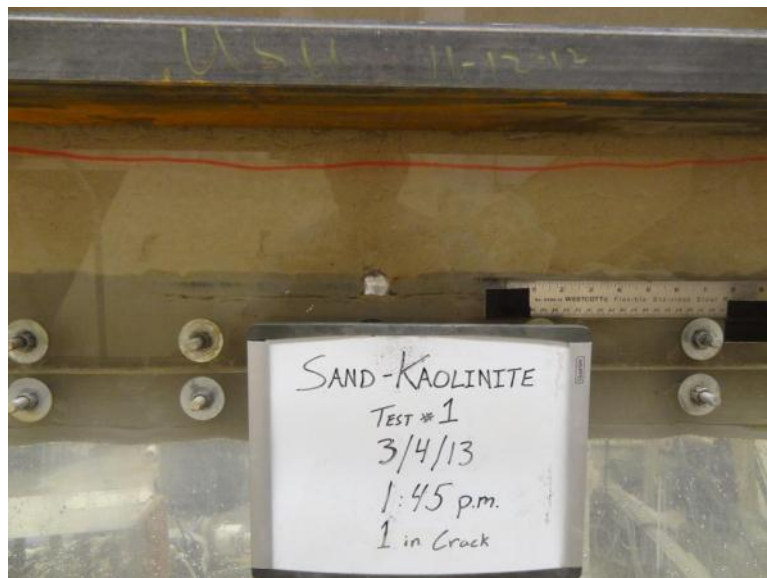


Figure A- 28. Test 1 on Sand with Clay during Cycle 1 discharge



Figure A- 29. Test 1 on Sand with Clay during Cycle 2 charge

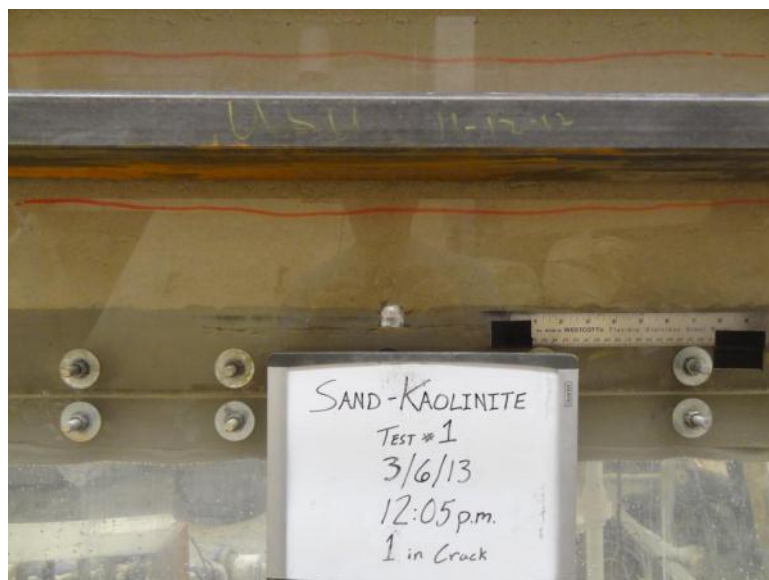


Figure A- 30. Test 1 on Sand with Clay during Cycle 2 discharge

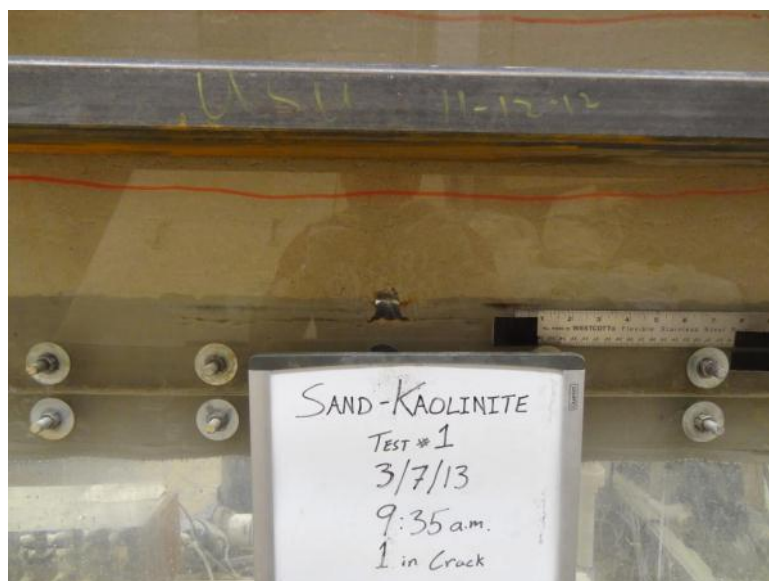


Figure A- 31. Test 1 on Sand with Clay during Cycle 3 charge



Figure A- 32. Test 1 on Sand with Clay during Cycle 4 charge

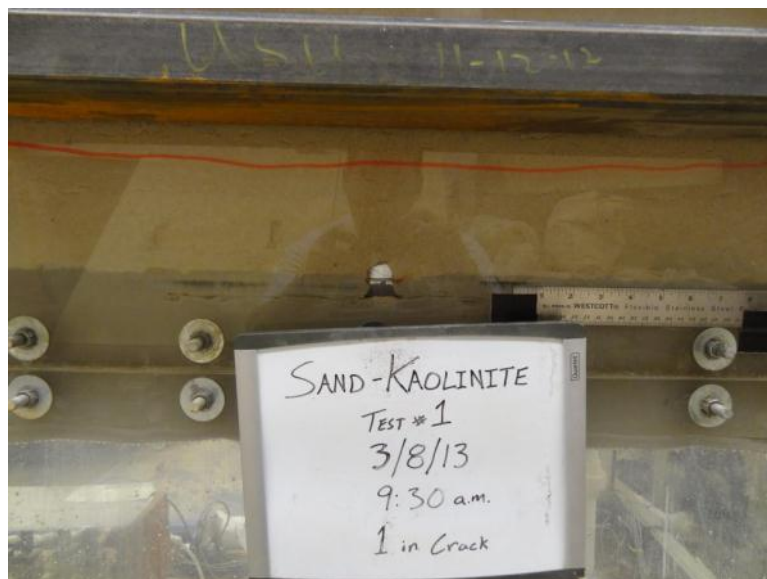


Figure A- 33. Test 1 on Sand with Clay during Cycle 4 discharge

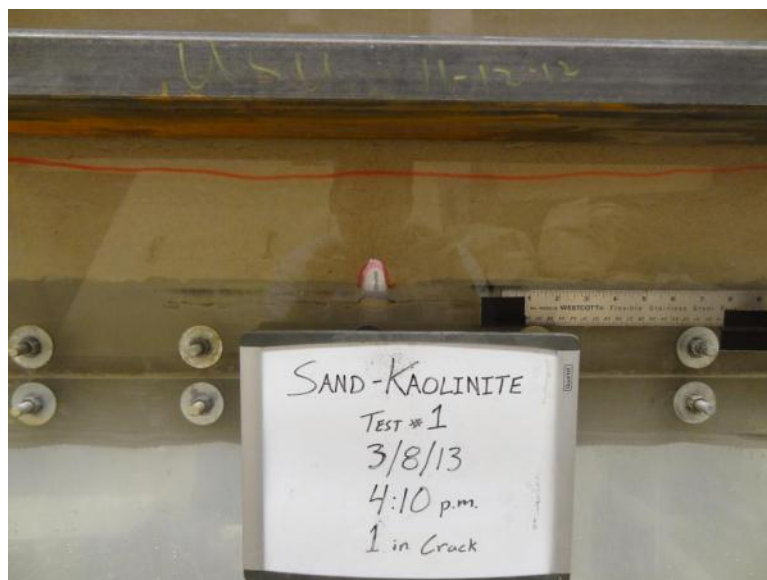


Figure A- 34. Test 1 on Sand with Clay during Cycle 5 discharge



Figure A- 35. Test 1 on Sand with Clay during Cycle 5 discharge



Figure A- 36. Test 1 on Sand with Clay during Cycle 6 charge



Figure A- 37. Test 1 on Sand with Clay during Cycle 6 discharge

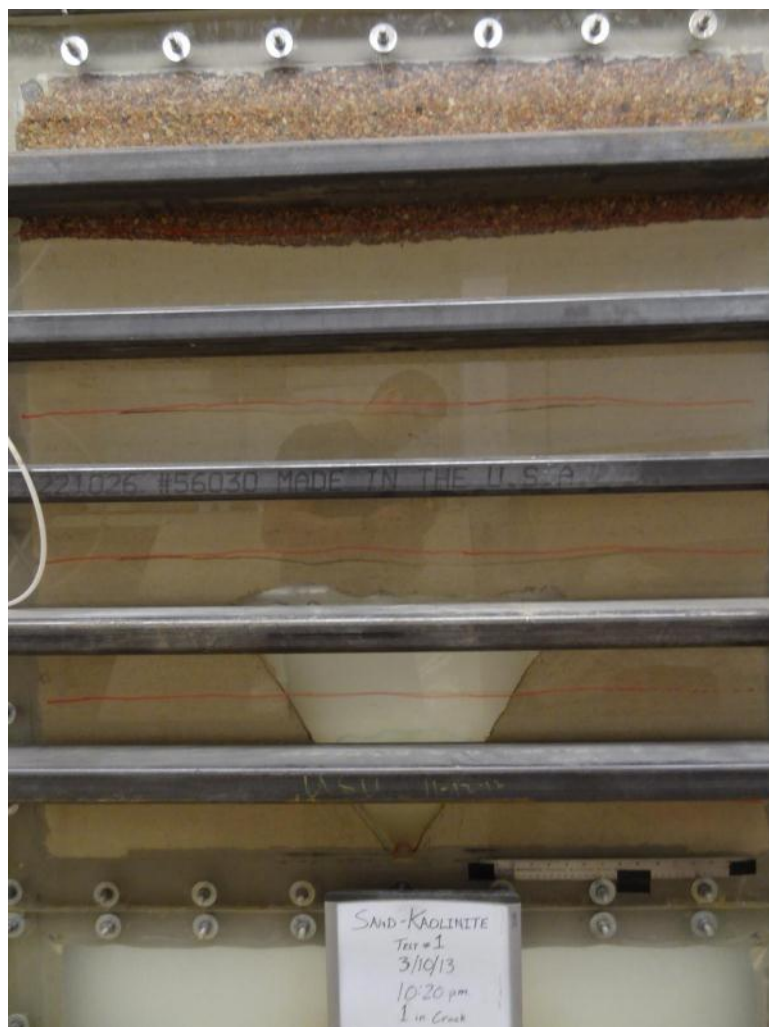


Figure A- 38. Test 1 on Sand with Clay during Cycle 8 charge

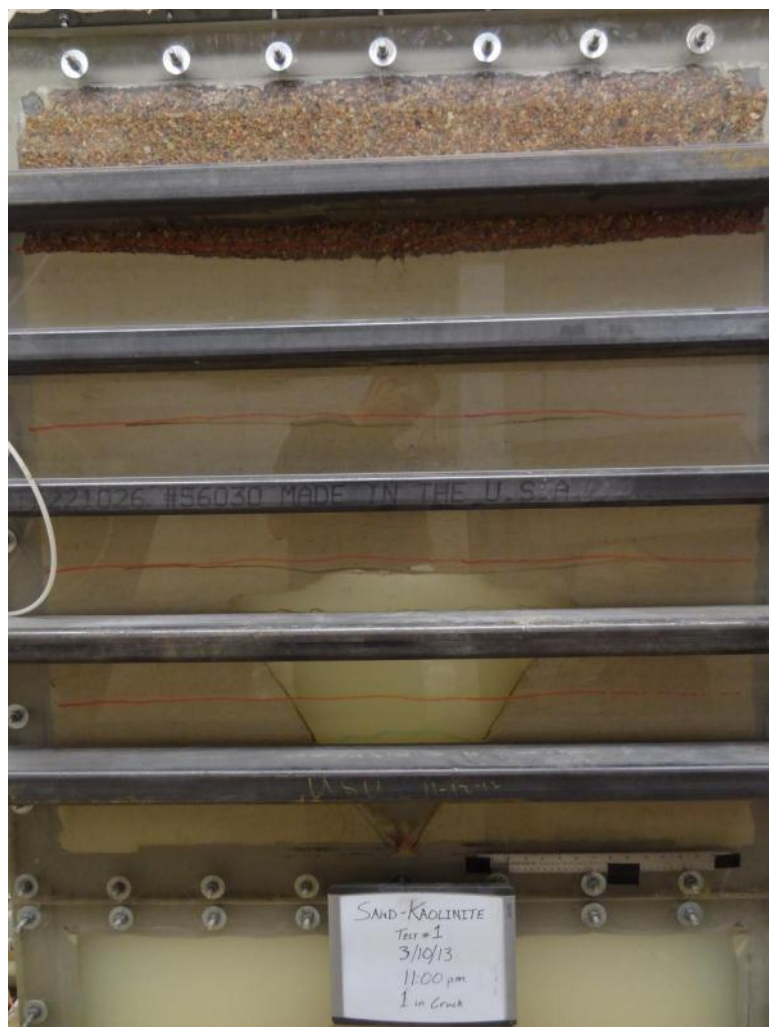


Figure A- 39. Test 1 on Sand with Clay during Cycle 8 charge



Figure A- 40. Test 1 on Sand with Clay during Cycle 8 charge

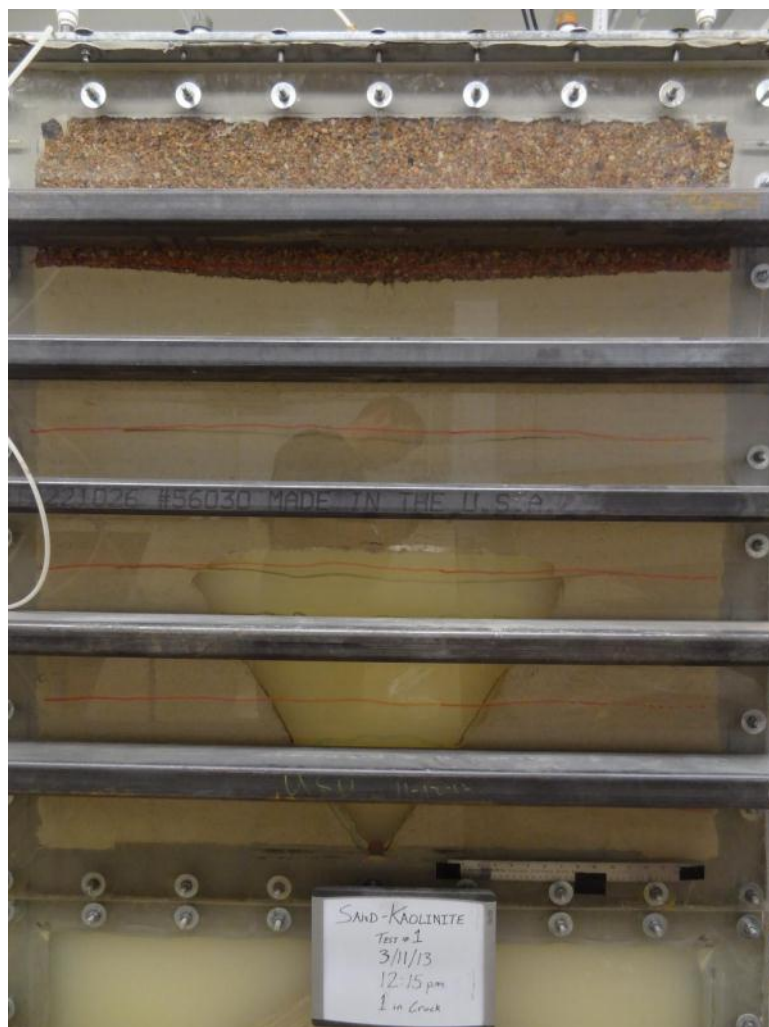


Figure A- 41. Test 1 on Sand with Clay during Cycle 9 charge

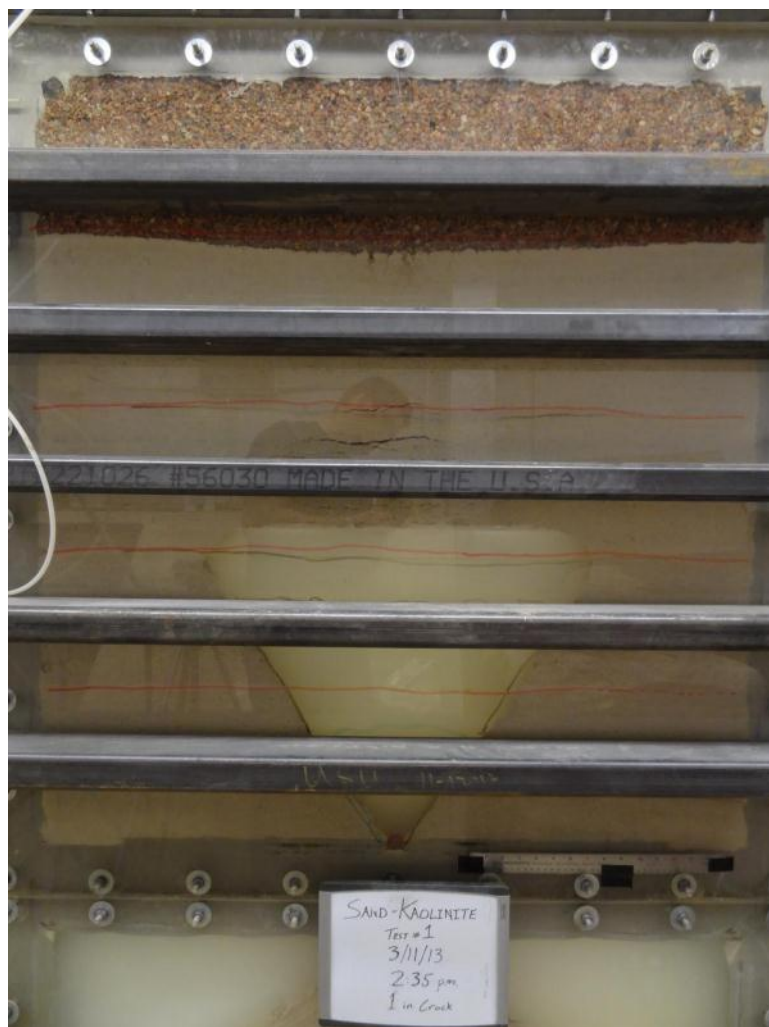


Figure A- 42. Test 1 on Sand with Clay during Cycle 9 discharge

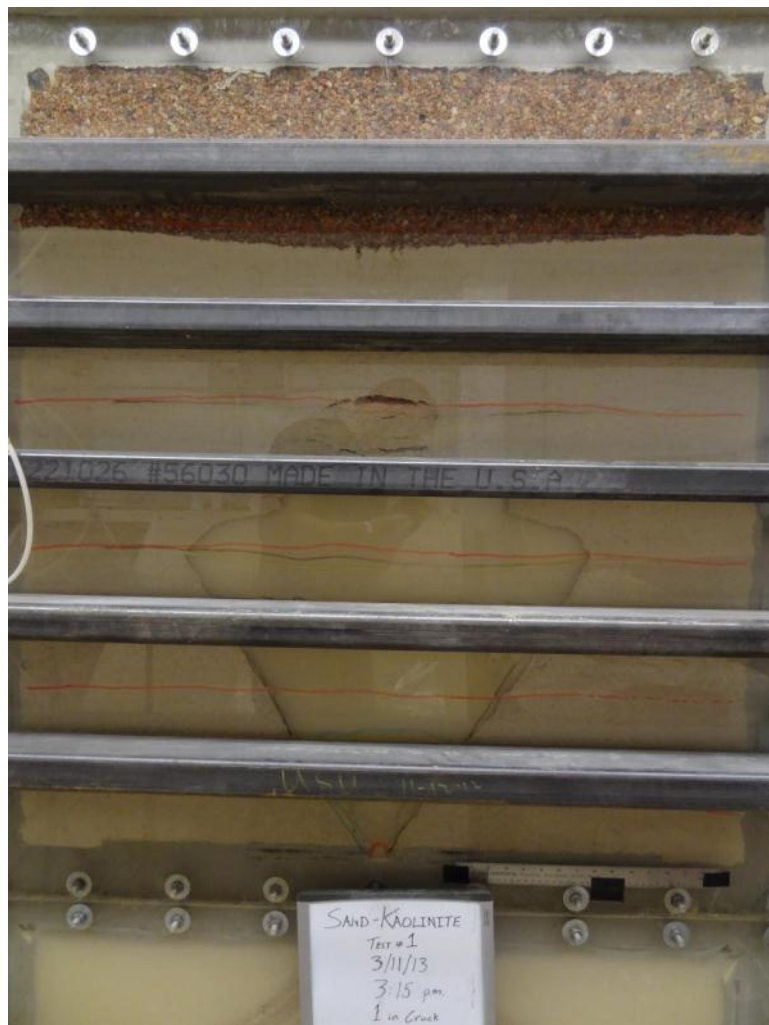


Figure A- 43. Test 1 on Sand with Clay during Cycle 9 discharge

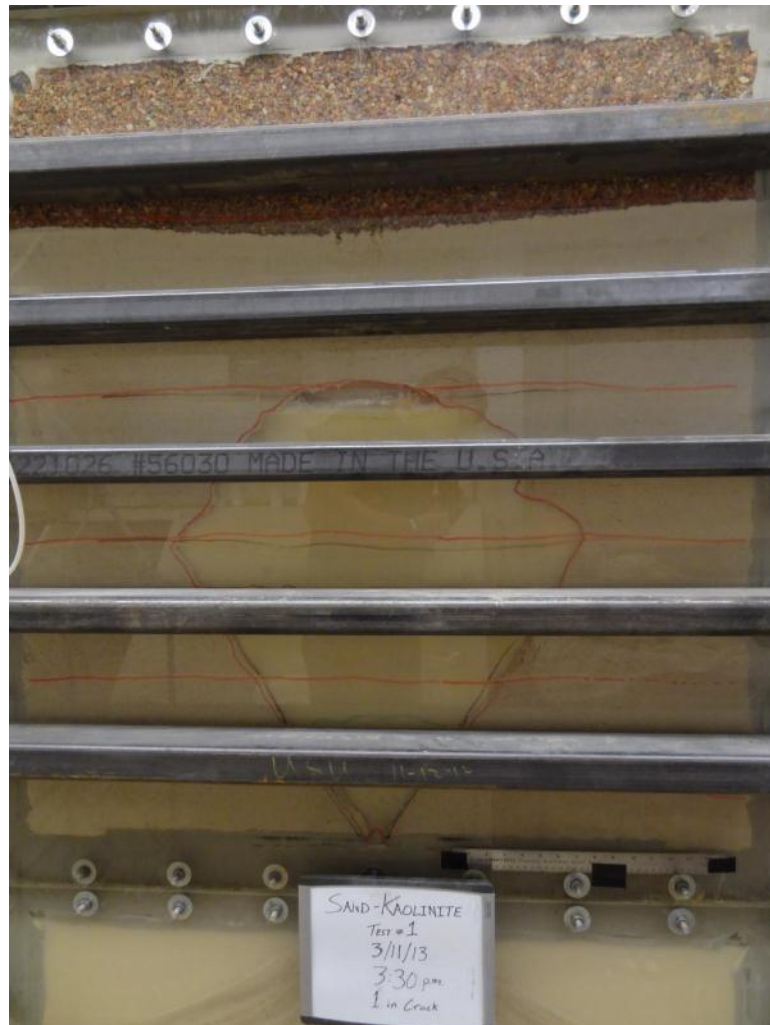


Figure A- 44. Test 1 on Sand with Clay during Cycle 9 discharge

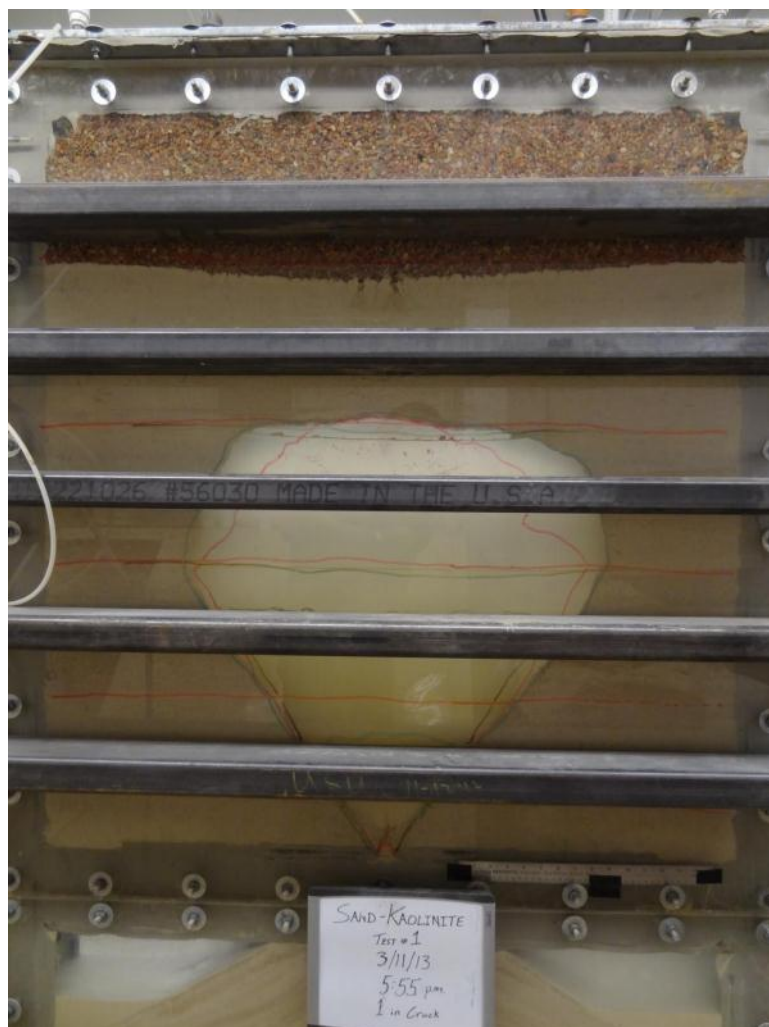


Figure A- 45. Test 1 on Sand with Clay during Cycle 10 charge

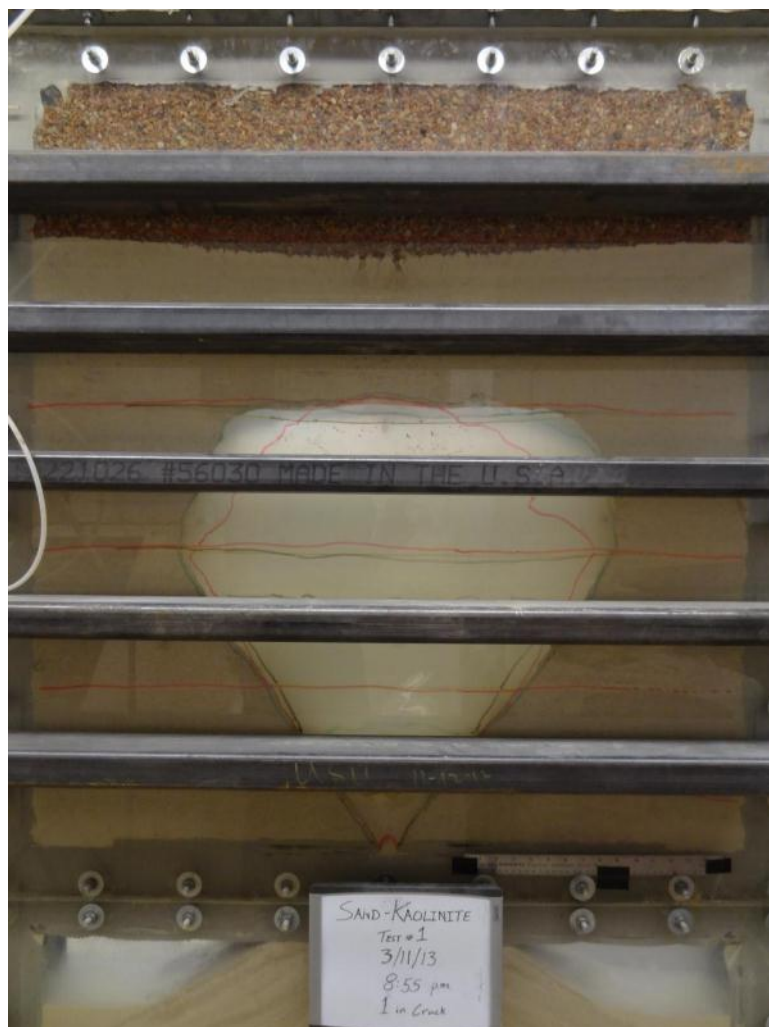


Figure A- 46. Test 1 on Sand with Clay during Cycle 10 discharge

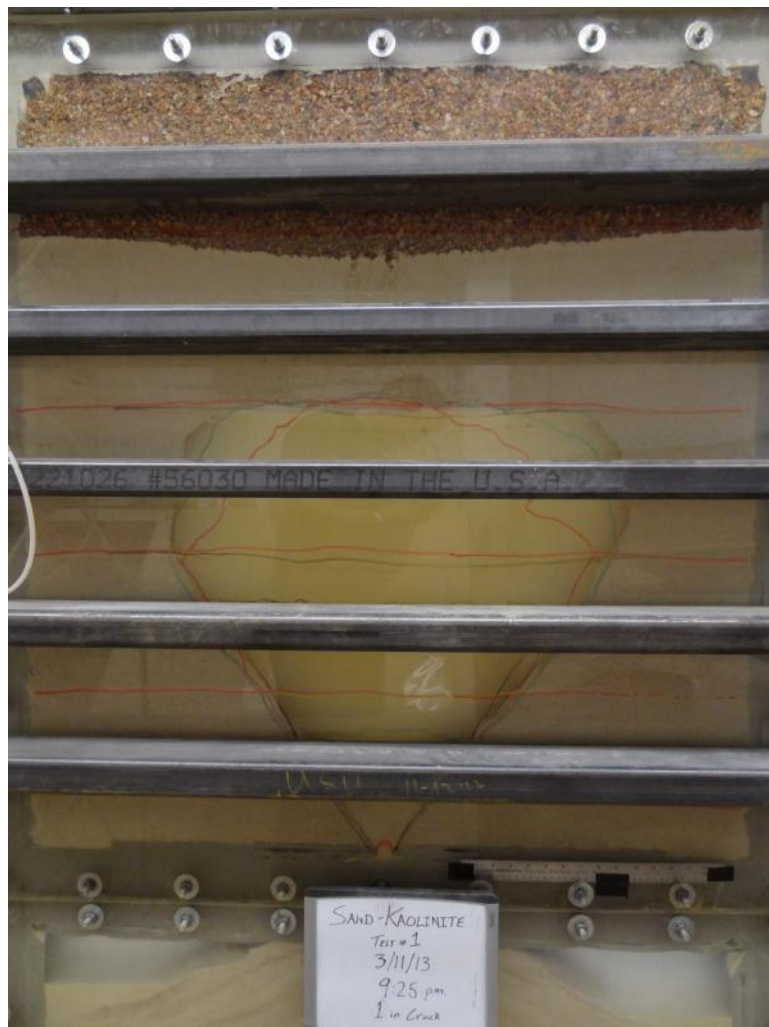


Figure A- 47. Test 1 on Sand with Clay during Cycle 10 discharge

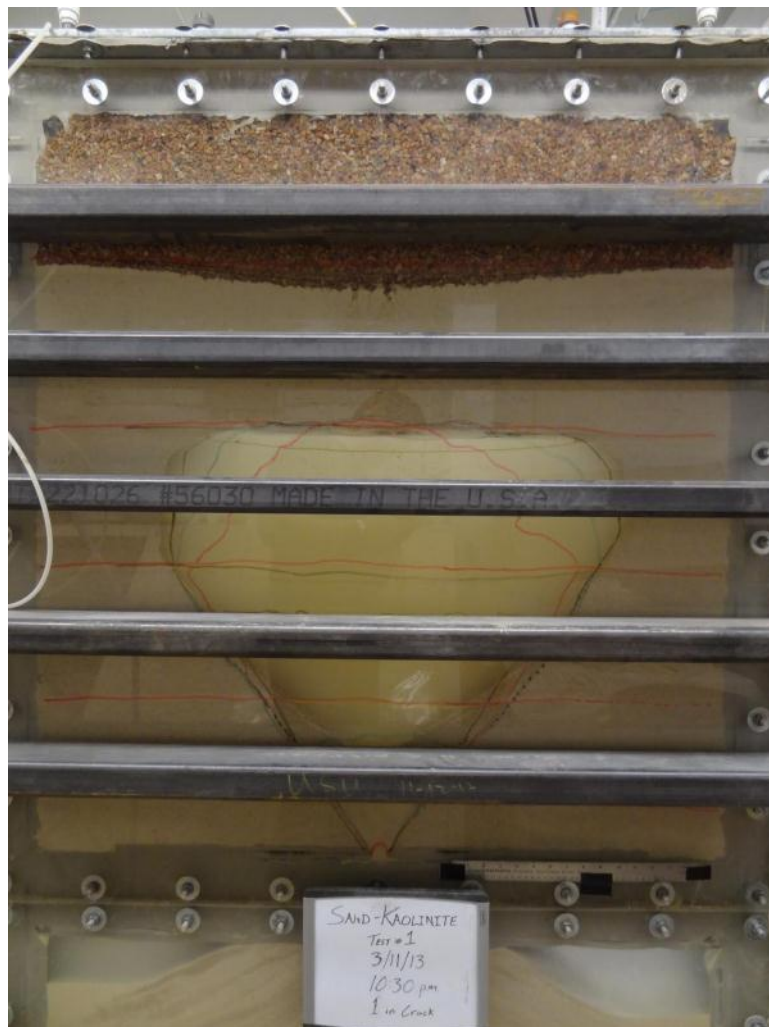


Figure A- 48. Test 1 on Sand with Clay during Cycle 10 discharge



Figure A- 49. Test 1 on Sand with Clay during Cycle 11 charge

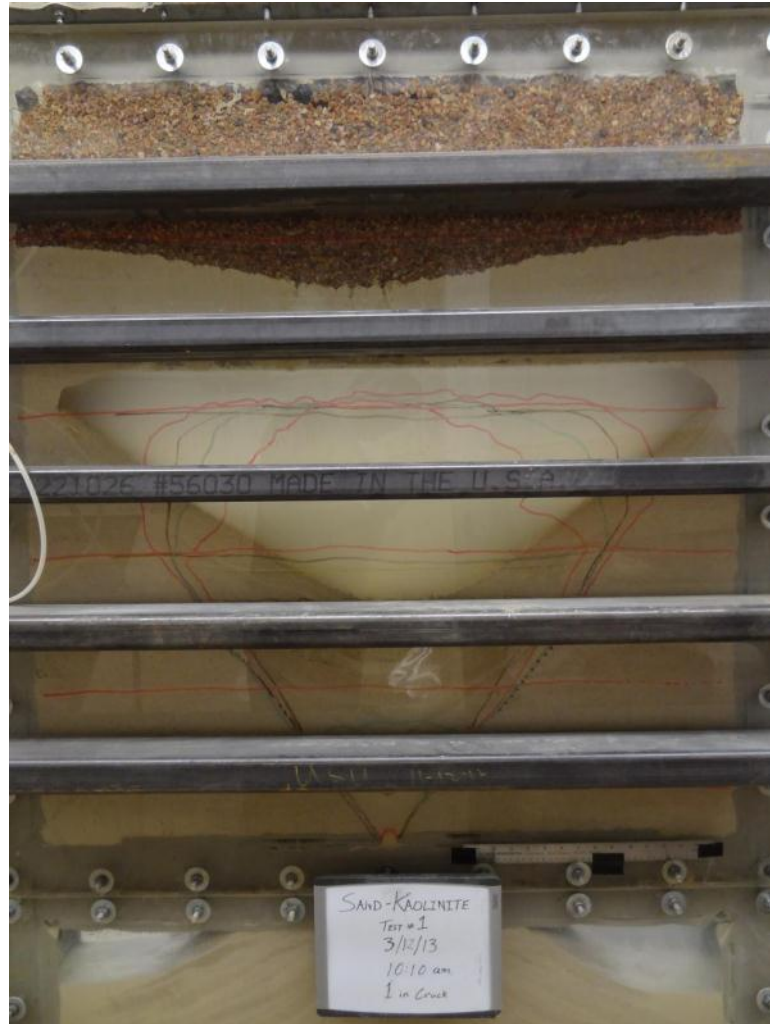


Figure A- 50. Test 1 on Sand with Clay during Cycle 11 discharge

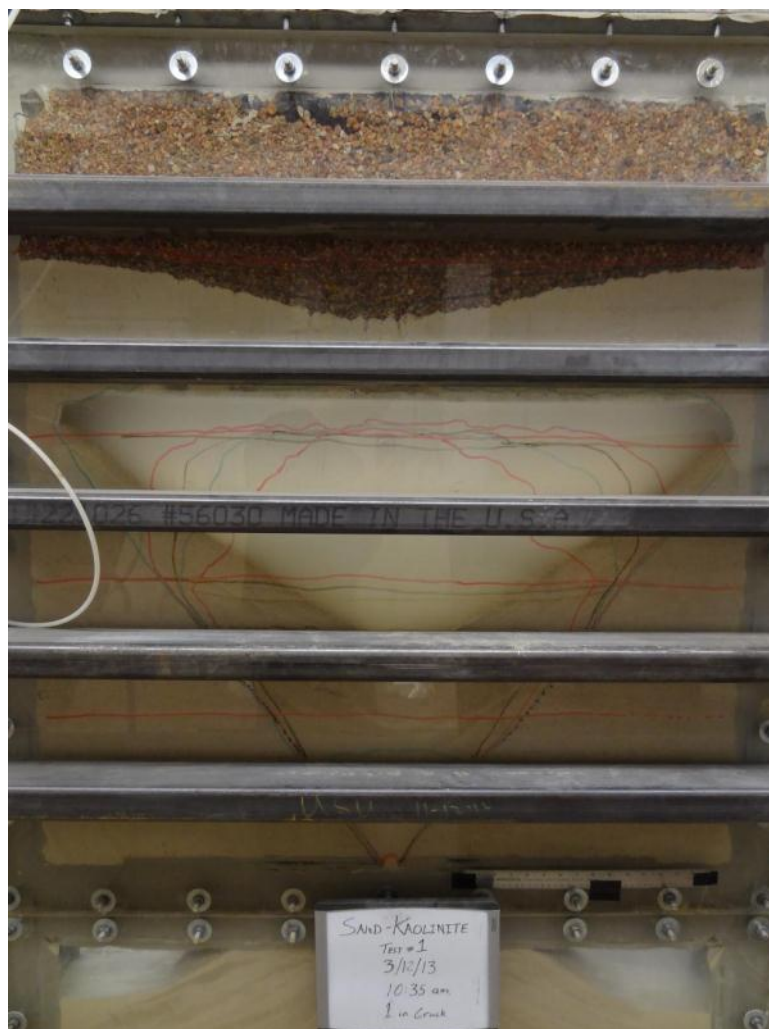


Figure A- 51. Test 1 on Sand with Clay during Cycle 11 discharge



Figure A- 52. Test 1 on Sand with Clay during Cycle 11 discharge

Teton Core of Embankment Test #1 Pictures:



Figure A- 53. Test 1 on Teton Core during Cycle 1 charge



Figure A- 54. Test 1 on Teton Core during Cycle 1 charge



Figure A- 55. Test 1 on Teton Core during Cycle 1 discharge



Figure A- 56. Test 1 on Teton Core during Cycle 2 charge



Figure A- 57. Test 1 on Teton Core during Cycle 2 discharge



Figure A- 58. Test 1 on Teton Core during Cycle 3 charge



Figure A- 59. Test 1 on Teton Core during Cycle 3 discharge



Figure A- 60. Test 1 on Teton Core during Cycle 4 charge



Figure A- 61. Test 1 on Teton Core during Cycle 4 discharge



Figure A- 62. Test 1 on Teton Core during Cycle 5 charge



Figure A- 63. Test 1 on Teton Core during Cycle 5 discharge



Figure A- 64. Test 1 on Teton Core during Cycle 6 charge



Figure A- 65. Test 1 on Teton Core during Cycle 6 discharge



Figure A- 66. Test 1 on Teton Core during Cycle 7 charge



Figure A- 67. Test 1 on Teton Core during Cycle 7 discharge



Figure A- 68. Test 1 on Teton Core during Cycle 8 charge



Figure A- 69. Test 1 on Teton Core during Cycle 8 discharge



Figure A- 70. Test 1 on Teton Core during Cycle 9 charge



Figure A- 71. Test 1 on Teton Core during Cycle 9 discharge



Figure A- 72. Test 1 on Teton Core during Cycle 11 charge



Figure A- 73. Test 1 on Teton Core during Cycle 11 discharge



Figure A- 74. Test 1 on Teton Core during Cycle 12 charge



Figure A- 75. Test 1 on Teton Core during Cycle 12 discharge



Figure A- 76. Test 1 on Teton Core during Cycle 13 charge



Figure A- 77. Test 1 on Teton Core during Cycle 13 discharge



Figure A- 78. Test 1 on Teton Core during Cycle 14 charge



Figure A- 79. Test 1 on Teton Core during Cycle 14 discharge



Figure A- 80. Test 1 on Teton Core during Cycle 15 charge



Figure A- 81. Test 1 on Teton Core during Cycle 15 discharge



Figure A- 82. Test 1 on Teton Core during Cycle 16 charge



Figure A- 83. Test 1 on Teton Core during Cycle 16 discharge



Figure A- 84. Test 1 on Teton Core during Cycle 17 charge



Figure A- 85. Test 1 on Teton Core during Cycle 17 discharge



Figure A- 86. Test 1 on Teton Core during Cycle 17 discharge



Figure A- 87. Test 1 on Teton Core during Cycle 17 discharge



Figure A- 88. Test 1 on Teton Core during Cycle 18 charge



Figure A- 89. Test 1 on Teton Core during Cycle 18 discharge



Figure A- 90. Test 1 on Teton Core during Cycle 18 discharge

Teton Core of Embankment Test #2 Pictures:

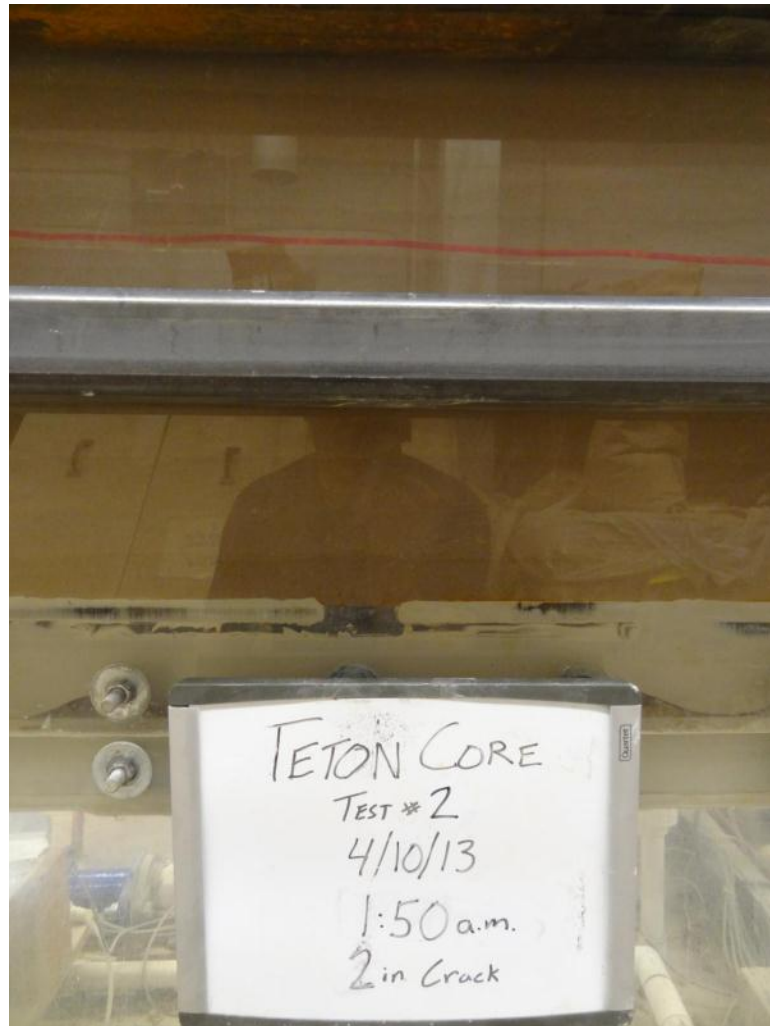


Figure A- 91. Test 2 on Teton Core during Cycle 1 charge

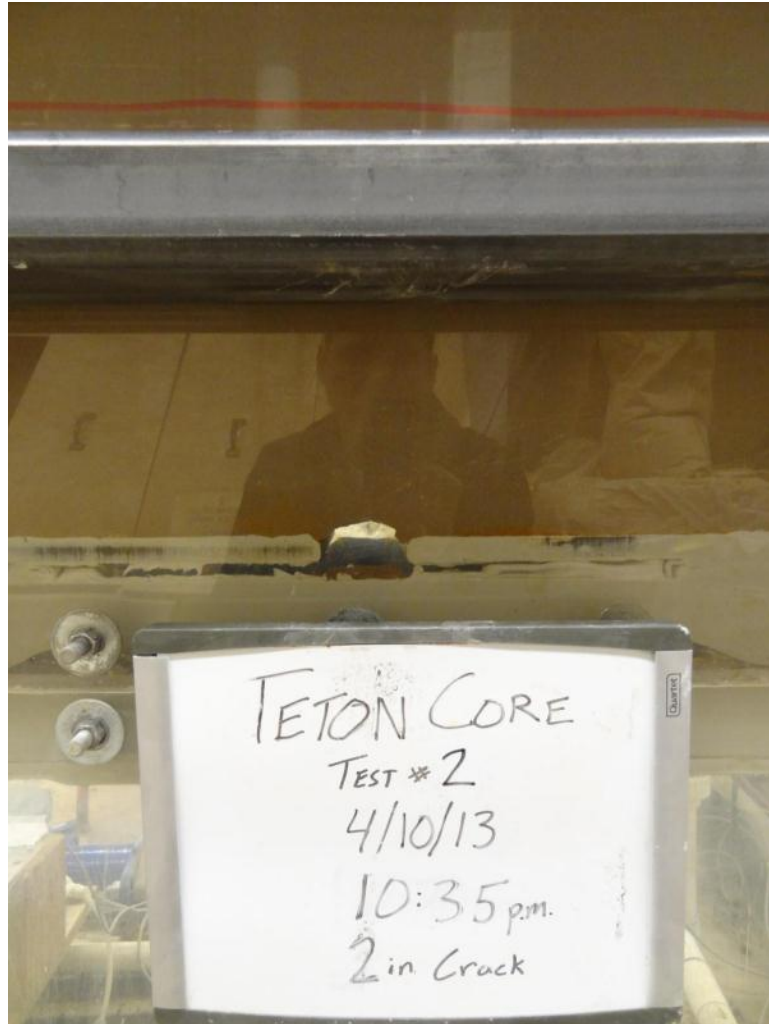


Figure A- 92. Test 2 on Teton Core during Cycle 1 charge

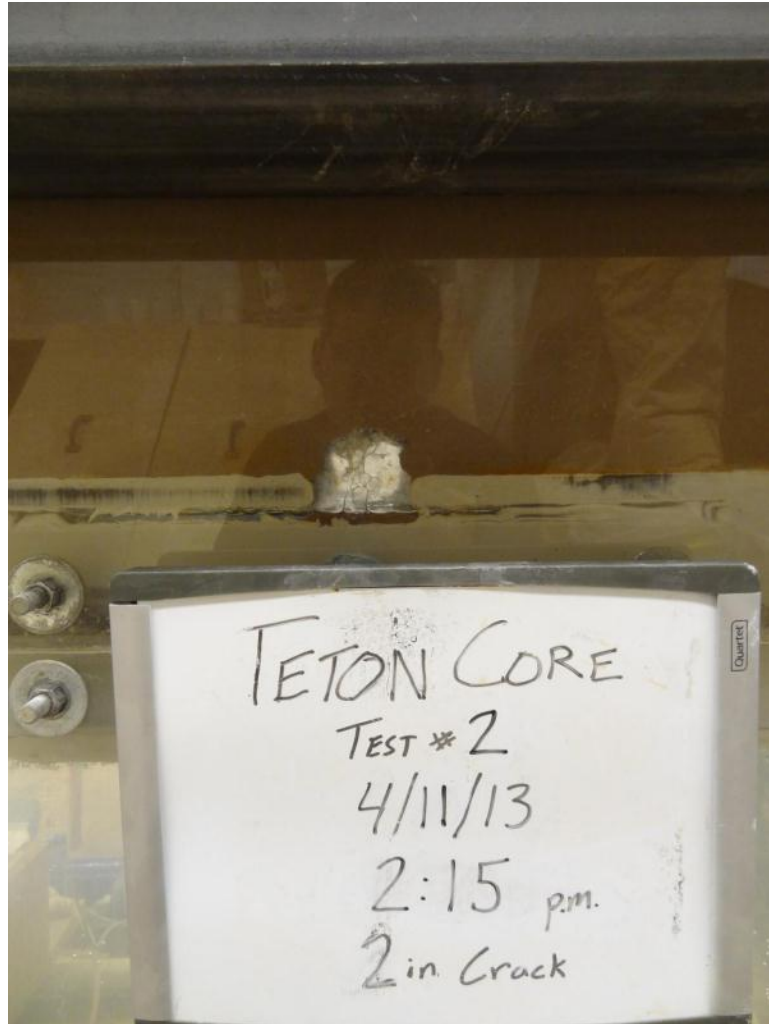


Figure A- 93. Test 2 on Teton Core during Cycle 1 discharge

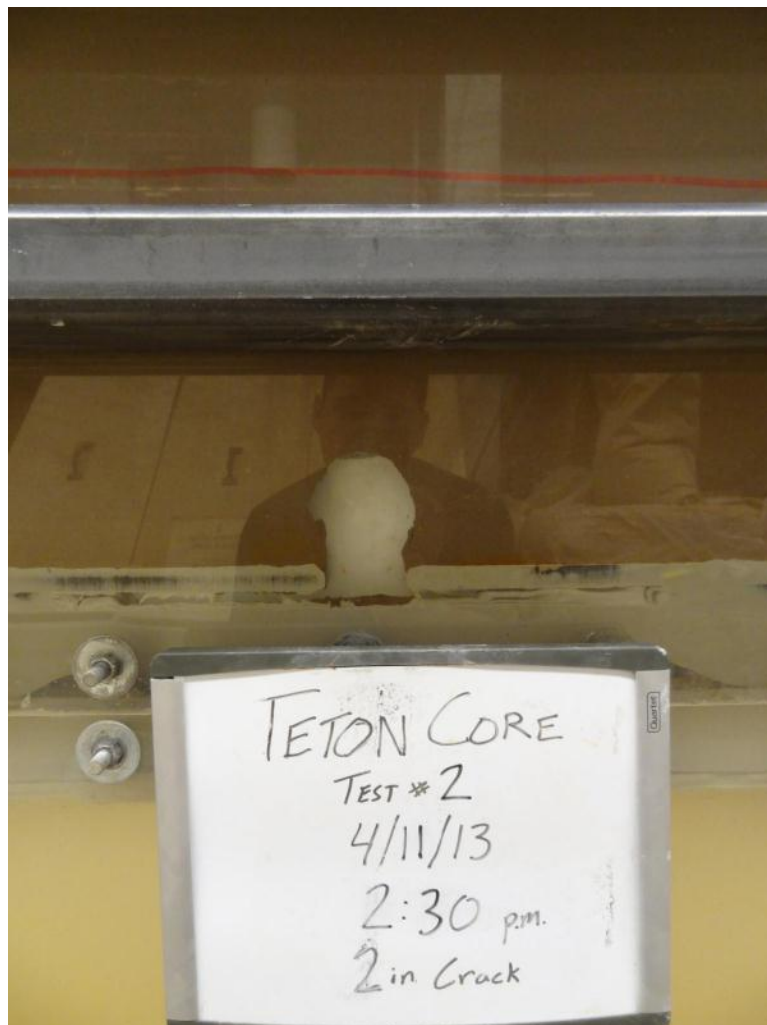


Figure A- 94. Test 2 on Teton Core during Cycle 2 charge

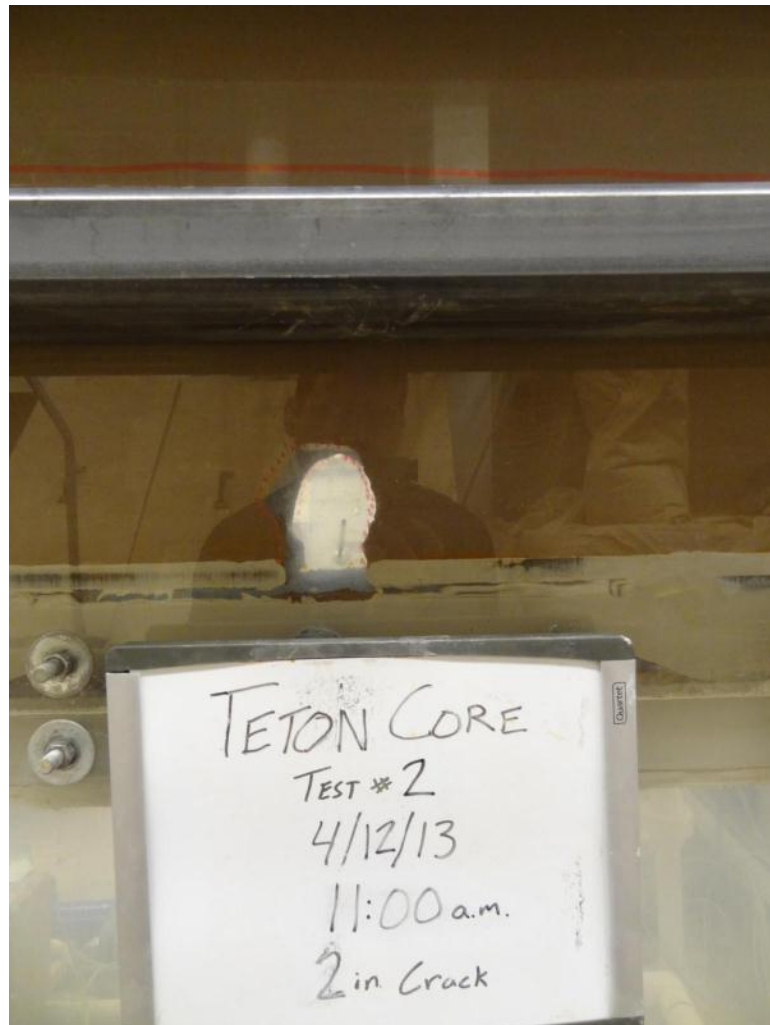


Figure A- 95. Test 2 on Teton Core during Cycle 2 charge

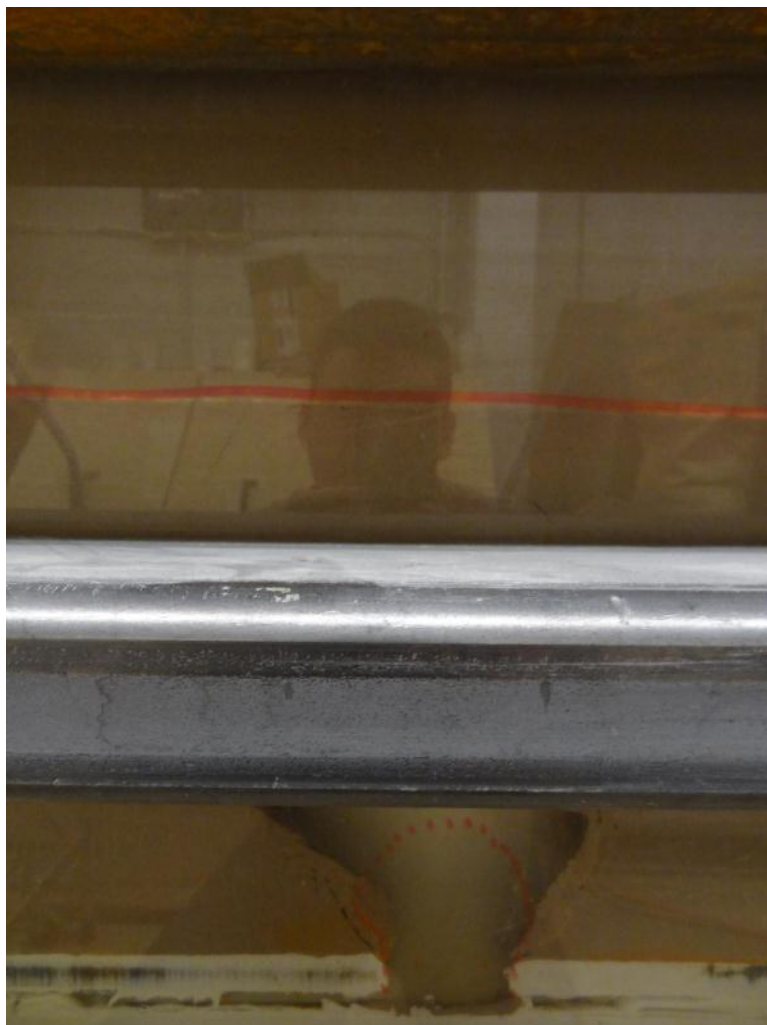


Figure A- 96. Test 2 on Teton Core during Cycle 2 discharge



Figure A- 97. Test 2 on Teton Core during Cycle 2 discharge



Figure A- 98. Test 2 on Teton Core during Cycle 2 discharge



Figure A- 99. Test 2 on Teton Core during Cycle 2 discharge

Teton Core of Embankment Test #3 Pictures:

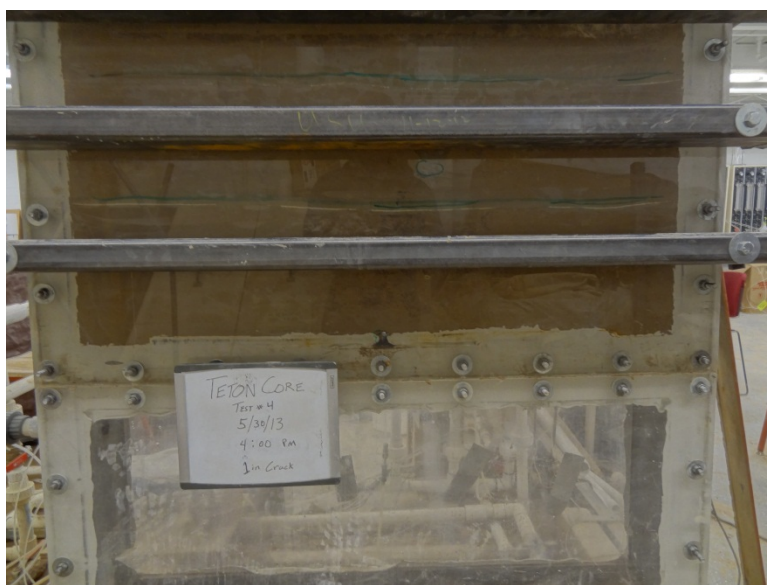


Figure A- 100. Test 3 on Teton Core with constant downward gradient



Figure A- 101. Test 3 on Teton Core with constant downward gradient



Figure A- 102. Test 3 on Teton Core with constant downward gradient

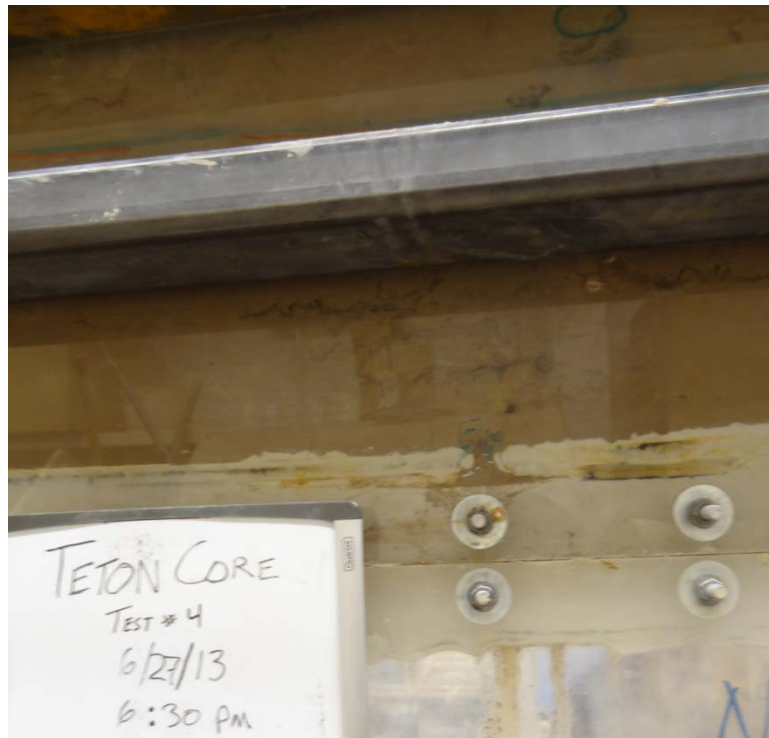


Figure A- 103. Test 3 on Teton Core with constant downward gradient



Figure A- 104. Test 3 on Teton Core with constant downward gradient



Figure A- 105. Test 3 on Teton Core with constant downward gradient

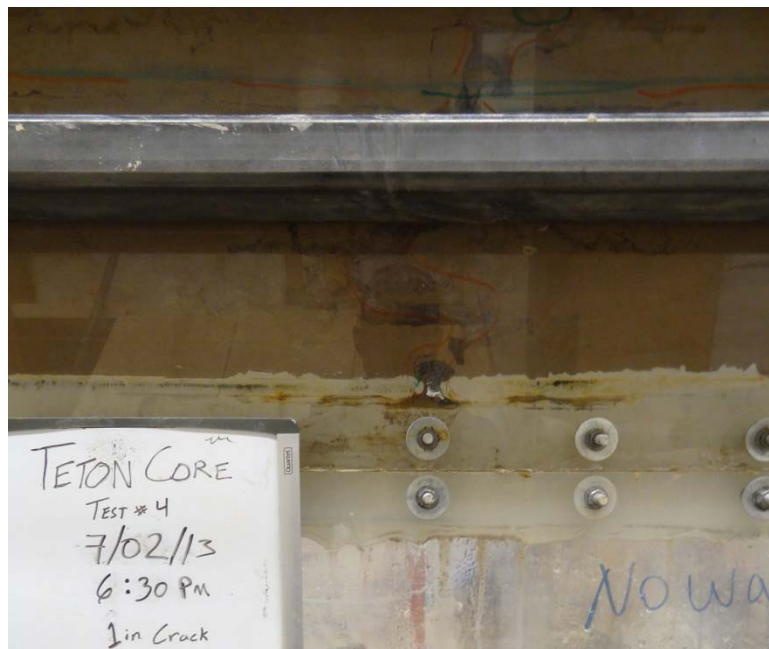


Figure A- 106. Test 3 on Teton Core with constant downward gradient



Figure A- 107. Test 3 on Teton Core with constant downward gradient



Figure A- 108. Test 3 on Teton Core with constant downward gradient



Figure A- 109. Test 3 on Teton Core with constant downward gradient



Figure A- 110. Test 3 on Teton Core with constant downward gradient

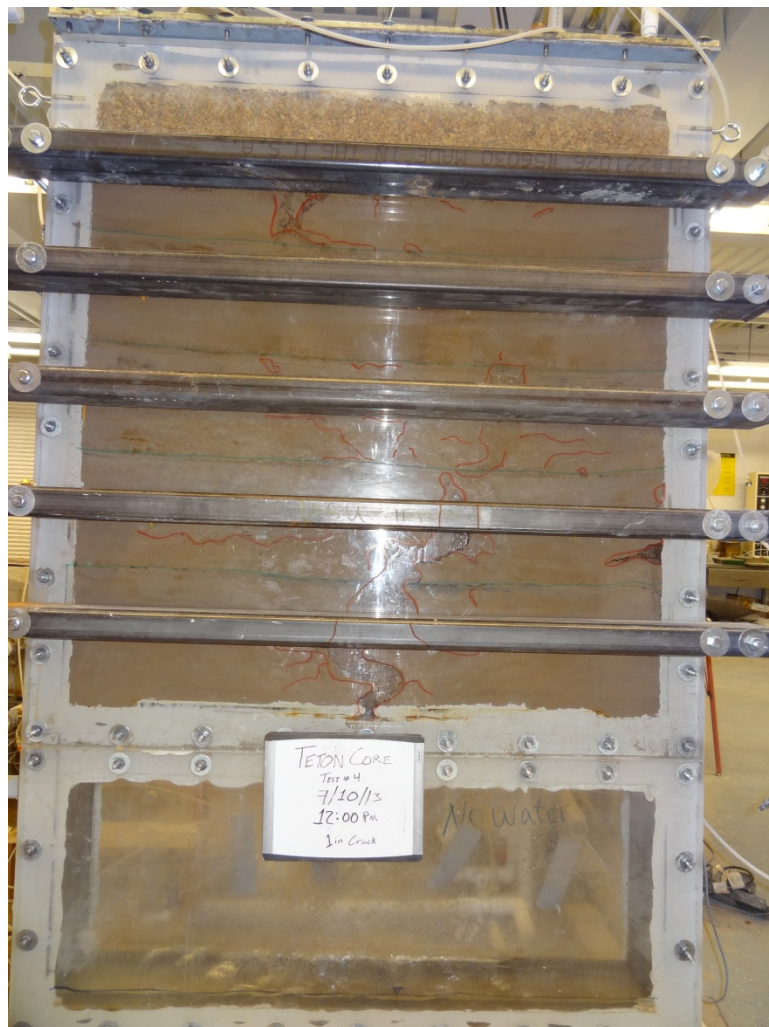


Figure A- 111. Test 3 on Teton Core with constant downward gradient



Figure A- 112. Test 3 on Teton Core with constant downward gradient